EBM Experimental Biology and Medicine

Volume 250 | Issue 4

Experimental Biology and Medicine

Editor-in-Chief

Nicola Conran
University of Campinas, Brazil

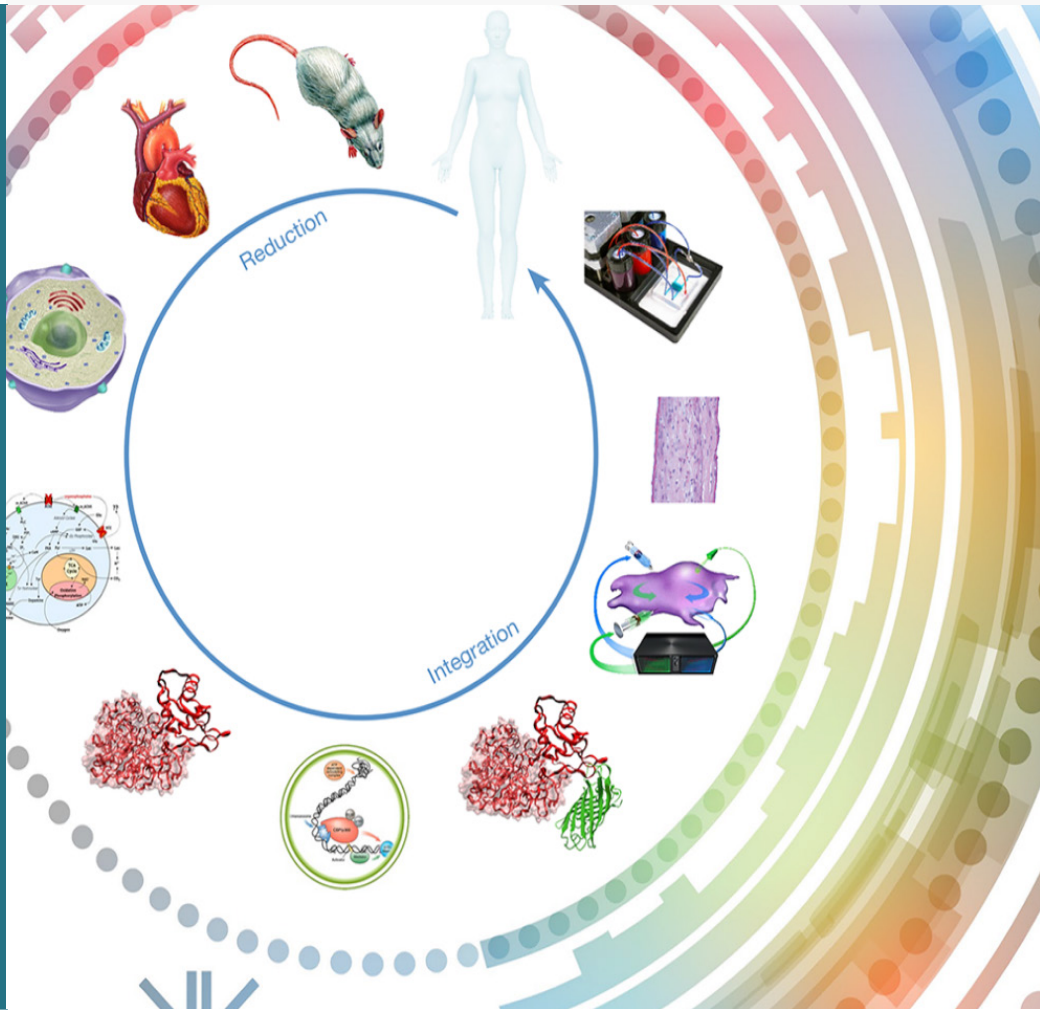

ISBN 978-2-8325-6395-3
DOI 10.3389/978-2-8325-6395-3

frontiers | Publishing Partnerships

Society for Experimental Biology and Medicine
3220 N Street NW, #179
Washington DC 20007, USA
Executive Director – ed@sebm.org

www.sebm.org

EBM Experimental Biology and Medicine

Editorial Board

ISSN 1535-3699
ISBN 978-2-8325-6395-3
DOI 10.3389/978-2-8325-6395-3

EBM Experimental Biology and Medicine

2025 | Volume 250 | Issue 4 | ISSN 1535-3699

Table of contents

Translational Research

Highlight

Original Research

Correction

Retraction

EBM Experimental Biology and Medicine

TYPE Brief Communication
PUBLISHED 01 May 2025
DOI 10.3389/ebm.2025.10387

OPEN ACCESS

*CORRESPONDENCE
Sunchai Payungporn,
sp.medbiochemcu@gmail.com

RECEIVED 25 September 2024
ACCEPTED 22 April 2025
PUBLISHED 01 May 2025

CITATION
Khamwut A, Nimnual J, Chomta N, Nimsamer P, Mayuramart O, Kaewsapsak P, Pasittungkul S, Poovorawan Y and Payungporn S (2025) Detection of respiratory syncytial virus based on RT-RPA and CRISPR-Cas12a. *Exp. Biol. Med.* 250:10387. doi: 10.3389/ebm.2025.10387

Detection of respiratory syncytial virus based on RT-RPA and CRISPR-Cas12a

Ariya Khamwut[1], Juthamas Nimnual[1], Nantinee Chomta[1], Pattaraporn Nimsamer[1,2], Oraphan Mayuramart[1], Pornchai Kaewsapsak[1,3], Siripat Pasittungkul[4], Yong Poovorawan[4] and Sunchai Payungporn[1,3]*

[1]Center of Excellence in Systems Microbiology, Faculty of Medicine, Chulalongkorn University, Bangkok, Thailand, [2]Division of Medical Bioinformatics, Research Department, Faculty of Medicine Siriraj Hospital, Mahidol University, Bangkok, Thailand, [3]Department of Biochemistry, Faculty of Medicine, Chulalongkorn University, Bangkok, Thailand, [4]Center of Excellence in Clinical Virology, Faculty of Medicine, Chulalongkorn University, Bangkok, Thailand

Abstract

Human respiratory syncytial virus (hRSV) is one of the most prevalent viruses infecting children globally. In this study, we employed the RT-RPA with CRISPR/Cas12a detection methodology to detect and differentiate RSV-A and RSV-B, particularly in resource-limited settings. The detection limit for RSV-A and RSV-B was approximately 10^2 and 10^3 copies/reaction, respectively. The assay revealed 100% specificity in detecting both RSV-A and RSV-B. Diagnostic accuracy was 90.32 and 93.55% for RSV-A and RSV-B, respectively, compared to RT-qPCR. These data indicate a proficient strategy for RSV screening, demonstrating promise for prospective applications in detecting diverse viral infections.

KEYWORDS

CRISPR-Cas12a, detection, isothermal amplification, RT-RPA, respiratory syncytial virus

Impact statement

This study presents a novel RSV detection method using RT-RPA and CRISPR/Cas12a, achieving high sensitivity and specificity. With detection limits of 10^2 and 10^3 copies/reaction for RSV-A and RSV-B, respectively, and diagnostic accuracy comparable to RT-qPCR, it offers a reliable, resource-efficient alternative for accurate RSV screening.

Introduction

The human respiratory syncytial virus (hRSV) is an enveloped (−) ssRNA virus belonging to the *Paramyxoviridae* family and is classified in the genus *Pneumovirus*. RSV has a single serotype divided into two major subgroups, RSV-A and RSV-B, each

comprising multiple genotypes [1–3]. The replication of hRSV occurs in both the upper and lower airways and is commonly disseminated through direct contact or aerosol inhalation [2, 4]. The predominant clinical presentation of RSV infection observed in children is bronchiolitis, a pathological condition affecting the lower respiratory tract, marked by airway obstruction. This condition may progress to complications such as pneumonia, respiratory failure, and mortality [5, 6].

Presently, preventive strategies rely on avoiding risk factors, patient isolation, and vaccination. However, existing vaccines primarily offer inadequate protection against RSV infection in older adults and high-risk individuals. Consequently, rapid diagnosis of RSV infection is essential to track and reduce the spread of diseases. The World Health Organization (WHO) advocates the utilization of a virus testing approach employing quantitative reverse transcription-polymerase chain reaction (qRT-PCR) conducted on throat or nasopharyngeal swabs (NP) [7, 8]. However, the use of qRT-PCR remains restricted because of the high cost of the devices, the need for a specialized molecular lab and specialists, and the 4-h detection turnaround time.

Interestingly, the U.S. Food and Drug Administration (FDA) recently approved the CRISPR-based diagnostic approach for more straightforward and rapid diagnosis [9]. This approach integrates the CRISPR/Cas system with recombinase polymerase amplification (RPA) to amplify and identify target regions within DNA sequences [10, 11]. The CRISPR-Cas12a technology, with its portable, rapid, and precise characteristics, holds immense promise in nucleic acid diagnostics, potentially transforming the field of virology and molecular diagnostics [12].

CRISPR-Cas12a, a CRISPR nuclease, possesses the capability to selectively degrade designated double-stranded DNA (dsDNA) and single-stranded DNA (ssDNA) that is complementary to the CRISPR RNA (crRNA). This process involves the utilization of the RuvC domain, resulting in the creation of staggered ends in the target DNA (*cis*-cleavage activity) after recognition of the protospacer adjacent motif (PAM) (5′-TTTV-3′) [13, 14]. After identifying the corresponding sequences to the CRISPR RNA (crRNA), the Cas protein cleaves the specific target. A matching DNA sequence triggers the collateral effect (*trans*-cleavage activity) of Cas12a. This activation separates the fluorescent reporter from the quencher, illuminating the fluorescent signal [15].

Despite extensive research on the CRISPR-Cas12a technology for the expeditious and precise detection of human respiratory viruses, there remains a constrained capacity for nucleic acid identification of RSV in clinical samples in relation to both subtypes, A and B. This limitation underscores the need for a more advanced and specific diagnostic tool. Therefore, the objective of this study is to establish an RT-RPA with a CRISPR/Cas12a-based technique specifically designed to identify RSV-A and RSV-B, a breakthrough that could revolutionize RSV diagnostics.

Materials and methods

Design and selection of primers and crRNA for specific RSV detection

Primers specific to the glycoprotein (G) genes of the human respiratory syncytial virus (RSV) and CRISPR RNA (crRNA) were meticulously designed to target the conserved region, and the sequences were selected from the NCBI database[1]. In designing crRNA, the selected sequences were adjacent to the PAM sequence (TTTV) [13], and the scaffold and T7 promoter sequence were then added to the 5′-end. This careful design process ensures the specificity and accuracy of our diagnostic tool. All primers and crRNAs used are presented in Table 1.

crRNA construction and purification

For crRNA construction, the annealing reaction consisted of 10 μL of a 2.5 μL of 10x ligation buffer, 10 μM of DNA template for crRNA, 10 μL of a 10 μM T7 promoter primer, and 2.5 μL of DEPC. The annealing process was as follows: 95°C for 3 min, 65°C for 3 min, 42°C for 5 min, and 37°C for 45 min. Subsequently, crRNA transcription was executed utilizing the RiboMAX™ Large Scale RNA Production System (Promega, United States), following the manufacturer's prescribed protocol. Post-transcription, the crRNA, consisting of approximately 40 nucleotides, underwent purification employing a miRNA isolation kit (Geneaid, Taiwan) and was subsequently quantified using the Qubit™ microRNA Assay Kit (Thermo Fisher Scientific, United States).

RT-RPA reaction setup and protocol

A commercial reverse transcription recombinase polymerase amplification (RT-RPA) kit (TwistDx, UK) was employed to perform the isothermal amplification of the RSV-A and RSV-B genes. In brief, the RT-RPA reaction was constituted by combining 29.5 μL of rehydration buffer, 2.4 μL of a 10 μM forward primer, 2.4 μL of a 10 μM reverse primer, 1 μL of 200 U/μL Reverse Aid RT (Thermo Fisher Scientific, United States), 4.2 μL of DEPC, and 1 μL of the RNA template. Subsequently, 280 nM of MgOAC was introduced to the cap, and the mixture was vortexed and spun down for 2 min. The mixture was incubated in a mini heating dry bath (Major Science, United States) at 39°C for 30 min, followed by a subsequent heat inactivation step at 75°C for 5 min.

1 https://www.ncbi.nlm.nih.gov/nuccore

TABLE 1 Oligonucleotides used in the study.

Assay	Primer name	Sequence (5′ ⟶ 3′)	Length (bp)	Product size (bp)
RT-RPA	RSVA-G-F282	ATACCTCACCCAGAATCCCCAGCTTGGAAT	30	391
	RSVA-G-R672	GGTTTGAGGTTTGRGATCTTTTTTGGTTGTCTT	33	
	RSVB-G-F39	CACTGCCAGTACTCTAGAAAAGACCTGGGA	30	384
	RSVB-G-R422	CTGCCTTTGGTTTGTGCTGTTGTATGGTGT	30	
crRNA	RSVA-G598	UAAUUUCUACUAAGUGUAGAUCAGGUUUUUUGUUUGGUAUU	41	
	RSVB-G154	UAAUUUCUACUAAGUGUAGAUGCAAUGAUAAUCUCAACCUC	41	

Note: The underline represents the spacer sequence.

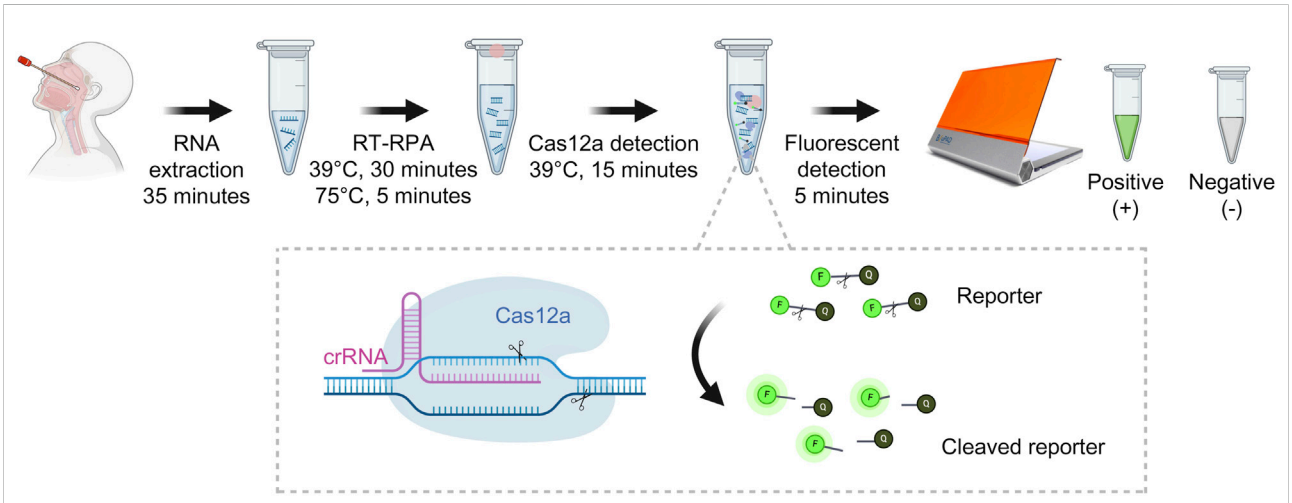

FIGURE 1
Detection of RSV-A and RSV-B based on RT-RPA and CRISPR-Cas12a (This figure was created with Biorender.com).

CRISPR/Cas12a cleavage assay procedure

Next, the CRISPR/Cas12a cleavage assay was conducted within a 15 μL reaction system. The mixture comprised 1.5 μL of 10x NEB buffer 2, 1.5 μL of 300 nM crRNA, 0.5 μL of 1 μM Cas12a (New England Biolabs, United States), 0.5 μL of 6 μM ssDNA probe labeled with FAM and BHQ1, 10 μL of DEPC, and 1 μL of RT-RPA template. Subsequently, the reaction mixtures underwent incubation in a mini heating dry bath (Major Science, United States) at 39°C for 15 min. The fluorescent signal was observed on a BluPAD Dual LED Blue/White Light Transilluminator (Bio-Helix, Taiwan) by the naked eye. The assay was conducted in triplicate, and the findings were based on consensus interpretations derived from three interpreters. The criteria for interpretation by the naked eye include the absence of fluorescence in negative samples, and a clear fluorescence or color change in positive samples. Positive results should be visibly distinguishable from negative controls, with the test sample showing a stronger signal than the background or controls.

Determining the limit of detection for RT-RPA and CRISPR-Cas12a

To determine the limit of detection, standard RNA was generated using RiboMAX™ Large Scale RNA Production System (Promega, United States) according to the manufacturer's protocol. Then, DNase I (Thermo Fisher Scientific, United States) was used to eliminate the DNA templates. Next, the synthesized standard RNA was purified and quantified using a miRNA isolation kit (Geneaid, Taiwan) and Qubit™ microRNA Assay Kit (Thermo Fisher Scientific, United States), respectively. Using a 10-fold serial dilution, synthetic standard RNAs with copy numbers ranging from 10^7 to 10 copies/μL were prepared. The limit of detection was determined by the RT-RPA followed by CRISPR-Cas12a detection. The fluorescent signal was observed on a BluPAD Dual LED Blue/White Light Transilluminator (Bio-Helix, Taiwan) by the naked eye.

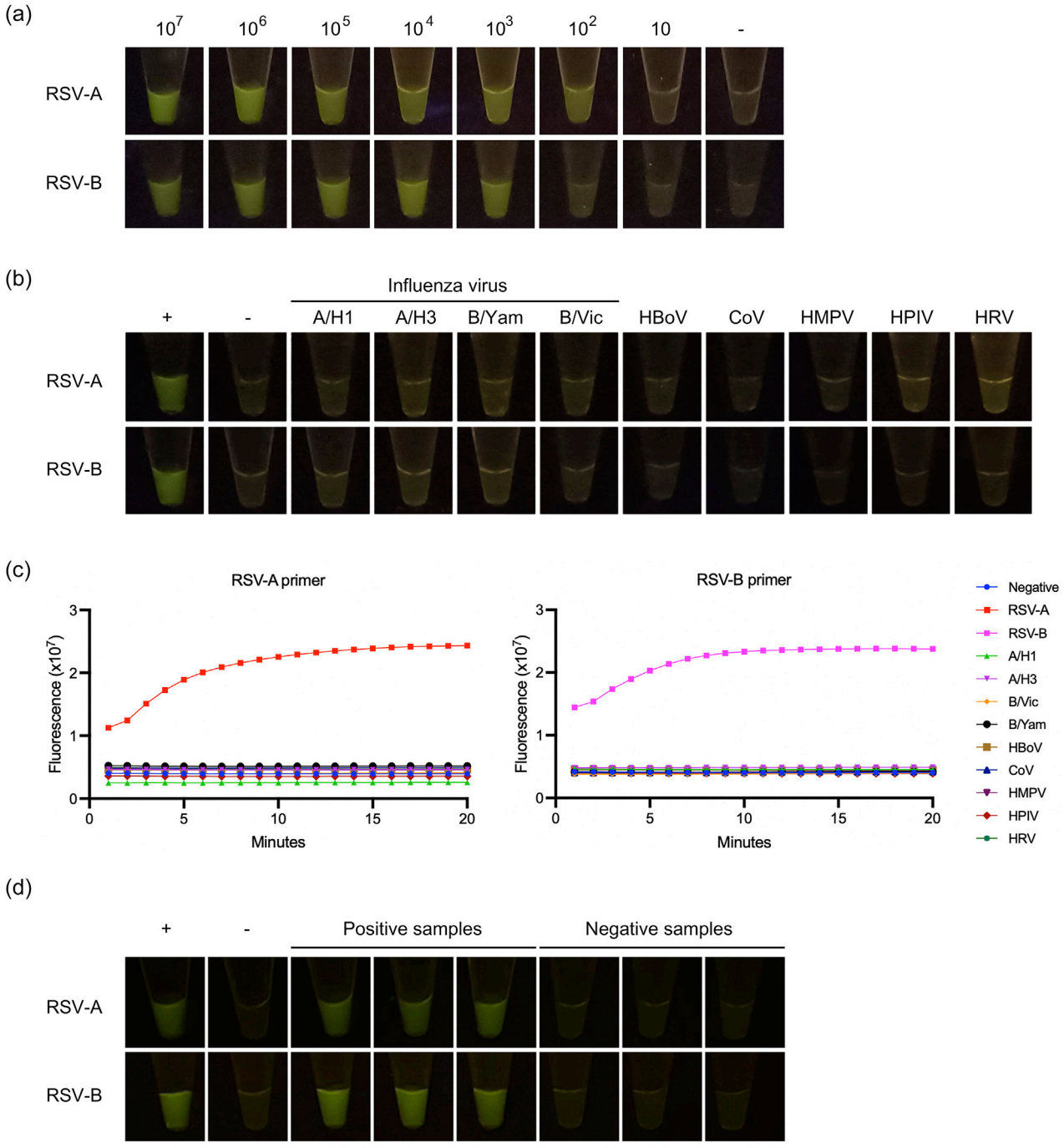

FIGURE 2
Detection of RSV-A and RSV-B based on RT-RPA and CRISPR-Cas12a. **(A)** The limit of detection. **(B)** The cross-reactivity testing against influenza viruses A (A/H1 and A/H3), influenza viruses B (B/Yam and B/Vic), human bocavirus (HBoV), coronavirus (CoV), human metapneumovirus (HMPV), human parainfluenza virus (HPIV), and human rhinovirus (HRV). **(C)** Cross-reactivity testing against other respiratory viruses was performed by qPCR using RT-RPA + CRISPR with RSV-A primers and RT-RPA + CRISPR with RSV-B primers. Dot plots show fluorescence intensity measurements taken from 1 to 15 min. **(D)** The representative of positive and negative detection.

TABLE 2 The performance of RT-RPA and CRISPR-Cas12a based assay.

Parameters	RSV-A	RSV-B
Total samples	93	93
True positive	30	21
True negative	54	66
False positive	0	0
False negative	9	6
Sensitivity	76.92%	77.78%
Specificity	100%	100%
Diagnostic accuracy	90.32%	93.55%

Cross-reactivity testing with various respiratory viruses

Next, cross-reactivity testing was conducted on diverse human respiratory viral samples, including influenza viruses A (A/H1 and A/H3), influenza viruses B (B/Yam and B/Vic), human bocavirus (HBoV), coronavirus (CoV), human metapneumovirus (HMPV), human parainfluenza virus (HPIV), and human rhinovirus (HRV). This assessment was carried out utilizing RT-RPA and CRISPR-Cas12a detection methodologies (n = 10 for each).

Calculation of sensitivity, specificity, and accuracy

The sensitivity, specificity, and accuracy were calculated using the web-based diagnostic test evaluation calculator MedCalc software[2] [16]. This web-based tool was utilized to calculate these metrics, ensuring a comprehensive analysis of the test performance. The formulas for calculating sensitivity, specificity, and accuracy are as follows:

$$\text{Sensitivity} = \frac{\text{True Positives (TP)}}{\text{True Positives (TP)} + \text{False Negatives (FN)}}$$

$$\text{Specificity} = \frac{\text{True Negatives (TN)}}{\text{True Negatives (TN)} + \text{False Positives (FP)}}$$

$$\text{Accuracy} = \frac{\text{True Positives (TP)} + \text{True Negatives (TN)}}{\text{True Positives (TP)} + \text{True Negatives (TN)} + \text{False Positives (FP)} + \text{False Negatives (FN)}}$$

2 https://www.medcalc.org/calc/diagnostic_test.php

RNA sample collection and verification

The RNA samples were obtained from the Center of Excellence in Clinical Virology, Chulalongkorn University. Briefly, nasopharyngeal swab samples (n = 93) were collected from patients with influenza-like illness (ILI). The viral RNA was extracted using a GenUP™ Virus RNA kit (Biotech Rabbit, German). The RSV-positive sample was verified by RT-qPCR as described in the previous study [17] (cut-off at Ct ≤ 38).

Results and discussion

A recently developed approach for pathogen detection incorporating isothermal amplification techniques (such as RPA) coupled with fluorescent detection utilizing the CRISPR-Cas system [10, 18, 19] has been developed and shown to be useful for higher-sensitivity nucleic acid pathogen identification [11, 20]. Our experimental protocol procedure took approximately 90 min, covering the entire process from RNA extraction to fluorescent detection (Figure 1). Meanwhile, the qRT-PCR revealed an approximately 4-h turn-around time and required a specialized molecular laboratory, expensive equipment, and well-trained staff.

A previous study has shown that RSV can be detected using the RPA coupled with the CRISPR-Cas approach at 10^4 copies/mL [21]. As illustrated in the results (Figure 2A), the LOD for RSV-A and RSV-B were estimated to be around 10^2 and 10^3 copies per reaction, respectively. The outcomes demonstrated that the primers and crRNA used in this investigation exhibited notable specificity against RSV-A and RSV-B viruses (Figure 2B). No cross-reactivity was discerned with other respiratory viruses (Figure 2B). Interestingly, our study can discriminate between the RSV-A and RSV-B subtypes (Figure 2C). In addition, RT-RPA with CRISPR-Cas12a assay was performed using RSV-A primers on RSV-B targets, and *vice versa*. The results showed that the primers could not amplify across subtypes (Supplementary Figure S1). The representative detection results were shown in Figure 2D.

In this study, the RSV-positive sample was verified by RT-qPCR. The results showed 39 and 27 RSV-A and RSV-B positive samples, respectively. Prior investigations indicated that RSV-A exhibited specificity and sensitivity values of 73.08% and 90%, respectively, while RSV-B demonstrated specificity and sensitivity figures of 42.86% and 93.33%, respectively [22]. Our study suggests a modest enhancement in the specificity (100%) of RSV-A and RSV-B detection compared to the gold-standard detection outcomes from RT-qPCR, as shown in Table 2. However, the current study demonstrates lower sensitivity, with values of 76.92% and 77.78% for RSV-A RSV-B, respectively (Table 2). In the case of RSV-A, the findings revealed 30 true positives, 0 false positives, 9 false negatives, and 54 true negatives. Conversely, for RSV-B, the results indicated

21 true positives, 0 false positives, 6 false negatives, and 66 true negatives. The undetected positive samples were associated with high Ct (cycle threshold) values, which could indicate a lower viral load in these samples. Furthermore, since multiple freeze-thaw cycles and storage may have caused RNA degradation. Additionally, the diagnostic accuracy for RSV-A and RSV-B was reported as 90.32% and 93.55%, respectively.

However, this research still has some limitations, including the challenges related to nonspecific amplification, variable sensitivity, isothermal conditions, guide RNA specificity, and the subjective nature of the readout. These highlight the importance of ongoing research and optimization for their practical and reliable application in diagnostics.

In conclusion, the benefits of this study include simplicity, quick turnaround time, affordability, and applicability in resource-constrained places. The assays would be helpful and appealing for systematic retesting of individuals and large-scale screening across many communities to isolate patients and prevent the spread of RSV.

Author contributions

AK: Formal Analysis, Methodology, Visualization, Writing – original draft. JN: Methodology, Writing – review and editing. NC: Methodology, Writing – review and editing. PN: Methodology, Writing – review and editing. OM: Methodology, Writing – review and editing. PK: Supervision, Writing – review and editing. SiP: Methodology, Writing – review and editing. YP: Supervision, Writing – review and editing. SuP: Conceptualization, Funding acquisition, Supervision, Writing – review and editing. All authors contributed to the article and approved the submitted version.

Data availability

The original contributions presented in the study are included in the article/Supplementary Material, further inquiries can be directed to the corresponding author.

Ethics statement

The experimental procedures in this investigation were approved by the Institutional Review Board, Faculty of Medicine, Chulalongkorn University (IRB No. 0352/67).

Funding

The author(s) declare that financial support was received for the research and/or publication of this article. This work was supported by the Research Grants for Talented Mid-Career Researchers, The National Research Council of Thailand (NRCT) (N41A640077); the Thailand Science Research and Innovation Fund, Chulalongkorn University (HEAF67300057); Ratchadapisek Somphot Fund, Faculty of Medicine, Chulalongkorn University (MDCU RA-MF-21/67); and Ratchadapisek Somphot Fund for Postdoctoral Fellowship, Chulalongkorn University.

Acknowledgments

We would like to thank the Center of Excellence in Clinical Virology, Faculty of Medicine, Chulalongkorn University, for kindly providing the samples.

Conflict of interest

The author(s) declared no potential conflicts of interest with respect to the research, authorship, and/or publication of this article.

Supplementary material

The Supplementary Material for this article can be found online at: https://www.ebm-journal.org/articles/10.3389/ebm.2025.10387/full#supplementary-material

References

1. Mufson MA, Orvell C, Rafnar B, Norrby E. Two distinct subtypes of human respiratory syncytial virus. *J Gen Virol* (1985) **66**(Pt 10):2111–24. doi:10.1099/0022-1317-66-10-2111

2. Collins PL, Fearns R, Graham BS. Respiratory syncytial virus: virology, reverse genetics, and pathogenesis of disease. *Curr Top Microbiol Immunol* (2013) **372**: 3–38. doi:10.1007/978-3-642-38919-1_1

3. Jorquera PA, Anderson L, Tripp RA. Human respiratory syncytial virus: an introduction. *Methods Mol Biol* (2016) **1442**:1–12. doi:10.1007/978-1-4939-3687-8_1

4. Krause CI. The ABCs of RSV. *The Nurse Pract* (2018) **43**:20–6. doi:10.1097/01.npr.0000544277.74514.55

5. Barr R, Green CA, Sande CJ, Drysdale SB. Respiratory syncytial virus: diagnosis, prevention and management. *Ther Adv Infect Dis* (2019) **6**: 2049936119865798. doi:10.1177/2049936119865798

6. Piedimonte G, Perez MK. Respiratory syncytial virus infection and bronchiolitis. *Pediatr In Rev* (2014) **35**:519–30. doi:10.1542/pir.35.12.519

7. Teirlinck AC, Broberg EK, Stuwitz Berg A, Campbell H, Reeves RM, Carnahan A, et al. Recommendations for respiratory syncytial virus surveillance at the national level. *Eur Respir J* (2021) **58**:2003766. doi:10.1183/13993003.03766-2020

8. Todd AK, Costa AM, Waller G, Daley AJ, Barr IG, Deng YM. Rapid detection of human respiratory syncytial virus A and B by duplex real-time RT-PCR. *J Virol Methods* (2021) **294**:114171. doi:10.1016/j.jviromet.2021.114171

9. Puig-Serra P, Casado-Rosas MC, Martinez-Lage M, Olalla-Sastre B, Alonso-Yanez A, Torres-Ruiz R, et al. CRISPR approaches for the diagnosis of human diseases. *Int J Mol Sci* (2022) **23**:1757. doi:10.3390/ijms23031757

10. Mayuramart O, Nimsamer P, Rattanaburi S, Chantaravisoot N, Khongnomnan K, Chansaenroj J, et al. Detection of severe acute respiratory syndrome coronavirus 2 and influenza viruses based on CRISPR-Cas12a. *Exp Biol Med (Maywood)* (2021) **246**:400–5. doi:10.1177/1535370220963793

11. Nimsamer P, Mayuramart O, Rattanaburi S, Chantaravisoot N, Saengchoowong S, Puenpa J, et al. Comparative performance of CRISPR-Cas12a assays for SARS-CoV-2 detection tested with RNA extracted from clinical specimens. *J Virol Methods* (2021) **290**:114092. doi:10.1016/j.jviromet.2021.114092

12. Wang B, Wang R, Wang D, Wu J, Li J, Wang J, et al. Cas12aVDet: a CRISPR/cas12a-based platform for rapid and visual nucleic acid detection. *Anal Chem* (2019) **91**:12156–61. doi:10.1021/acs.analchem.9b01526

13. Paul B, Montoya G. CRISPR-Cas12a: functional overview and applications. *Biomed J* (2020) **43**:8–17. doi:10.1016/j.bj.2019.10.005

14. Dronina J, Samukaite-Bubniene U, Ramanavicius A. Towards application of CRISPR-Cas12a in the design of modern viral DNA detection tools (Review). *J Nanobiotechnology* (2022) **20**:41. doi:10.1186/s12951-022-01246-7

15. Wang Y, Yang T, Liu G, Xie L, Guo J, Xiong W. Application of CRISPR/Cas12a in the rapid detection of pathogens. *Clinica Chim Acta* (2023) **548**:117520. doi:10.1016/j.cca.2023.117520

16. Schoonjans F, Zalata A, Depuydt CE, Comhaire FH. MedCalc: a new computer program for medical statistics. *Computer Methods Programs Biomed* (1995) **48**:257–62. doi:10.1016/0169-2607(95)01703-8

17. Thongpan I, Suntronwong N, Vichaiwattana P, Wanlapakorn N, Vongpunsawad S, Poovorawan Y. Respiratory syncytial virus, human metapneumovirus, and influenza virus infection in Bangkok, 2016-2017. *PeerJ* (2019) **7**:e6748. doi:10.7717/peerj.6748

18. Mao X, Xu M, Luo S, Yang Y, Zhong J, Zhou J, et al. Advancements in the synergy of isothermal amplification and CRISPR-cas technologies for pathogen detection. *Front Bioeng Biotechnol* (2023) **11**:1273988. doi:10.3389/fbioe.2023.1273988

19. Li X, Zhu S, Zhang X, Ren Y, He J, Zhou J, et al. Advances in the application of recombinase-aided amplification combined with CRISPR-Cas technology in quick detection of pathogenic microbes. *Front Bioeng Biotechnol* (2023) **11**:1215466. doi:10.3389/fbioe.2023.1215466

20. Chen JS, Ma E, Harrington LB, Da Costa M, Tian X, Palefsky JM, et al. CRISPR-Cas12a target binding unleashes indiscriminate single-stranded DNase activity. *Science* (2018) **360**:436–9. doi:10.1126/science.aar6245

21. Hongdan G, Yao D, Qiang C, Meng H, Xiaorong L, Zhihao X, et al. A multiplex recombinase polymerase amplification assay combined with CRISPR/Cas12a for the detection of respiratory syncytial virus and respiratory adenovirus. *J Int Med Res* (2024) **52**:3000605231223083. doi:10.1177/03000605231223083

22. Gong L, Wang X, Li Z, Huang G, Zhang W, Nie J, et al. Integrated trinity test with RPA-CRISPR/cas12a-fluorescence for real-time detection of respiratory syncytial virus A or B. *Front Microbiol* (2022) **13**:819931. doi:10.3389/fmicb.2022.819931

EBM Experimental Biology and Medicine

TYPE Original Research
PUBLISHED 01 May 2025
DOI 10.3389/ebm.2025.10493

OPEN ACCESS

*CORRESPONDENCE
Xingjian Niu,
niuxingjian@hrbmu.edu.cn

†These authors have contributed equally to this work

RECEIVED 16 January 2025
ACCEPTED 14 April 2025
PUBLISHED 01 May 2025

CITATION
Hu Y, Li J, Wang M, Wang X, Li J, Ji H and Niu X (2025) Pan-immune-inflammation value predicts survival in inflammatory breast cancer patients. *Exp. Biol. Med.* 250:10493. doi: 10.3389/ebm.2025.10493

Pan-immune-inflammation value predicts survival in inflammatory breast cancer patients

Yingjia Hu[1‡], Jian Li[1‡], Mingyu Wang[2‡], Xinyi Wang[3], Jiankang Li[4,5], Hongfei Ji[4,5] and Xingjian Niu[1*]

[1]Department of Medical Oncology, Harbin Medical University Cancer Hospital, Harbin Medical University, Harbin, Heilongjiang, China, [2]Department of General Surgery, The Second Affiliated Hospital of Harbin Medical University, Harbin Medical University, Harbin, Heilongjiang, China, [3]Department of Endocrinology, Health Management Center, Tianjin Union Medical Center, Nankai University, Tianjin, China, [4]Institute of Cancer Prevention and Treatment, Harbin Medical University, Harbin, Heilongjiang, China, [5]Department of Biochemistry and Molecular Biology, Heilongjiang Academy of Medical Sciences, Harbin, Heilongjiang, China

Abstract

Inflammatory breast cancer (IBC) is a rare and aggressive breast cancer subtype with poor survival. Identifying novel biomarkers is needed to predict survival for this highly progressive form of breast cancer. In this retrospective study, we investigated pan-immune-inflammation value (PIV), a novel immune-inflammation-based biomarker which combined the peripheral blood parameters (lymphocytes, monocytes, neutrophils, and platelets) in a retrospective cohort of 143 IBC patients. Then we explored the difference of PIV levels in IBC and non-IBC cohorts and the relationship between PIV and clinical characteristics in IBC patients. The survival rates of disease-free survival (DFS) and overall survival (OS) in IBC patients were analyzed and univariate and multivariate statistics were used to evaluate the prognostic value. PIV had the most significantly predictive value in IBC patients compared with other peripheral blood parameters. The mean PIV value in IBC patients was significantly higher than non-IBC patients, and the significant difference between the IBC and non-IBC was also observed in subgroups with different clinical stages and pathologic types. Furthermore, PIV performed an extensive systemic immune prognostic factor on both DFS and OS in IBC patients, and PIV was identified an independent prognostic indicator for survival outcome in IBC patients in univariate and multivariate models. Our retrospective study demonstrated the prognostic value of PIV in IBC patients, suggesting the potential application of PIV in IBC treatment outcomes. PIV would also provide some insights into the mechanisms underlying the role of immune and inflammation in IBC development and progression.

KEYWORDS

inflammatory breast cancer, pan-immune-inflammation value, prognosis, biomarker, immune

Impact Statement

In this work, we identified pan-immune-inflammation value (PIV), a novel immune-inflammation-based biomarker, showed a significantly predictive value in IBC patients, and it's the first time to retrospectively evaluate the predictive value of PIV in IBC patients. We found that PIV had the most significantly predictive value in IBC patients compared with other peripheral blood parameters, and PIV was considered as a favorable independent prognostic indicator in IBC patients. Furthermore, the mean PIV value in IBC patients was significantly higher than non-IBC patients, which might provide some insights into the mechanisms underlying the role of immune and inflammation in IBC development and progression compared with non-IBC. Our retrospective study demonstrated the prognostic value of PIV in IBC patients, suggesting the potential application of PIV in IBC treatment outcomes.

Introduction

Inflammatory breast cancer (IBC) is a rapidly advancing and highly aggressive form of breast cancer [1, 2]. Despite being a relatively rare subtype, IBC accounts for approximately 10% of all breast cancer related deaths [3]. Since no IBC-specific target and treatment strategy have been identified, IBC is mainly treated with the anthracycline/taxane-based chemotherapy with or without anti-HER2 therapy similar to non-IBC [4]. However, patients suffered with IBC usually have shorter survival time and worse prognosis compared with non-IBC cases [5], and there is still controversy about the prognostic evaluation of IBC. Therefore, it is essential to identify novel biomarkers to predict survival, which will contribute to make accurate treatment plans to benefit IBC patients.

Characterized by involvement of skin, the clinicopathological features of IBC are due to the lymphatic obstruction caused by widespread of tumor emboli [6]. There is evidence supporting that the contact between cancer cells and tumor microenvironment (TME) is required for the unique emboli form of IBC [6, 7]. Recent studies have revealed the contributions of the TME to the progressive and invasive behavior of IBC, such as immune evasion and chemotherapy resistance [6, 8, 9]. Among the components in TME, tumor associated macrophages are considered the main immune inflammatory cells of the TME in IBC, which usually polarize to alternatively activated M2 macrophages and act as immunosuppressive cells to induce tumor metastasis [8, 10, 11]. Besides, tumor-infiltrated lymphocytes (TILs) also participate in the controlling and transforming of TME in IBC and play a significant role in initiation and progression of tumor [7]. These individual cells within the TME collectively lead to a unique immune microenvironment of IBC, which provides a novel perspective on investigating the immune features of IBC and evaluating the IBC-associated immune inflammatory markers for forecasting the prognosis and adopting suitable therapeutic strategies.

Over past few years, a number of immune inflammatory biomarkers such as neutrophil to lymphocyte ratio (NLR), platelet to lymphocyte ratio (PLR), and monocyte to lymphocyte ratio (MLR), are based on blood parameters and easy to evaluate, which have been widely studied and showed their values in predicting the prognosis of breast cancer [12–14]. Given the complexity of the TME in IBC, the pan-immune-inflammation value (PIV) may provide additional information [14]. PIV is a kind of novel score index that combines the counts of these immune inflammatory cells involved may provide more relevant information [15–21]. It was initially used as a tool to predict survival of advanced colorectal cancer [16], and has been gradually discovered its potential value in many other cancer subtypes, especially in breast cancer [15, 17, 18, 22]. However, there is currently no available PIV data could assess the treatment efficacy of IBC. In this article, we conducted a single-center, retrospective assessment, aiming at illustrating prognostic significance of PIV in IBC patients and providing a novel immune biomarker for IBC patients.

Materials and methods

Patient population

Patients clinically diagnosed with IBC in the Harbin Medical University Cancer Hospital during January 2010 to December 2023 were enrolled into this current retrospective, single-center investigation. All cases (n = 143) were clinically defined according to international consensus criteria that the patient exhibited typical clinical features of IBC and fulfilled the pathological T4d diagnosis [1]. The clinic-pathological data of patients, including age, TNM stage, histopathological information (receptor subtype, pathological type, grade, Ki67 and P53 status), body mass index [BMI, as weight (kg) divided by the square of height (m^2)] [23] and follow-up details, were collected in accordance with the ethical principles outlined in the Helsinki Declaration regarding research involving human subjects. Neoadjuvant chemotherapy was administered in stage III IBC patients, which was anthracycline-based, incorporating taxanes. Anti-HER2 targeted therapy was combined with the chemotherapy in the cases with HER2-positive status. Subsequently, patients who underwent mastectomy and axillary lymph node dissection were subjected to chemotherapy, endocrine therapy and radiotherapy. However, for stage IV IBC patients, salvage therapies including chemotherapy, anti-HER2 targeted therapy and endocrine therapy were applied according to the molecular subtypes. To evaluate

TABLE 1 Baseline clinico-pathological parameters of patients in IBC cohorts and non-IBC control cohorts.

Characteristics	Total (n = 311)	IBC (n = 143)	Non-IBC (n = 168)
Age, y			
Median	53.0	54.5	51.5
Range	27–85	28–85	27–82
Stage			
I-IIIa	72 (23.2%)	0 (0.0%)	72 (42.9%)
IIIb	124 (39.9%)	99 (69.2%)	25 (14.9%)
IIIc	58 (18.6%)	23 (16.1%)	35 (20.8%)
IV	75 (24.1%)	21 (14.7%)	36 (21.4%)
Receptor subtype			
$HR^+/HER2^-$	123 (39.5%)	57 (39.9%)	66 (39.3%)
$HER2^+$	119 (38.3%)	55 (38.5%)	64 (38.1%)
TNBC	69 (22.2%)	31 (21.7%)	38 (22.6%)
Pathological type			
Ductal	263 (84.6%)	123 (86.0%)	140 (83.3%)
Lobular	25 (8.0%)	9 (6.3%)	16 (9.5%)
Mixed/other	23 (7.4%)	11 (7.7%)	12 (7.1%)
Grade			
1	9 (2.9%)	2 (1.4%)	7 (4.2%)
2	177 (56.9%)	80 (55.9%)	97 (57.7%)
3	125 (40.2%)	61 (42.7%)	64 (38.1%)
Ki67 status			
Median	33.0%	31.0%	34.0%
Range	0–80%	0–80%	0–80%
P53 status			
Positive	134 (43.1%)	62 (43.4%)	72 (42.9%)
Negative	177 (56.9%)	81 (56.6%)	96 (57.1%)
Body mass index (BMI)			
<25	45 (14.5%)	17 (11.9%)	28 (16.7%)
25- <30	128 (41.2%)	54 (37.8%)	74 (44.0%)
30- <35	91 (29.3%)	41 (28.7%)	50 (29.8%)
≥35	47 (15.1%)	31 (21.7%)	16 (9.5%)

P-values were shown in bold values if they had statistical significance.

whether the peripheral blood parameters were correlated with the phenotype or with advanced stage in IBC, 168 non-IBC patients were also collected between January 2010 and December 2023 at Harbin Medical University Cancer Hospital. This non-IBC group was randomly sampled to match the IBC cases in the same period and the molecular subtypes when diagnosed. Patients who underwent immunomodulatory treatment or had hematological disease and a history of malignancies were excluded. This study

TABLE 2 Predictive values of PIV, MLR, PLR and NLR on IBC survival.

Parameters	AUC	95% CI	Cut-off	Sensitivity (%)	Specificity (%)	*P*-value
PIV	0.725	0.631–0.818	284.66	69.2	71.2	**<0.001**
MLR	0.583	0.476–0.690	0.25	53.8	59.6	0.127
PLR	0.634	0.535–0.732	162.14	59.0	68.3	**0.014**
NLR	0.622	0.518–0.727	2.50	59.0	65.4	**0.025**

Abbreviations: AUC, the area under the curve; CI, confidence interval; PIV, pan-immune-inflammation-value; MLR, monocyte-to-lymphocyte ratio; PLR, platelet-to-lymphocyte ratio; NLR, neutrophil-to-lymphocyte ratio.
P-values were shown in bold values if they had statistical significance.

was approved by the Ethics Committee of Harbin Medical University Cancer Hospital, and all patients had written informed consent.

Blood count collection

The pre-treatment peripheral blood data of neutrophil count, lymphocyte count, monocyte count and platelet count were obtained 1 week before any treatment. The absolute counts of neutrophils, lymphocytes, monocytes, and platelets were used to investigate NLR, MLR, and PLR. The PIV was calculated as neutrophil count × platelet count × monocyte count/ lymphocyte count [14].

Follow-up

Patients were regularly followed up using a system that combined telephone communication and the follow-up department. The recorded information included patients' health status, disease progression and date of mortality. DFS (disease-free survival) was calculated as the period (in months) from disease diagnosis until disease recurrence or death. OS (overall survival) was calculated as the time (in months) from disease diagnosis to the date of death due to any cause. The last follow-up date was considered as the survival study endpoint for all patients.

Statistical analysis

ROC curve analysis was performed to determine the cut-off values for PIV, NLR, MLR, and PLR, taking disease recurrence or death as the endpoint of interest. Correlations between high or low PIV groups and clinicopathological features were analyzed using the $\chi 2$ or the Fisher's exact test when appropriate. Two-tailed, unpaired Student's t tests and one way ANOVA were used to analyze the statistical significance of PIV with clinical parameters between IBC and non-IBC patients. Kaplan-Meier curves were used to visualize survival probabilities over time, the log-rank test was employed to compare survival curves between groups based on the indicator. The Cox regression analyses were conducted to evaluate the influence of clinic-pathological parameters on clinical survival outcomes. All statistical analyses were performed using SPSS 20.0 statistics software (IBM, USA). Statistical significance was defined as $p < 0.05$ (two-tailed).

Results

Study population

A total of 143 IBC and matched-pair 168 non-IBC patients were enrolled in our study and the clinical-pathological features were described in Table 1. The median age of the IBC patients was 54.5 years (ranging from 28 to 85 years), higher than non-IBC patients with a median age of 51.5 years (ranging from 28 to 85 years). IBC patients were classified into IIIb (69.2%), IIIc (16.1%) and IV (14.7%) stage due to the T4d diagnosis according to the TNM-UICC [24], however in non-IBC patients, 72 patients (42.9%) were in I-IIIa stage. Compared with non-IBC patients, more IBC patients had BMI ≥35 (21.7% vs. 9.5%). The percentage of the molecular subtypes, pathological type, tumor grade and P53 status were similar in IBC and non-IBC cases.

Prognostic values of blood-based biomarkers in IBC

To investigate the predictive value of immune biomarkers in IBC, ROC curve analysis was conducted and the area under curves (AUC) and cut-off values of PIV and other related biomarkers (MLR, PLR, and NLR) were shown in Figure 1; Table 2. Compared with other markers, PIV showed a better prognostic significance of IBC (AUC = 0.725, $P < 0.001$). Although PLR (AUC = 0.634, $P = 0.014$) and NLR (AUC = 0.622, $P = 0.025$) also had predictive values in IBC, the sensitivity and specificity of them were lower than PIV. Therefore, we considered PIV as the most significantly predictive value in IBC patients, and the cut-off value for the PIV was determined as 284.66.

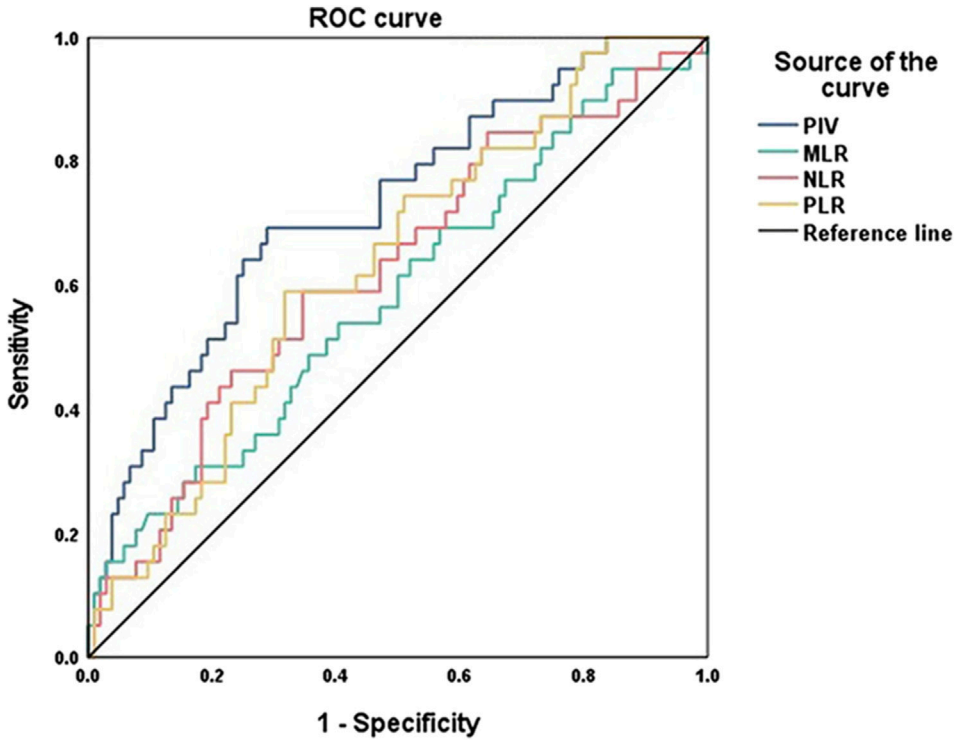

FIGURE 1
ROC curve analysis of PIV, MLR, PLR and NLR values in IBC patients.

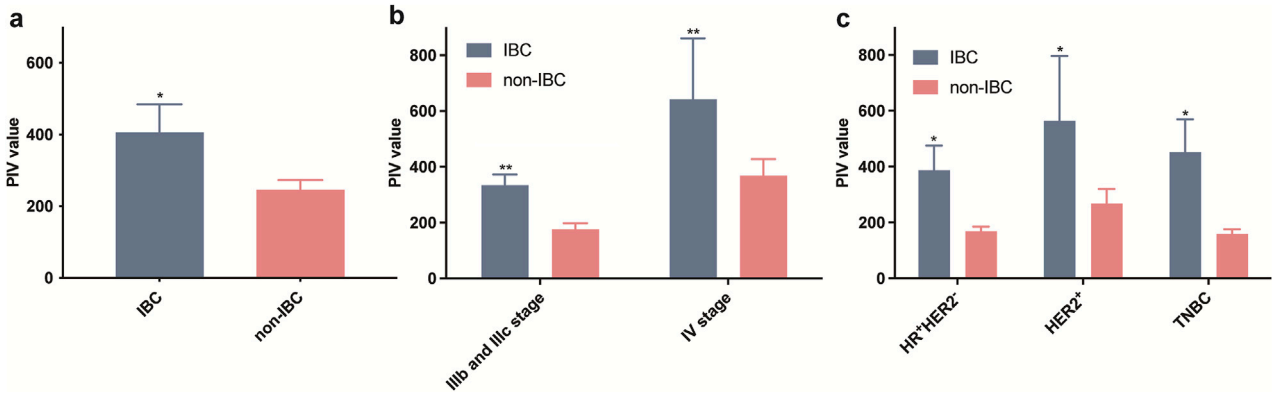

FIGURE 2
Comparison of PIV values in all IBC and non-IBC patients **(a)** as well as in different stages **(b)** and receptor subtypes **(c)** among IBC and non-IBC patients.

PIV distinguished IBC from non-IBC cohorts

Since PIV was a comprehensive immune-associated biomarker, we explored whether IBC had different PIV levels compared to non-IBC cohorts. Overall, the mean PIV values of IBC were significantly higher than that in non-IBC patients (Figure 2A). Furthermore, patients were categorized by different clinical stages or receptor subtypes. The results showed that stage IV tumors had higher PIV values in both IBC and non-IBC groups, and the mean PIV values in IBC were also higher than non-IBC patients whether their tumors were stage IIIb, IIIc and IV (Figure 2B). According to receptor subtypes, the patients were classified into HR (hormone

TABLE 3 PIV distribution according to clinico-pathological characteristics in IBC.

Characteristics	Total (n = 143)	PIV < 284.66 (n = 85)	PIV ≥ 284.66 (n = 58)	*P*-value
Age, y				
≤50	51 (35.7%)	29 (34.1%)	22 (37.9%)	0.640
>50	92 (64.3%)	56 (65.9%)	36 (62.1%)	
Stage				
IIIb	99 (69.2%)	60 (70.6%)	39 (67.2%)	**0.040**
IIIc	23 (16.1%)	9 (10.6%)	14 (24.1%)	
IV	21 (14.7%)	16 (18.8%)	5 (8.6%)	
Receptor subtype				
$HR^+/HER2^-$	57 (39.9%)	35 (41.2%)	22 (37.9%)	0.839
$HER2^+$	55 (38.5%)	31 (36.5%)	24 (41.4%)	
TNBC	31 (21.7%)	19 (22.4%)	12 (20.7%)	
Pathological type				
Ductal	123 (86.0%)	75 (88.2%)	48 (82.8%)	**0.047**
Lobular	9 (6.3%)	2 (2.4%)	7 (12.1%)	
Mixed/other	11 (7.7%)	8 (9.4%)	3 (5.2%)	
Grade				
1	2 (1.4%)	2 (2.4%)	0 (0.0%)	0.476
2	80 (55.9%)	48 (56.5%)	32 (55.2%)	
3	61 (42.7%)	35 (41.2%)	26 (44.8%)	
Ki67 status				
<20%	49 (34.3%)	30 (35.3%)	19 (32.8%)	0.754
≥20%	94 (65.7%)	55 (64.7%)	39 (67.2%)	
P53 status				
Positive	62 (43.4%)	35 (41.2%)	27 (46.6%)	0.524
Negative	81(56.6%)	50 (58.8%)	31 (53.4%)	
Body mass index (BMI)				
<25	17 (11.9%)	12 (14.1%)	5 (8.6%)	0.282
25- <30	54 (37.8%)	34 (40.0%)	20 (34.5%)	
30- <35	41 (28.7%)	25 (29.4%)	16 (27.6%)	
≥35	31 (21.7%)	14 (16.5%)	17 (29.3%)	

P-values were shown in bold values if they had statistical significance.

receptor)$^+$HER2$^-$, $HER2^+$ and TNBC (triple negative breast cancer) subtypes, and we found that PIV was significantly elevated in IBC cases in all pathological types (Figure 2C). These results indicated that the PIV in IBC patients was a characteristic biomarker, which could distinguish IBC from non-IBC cohorts.

IBC patient characteristics according to PIV value

To further investigate the role of PIV in IBC, the IBC patients were classified into high or low PIV groups according to the calculated PIV cut-off value of 284.66. A

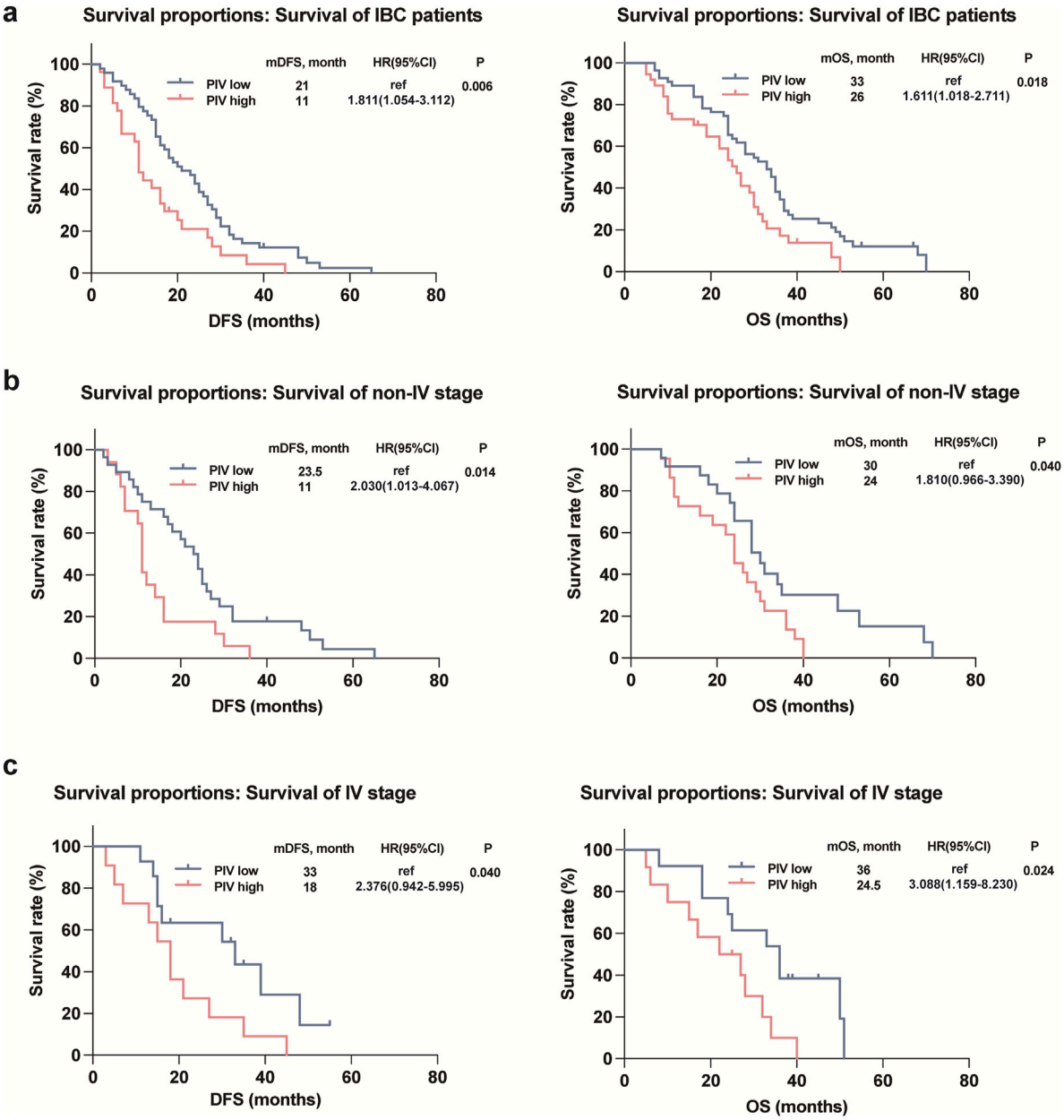

FIGURE 3
Kaplan-Meier curves for DFS and OS in the IBC patients **(a)** as well as the IBC patients with different stages **(b, c)** according to PIV.

comprehensive overview of clinical-pathological features according to PIV are summarized in Table 3. In our study population, 58 (40.6%) patients presented a high PIV, which displayed a higher incidence of lobular pathological type (P = 0.047) and advanced tumor stage (P = 0.040), suggesting a more aggressive metastasis profile in high PIV group. However, there were no significant differences in age, receptor subtype, grade, ki-67 status, p53 status, and BMI.

Survival outcomes according to PIV value in IBC patients

Kaplan-Meier plots illustrated the relationship of PIV value with DFS and OS of IBC patients, and the results showed that the survival outcomes of IBC patients in the high PIV group were markedly worse than that in the low PIV group in both DFS and OS rates (Figure 3A). Furthermore, to better comprehend the impact of PIV on the prognosis of IBC patients in clinical stages and pathological

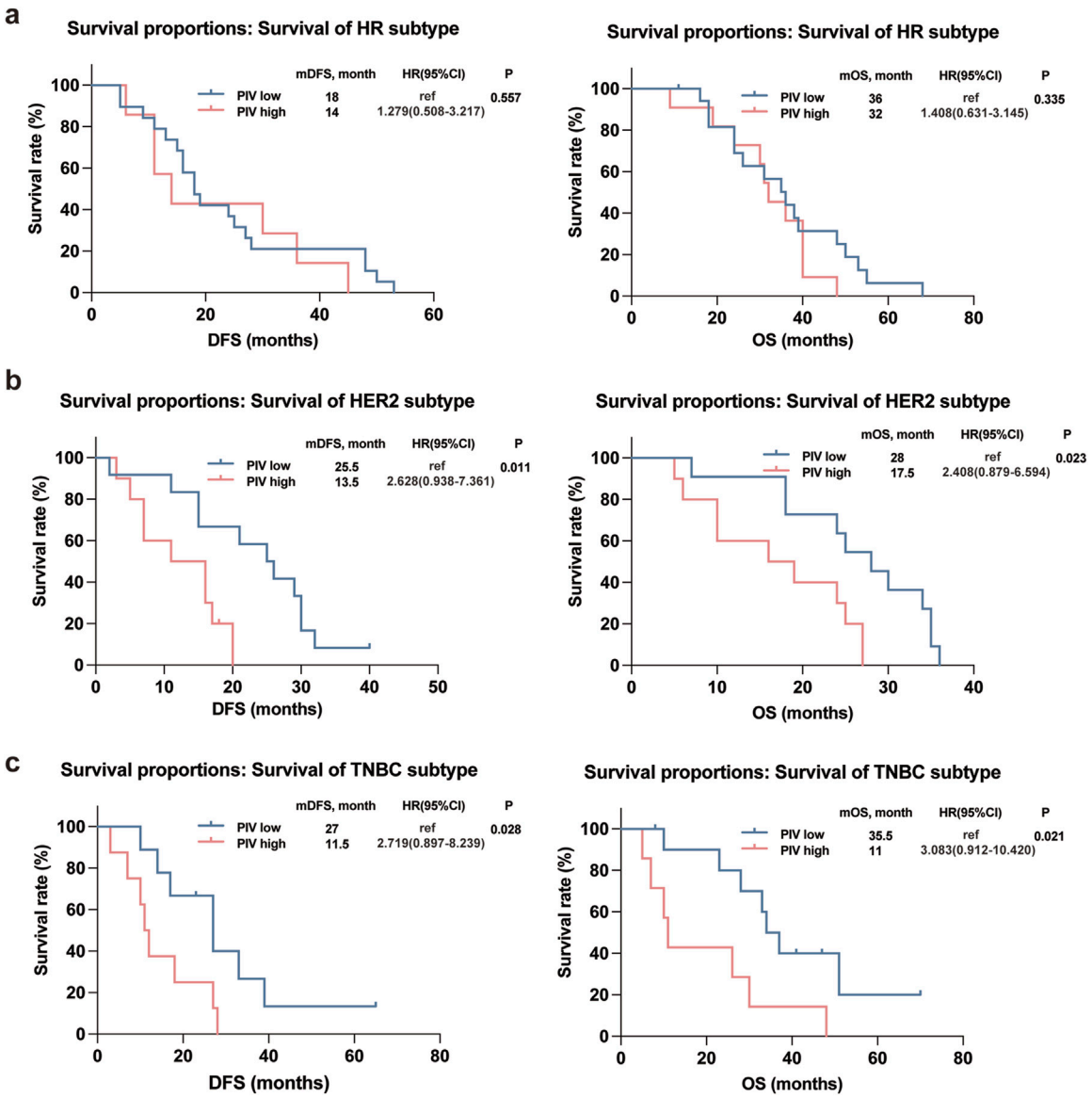

FIGURE 4
Kaplan-Meier curves for DFS and OS in the IBC patients with different subtypes according to PIV: HR subtype **(a)**; HER2 subtype **(b)**; TNBC subtype **(c)**.

types under various conditions, we conducted subgroup analyses and observed that similar results were observed in different clinical stages (non-IV and IV stage) of IBC patients (Figures 3B,C). However, in terms of different pathological subtypes, no significant difference in DFS or OS rates was observed in $HR^{+}HER2^{-}$ IBC patients based on high or low PIV values (Figure 4A), but $HER2^{+}$ and TNBC IBC patients in high PIV group had statistically significantly worse survival rates (Figures 4B,C). As a result of univariate and multivariate analyses, PIV all appeared as an independent predictor in DFS and OS outcomes (Table 4). Besides, in multivariate analysis comprising the variables, MLR caused a statistically significant difference in DFS and OS survival outcomes, and P53 made a difference in DFS survival (Table 4). These results indicated that PIV was an independent value to predict survival in IBC patients.

Discussion

In this study, we investigated PIV, a novel immune-inflammation-based biomarker which contained the majority of immune inflammatory cell components in peripheral blood (lymphocytes, monocytes, neutrophils, and platelets), in a retrospective cohort of 143 IBC patients. First, we demonstrated that PIV had the most

TABLE 4 Univariate and Multivariate analysis of prognostic factors for survival in IBC patients.

Covariate	DFS				OS			
	Univariable		Multivariable		Univariable		Multivariable	
	HR (95%CI)	P-value	HR (95%CI)	P-value	HR (95%CI)	P-value	HR (95%CI)	*P*-value
Age, y (≤50 vs. >50)	0.971 (0.601–1.569)	0.905	0.989 (0.575–1.701)	0.969	0.972 (0.612–1.545)	0.906	1.118 (0.665–1.877)	0.674
Stage (IIIb and IIIc vs. IV)	0.883 (0.660–1.182)	0.404	0.795 (0.584–1.081)	0.143	0.931 (0.709–1.222)	0.607	0.876 (0.661–1.162)	0.359
Receptor subtype ($HR^+/HER2^-$ vs. $HER2^+$ vs. TNBC)	1.052 (0.796–1.391)	0.722	1.060 (0.754–1.490)	0.736	1.115 (0.850–1.462)	0.433	1.268 (0.918–1.751)	0.149
Pathological type (ductal vs. lobular vs. mixed/other)	1.059 (0.689–1.626)	0.795	0.848 (0.503–1.432)	0.538	1.073 (0.746–1.543)	0.705	0.946 (0.620–1.444)	0.797
Grade (1 vs. 2 vs. 3)	1.062 (0.847–1.332)	0.603	1.118 (0.863–1.447)	0.398	1.054 (0.845–1.314)	0.641	1.166 (0.911–1.491)	0.222
Ki67 status (<20% vs. ≥20%)	1.139 (0.710–1.827)	0.588	1.056 (0.606–1.840)	0.848	1.057 (0.674–1.654)	0.809	0.828 (0.490–1.397)	0.479
P53 status (positive vs. negative)	1.512 (0.948–2.412)	0.082	1.965 (1.113–3.467)	**0.020**	1.142 (0.734–1.778)	0.556	1.227 (0.734–2.050)	0.435
BMI (<25 and 25- <30 vs. 30- <35 and ≥35	1.037 (0.647–1.663)	0.880	1.233 (0.698–2.177)	0.470	1.312 (0.833–2.066)	0.241	1.382 (0.837–2.281)	0.206
PIV (<284.66 vs. ≥284.66)	1.637 (1.032–2.596)	0.036	1.928 (1.098–3.387)	**0.022**	1.580 (1.017–2.455)	0.042	1.991 (1.182–3.353)	**0.010**
MLR (<0.25 vs. ≥0.25)	0.781 (0.494–1.236)	0.292	0.401 (0.211–0.762)	**0.005**	0.817 (0.525–1.273)	0.372	0.405 (0.219–0.748)	**0.004**
NLR (<162.14 vs. ≥162.14)	1.161 (0.738–1.827)	0.519	1.050 (0.504–2.187)	0.897	1.298 (0.833–2.023)	0.249	1.640 (0.885–3.037)	0.116
PLR (<2.50 vs. ≥2.50)	1.185 (0.747–1.882)	0.471	1.514 (0.772–2.967)	0.227	1.183 (0.755–1.853)	0.464	1.400 (0.770–2.547)	0.270

significantly predictive value in IBC patients. The mean PIV value in IBC patients was significantly higher compared to non-IBC patients, and the significant difference between the IBC and non-IBC was also observed in subgroups with different pathologic types and different clinical stages. Our results were in line with the well-documented perception that there was a distinct immune features and characteristic inflammation markers for IBC. Furthermore, PIV performed an extensive and favorable systemic immune prognostic factor on both DFS and OS in IBC patients, and PIV was identified an independent prognostic indicator for survival outcome in IBC patients with univariate and multivariate analyses. To our knowledge, these are novel results to estimate the prognostic value of PIV in IBC cohort.

Peripheral immune components or system is the fundamental for the orchestration and maintenance of the tumor-perturbed immune system, and also provide effective biomarkers for the diagnosis and prognosis of cancer and response to therapy [14, 25, 26]. There are studies that focusing on the immune profile of IBC, and the heterogeneous immune landscape of IBC was pointed out, which has improved our understanding of the immune characteristics of IBC [27]. In our study, PIV value in IBC patients was significantly higher compared with non-IBC patients, not only observed in different pathologic types, but also in different clinical stages, suggesting a potential distinct immune feature in IBC, that specific immune cell types of IBC may play a role in the progression and response of therapy.

Previous studies have usually used single immune component counting or the ratio of two to reflect peripheral immune system status in the prognostic modelling of IBC [12]. Lymphocytes are pivotal and multifaceted components in the anti-tumor immune response [28]. Recent research has shown that heterogeneous immune profiles in patients with IBC could impact on cancer immunity and be associated with clinical response [27]. It has been previously described that the most remarkable feature of peripheral blood in IBC was extreme lymphopenia that was highly correlated with the IBC disease itself rather than with treatment, and showed significant reduction in most subpopulations of lymphocytes [7]. As equivalently matched opponents with lymphocytes, circulating monocytes are another essential phenotype of myeloid immune cells, which are trafficked to the TME, divided into different subpopulations, and eventually

contribute to local immunosuppression [29]. Previous studies have found that monocytes counting in the IBC peripheral blood was more than in non-IBC patients [11].

In contrast to the predominant contributions of the above-mentioned types, there are a couple of other components in peripheral blood, such as neutrophils and platelets [30, 31]. Neutrophils and platelets are thought to be frequently replenished from common myeloid progenitor (CMP) shared with monocytes [14]. Despite being great enrichment in peripheral immune system and accumulating in a wide range of cancer, neutrophils and platelets have been implicated to emerge as not isolated performers, but rather the key mediators and crosstalk in the cancer immune systems [30]. Previous studies demonstrated that integration index (neutrophil to lymphocyte ratio or platelets to lymphocyte ratio) was associated with tumor burden and clinical parameters, such as the optimal candidate biomarker for IBC patients [12].

Compared to previous indicators (counting or ratio) with fragmented, partial information, PIV has served as comprehensive, integrated peripheral immune biomarker incorporating the globally immune components (lymphocytes, monocytes, neutrophils, and platelets) [15–17, 21, 32]. PIV initially emerged as the prognostic indicator for patients with metastatic colorectal cancer [16], and the similar prognostic significance of PIV has been well established in various malignant tumors and immune and inflammation-related disorders [19–21]. In this study, the result showed that PIV could provide more effective value in IBC compared with other prognostic markers, MLR, NLR, and PLR. This finding was similar to the results from retrospective studies in the literature of breast cancer not only in advanced stage but also in the early-stage breast cancer patients [15, 17, 18, 22, 33]. When PIV value was applied for stratification of IBC patients, it became evident that higher PIV was associated with a more unfavorable prognosis. Our study findings indicated a pronounced inverse relationship between elevated PIV levels and both DFS and OS in patients. Moreover, based on both univariate and multivariate COX regression analyses, we observed that PIV was an independent value to predict survival in IBC patients.

The present study had some limitations. First, it was a retrospective study by single-center design, and IBC showed a relatively rare incidence, with a limited number of IBC patients, which might lead to unanticipated biases, such as selection, information and confounding biases. Second, although we excluded the patients who received immunomodulatory treatment, there existed other conditions influencing the blood-based biomarkers. Third, our study did not incorporate tumor genomic or immune microenvironmental data, which may influence IBC outcomes. Besides, although we have incorporated the metabolic indicator BMI in our study, other metabolic comorbidities such as diabetes and metabolic syndrome, which may influence systemic inflammation. Finally, more detailed analysis, such as the interplay between molecular subtype, lymphovascular invasion or host metabolic status with tumor-associated inflammation in IBC remains unexplored, which are warranting future prospective studies. Although we have employed multiple strategies to minimize the biases, further validation through randomized multicenter studies is needed to be conducted to confirm observation in this study.

Conclusion

In summary, this translational retrospective study demonstrated the prognostic significance of PIV in IBC patients, which outperformed other blood-based immune markers, suggesting its potential application in predicting IBC treatment outcomes. Higher PIV value in IBC patients compared with subtype-matched cohort would also provide some insights into the mechanisms underlying the role of immune and inflammation in IBC development and progression.

Author contributions

All authors contributed to the study conception and design. Material preparation, data collection and analysis were performed by YH, JL, MW, XW, and JL. The first draft of the manuscript was written by XN and HJ and all authors commented on previous versions of the manuscript. All authors contributed to the article and approved the submitted version.

Data availability

The raw data supporting the conclusions of this article will be made available by the authors, without undue reservation.

Ethics statement

The studies involving humans were approved by Harbin Medical University Cancer Hospital. The studies were conducted in accordance with the local legislation and institutional requirements. The participants provided their written informed consent to participate in this study.

Funding

The author(s) declare that financial support was received for the research and/or publication of this article. This work was supported by the Haiyan Foundation of Harbin Medical University Cancer Hospital under Grant No. JJZD2024-18, Harbin Medical University Cancer Hospital Top Young Talent Project under Grant No. BJQN2021-03, and the National Science Foundation of Heilongjiang Province under grant Nos PL2024H179 and LH2023H085.

Conflict of interest

The author(s) declared no potential conflicts of interest with respect to the research, authorship, and/or publication of this article.

Generative AI statement

The authors declare that no Generative AI was used in the creation of this manuscript.

References

1. Manai M, Finetti P, Mejri N, Athimni S, Birnbaum D, Bertucci F, et al. Inflammatory breast cancer in 210 patients: a retrospective study on epidemiological, anatomo-clinical features and therapeutic results. *Mol Clin Oncol* (2019) **10**:223–30. doi:10.3892/mco.2018.1773

2. van Uden DJP, van Laarhoven HWM, Westenberg AH, de Wilt JHW, Blanken-Peeters CFJM. Inflammatory breast cancer: an overview. *Crit Rev Oncology/Hematology* (2015) **93**:116–26. doi:10.1016/j.critrevonc.2014.09.003

3. Hester RH, Hortobagyi GN, Lim B. Inflammatory breast cancer: early recognition and diagnosis is critical. *Am J Obstet Gynecol* (2021) **225**:392–6. doi:10.1016/j.ajog.2021.04.217

4. Dawood S, Merajver SD, Viens P, Vermeulen PB, Swain SM, Buchholz TA, et al. International expert panel on inflammatory breast cancer: consensus statement for standardized diagnosis and treatment. *Ann Oncol* (2011) **22**:515–23. doi:10.1093/annonc/mdq345

5. Hance KW, Anderson WF, Devesa SS, Young HA, Levine PH. Trends in inflammatory breast carcinoma incidence and survival: the surveillance, epidemiology, and end results program at the National Cancer Institute. *JNCI: J Natl Cancer Inst* (2005) **97**:966–75. doi:10.1093/jnci/dji172

6. Lim B, Woodward WA, Wang X, Reuben JM, Ueno NT. Inflammatory breast cancer biology: the tumour microenvironment is key. *Nat Rev Cancer* (2018) **18**:485–99. doi:10.1038/s41568-018-0010-y

7. Fernandez SV, MacFarlane AW, Jillab M, Arisi MF, Yearley J, Annamalai L, et al. Immune phenotype of patients with stage IV metastatic inflammatory breast cancer. *Breast Cancer Res* (2020) **22**:134–16. doi:10.1186/s13058-020-01371-x

8. Quail DF, Joyce JA. Microenvironmental regulation of tumor progression and metastasis. *Nat Med* (2013) **19**:1423–37. doi:10.1038/nm.3394

9. Huang A, Cao S, Tang L. The tumor microenvironment and inflammatory breast cancer. *J Cancer* (2017) **8**:1884–91. doi:10.7150/jca.17595

10. Su S, Liu Q, Chen J, Chen J, Chen F, He C, et al. A positive feedback loop between mesenchymal-like cancer cells and macrophages is essential to breast cancer metastasis. *Cancer Cell* (2014) **25**:605–20. doi:10.1016/j.ccr.2014.03.021

11. Di Bonito M, Cantile M, Botti G. Pathological and molecular characteristics of inflammatory breast cancer. *Transl Cancer Res* (2019) **8**:S449–S456. doi:10.21037/tcr.2019.03.24

12. Van Berckelaer C, Van Geyt M, Linders S, Rypens C, Trinh XB, Tjalma WAA, et al. A high neutrophil-lymphocyte ratio and platelet-lymphocyte ratio are associated with a worse outcome in inflammatory breast cancer. *The Breast* (2020) **53**:212–20. doi:10.1016/j.breast.2020.08.006

13. Pivatto Júnior F, Santos ÂBS, Englert EF, Mazzutti G, Costa GOM, Saffi MAL, et al. Monocyte-to-lymphocyte ratio as predictor of cancer therapy-related cardiotoxicity in patients with breast cancer: a pilot cohort study. *Breast Cancer Res Treat* (2023) **200**:355–62. doi:10.1007/s10549-023-06979-z

14. Xie J, Guo Z, Zhu Y, Ma M, Jia G. Peripheral blood inflammatory indexes in breast cancer: a review. *Medicine* (2023) **102**:E36315. doi:10.1097/md.0000000000036315

15. Qi X, Qiao B, Song T, Huang D, Zhang H, Liu Y, et al. Clinical utility of the pan-immune-inflammation value in breast cancer patients. *Front Oncol* (2023) **13**:1223786. doi:10.3389/FONC.2023.1223786

16. Fucà G, Guarini V, Antoniotti C, Morano F, Moretto R, Corallo S, et al. The Pan-Immune-Inflammation Value is a new prognostic biomarker in metastatic colorectal cancer: results from a pooled-analysis of the Valentino and TRIBE first-line trials. *Br J Cancer* (2020) **123**:403–9. doi:10.1038/s41416-020-0894-7

17. Lin F, Zhang LP, Xie SY, Huang HY, Chen XY, Jiang TC, et al. Pan-immune-inflammation value: a new prognostic index in operative breast cancer. *Front Oncol* (2022) **12**:830138. doi:10.3389/FONC.2022.830138

18. Sahin TK, Akyildiz A, Dogan OT, Kavgaci G, Guven DC, Aksoy S. Prognostic significance of pan-immune-inflammation value in patients with HER2-positive metastatic breast cancer treated with trastuzumab emtansine. *Pharmaceuticals (Basel)* (2024) **17**:824. doi:10.3390/ph17070824

19. Gambichler T, Said S, Abu Rached N, Scheel CH, Susok L, Stranzenbach R, et al. Pan-immune-inflammation value independently predicts disease recurrence in patients with Merkel cell carcinoma. *J Cancer Res Clin Oncol* (2022) **148**:3183–9. doi:10.1007/s00432-022-03929-y

20. Fu M, Zhang X, Shen F, Ma J, Li Z. Prognostic value of peripheral blood neutrophil/lymphocyte ratio, platelet/lymphocyte ratio, pan-immune-inflammation value and systemic immune-inflammation index for the efficacy of immunotherapy in patients with advanced gastric cancer. *Immunotherapy* (2024) **16**:551–63. doi:10.2217/imt-2024-0031

21. Topkan E, Selek U, Kucuk A, Pehlivan B. Low pre-ChemoradiotherapyPan-immune-inflammation value (PIV) measures predict better survival outcomes in locally advanced pancreatic adenocarcinomas. *J Inflamm Res* (2022) **15**:5413–23. doi:10.2147/jir.s385328

22. Provenzano L, Lobefaro R, Ligorio F, Zattarin E, Zambelli L, Sposetti C, et al. The pan-immune-inflammation value is associated with clinical outcomes in patients with advanced TNBC treated with first-line, platinum-based chemotherapy: an institutional retrospective analysis. *Ther Adv Med Oncol* (2023) **15**:17588359231165978. doi:10.1177/17588359231165978

23. Schairer C, Laurent CA, Moy LM, Gierach GL, Caporaso NE, Pfeiffer RM, et al. Obesity and related conditions and risk of inflammatory breast cancer: a nested case–control study. *Breast Cancer Res Treat* (2020) **183**:467–78. doi:10.1007/s10549-020-05785-1

24. Fouad TM, Barrera AMG, Reuben JM, Lucci A, Woodward WA, Stauder MC, et al. Inflammatory breast cancer: a proposed conceptual shift in the UICC-AJCC TNM staging system. *The Lancet Oncol* (2017) **18**:e228–e232. doi:10.1016/s1470-2045(17)30192-4

25. Yang R, Chang Q, Meng X, Gao N, Wang W. Prognostic value of Systemic immune-inflammation index in cancer: a meta-analysis. *J Cancer* (2018) **9**:3295–302. doi:10.7150/jca.25691

26. Gianni C, Palleschi M, Schepisi G, Casadei C, Bleve S, Merloni F, et al. Circulating inflammatory cells in patients with metastatic breast cancer: implications for treatment. *Front Oncol* (2022) **12**:882896. doi:10.3389/fonc.2022.882896

27. Bertucci F, Boudin L, Finetti P, Van Berckelaer C, Van Dam P, Dirix L, et al. Immune landscape of inflammatory breast cancer suggests vulnerability to immune checkpoint inhibitors. *Oncoimmunology* (2021) **10**:1929724. doi:10.1080/2162402X.2021.1929724

28. Sharma P, Hu-Lieskovan S, Wargo JA, Ribas A. Primary, adaptive, and acquired resistance to cancer immunotherapy. *Cell* (2017) **168**:707–23. doi:10.1016/j.cell.2017.01.017

29. Mego M, Gao H, Cohen EN, Anfossi S, Giordano A, Sanda T, et al. Circulating tumor cells (CTC) are associated with defects in adaptive immunity in patients with inflammatory breast cancer. *J Cancer* (2016) **7**:1095–104. doi:10.7150/jca.13098

30. Stoiber D, Assinger A. Platelet-leukocyte interplay in cancer development and progression. *Cells* (2020) **9**:855. doi:10.3390/CELLS9040855

31. Sagiv JY, Michaeli J, Assi S, Mishalian I, Kisos H, Levy L, et al. Phenotypic diversity and plasticity in circulating neutrophil subpopulations in cancer. *Cell Rep* (2015) **10**:562–73. doi:10.1016/j.celrep.2014.12.039

32. Guven DC, Sahin TK, Erul E, Kilickap S, Gambichler T, Aksoy S. The association between the Pan-Immune-Inflammation value and cancer prognosis: a systematic review and meta-analysis. *Cancers* (2022) **14**:2675. doi:10.3390/cancers14112675

33. Şahin AB, Cubukcu E, Ocak B, Deligonul A, Oyucu Orhan S, Tolunay S, et al. Low pan-immune-inflammation-value predicts better chemotherapy response and survival in breast cancer patients treated with neoadjuvant chemotherapy. *Sci Rep* (2021) **11**:14662. doi:10.1038/s41598-021-94184-7

EBM Experimental Biology and Medicine

TYPE Original Research
PUBLISHED 30 April 2025
DOI 10.3389/ebm.2025.10469

OPEN ACCESS

*CORRESPONDENCE
Honggang Liu,
liuhonggang_zy@163.com

RECEIVED 13 December 2024
ACCEPTED 17 April 2025
PUBLISHED 30 April 2025

CITATION
Zhang Y and Liu H (2025) Aberrant DNMT1-mediated DACH1 methylation is associated with colorectal adenoma-to-carcinoma progression.
Exp. Biol. Med. 250:10469.
doi: 10.3389/ebm.2025.10469

Aberrant DNMT1-mediated DACH1 methylation is associated with colorectal adenoma-to-carcinoma progression

Yan Zhang[1,2] and Honggang Liu[1]*

[1]Department of Pathology, Beijing Tongren Hospital, Capital Medical University, Beijing, China,
[2]Department of Pathology, Beijing Changping Traditional Chinese Medicine Hospital, Beijing, China

Abstract

Colorectal cancer (CRC) remains a major contributor to cancer-related morbidity and mortality. While Dachshund homolog 1 (DACH1) was recognized as a critical regulator in cancer progression, its role in promoting or suppressing tumor development remains a subject of ongoing debate. This study aimed to elucidate the role of DACH1 in CRC progression and its underlying regulation mechanisms. The expression levels of Methyltransferase 1 (DNMT1) and DACH1, as well as its methylation status were assessed through a combination of TCGA data analysis and experimental validation using immunohistochemistry, PCR, methylation-specific PCR, and bisulfite sequencing RCR on 120 clinical samples, comprising normal mucosa, adenomas, and adenocarcinomas. The relationships among them were evaluated using Pearson or Spearman correlation analysis. The associations between the DACH1 and DNMT1 levels and clinicopathological parameters were examined to determine their clinical relevance. A progressive decrease in DACH1 expression and a concomitant increase in DACH1 promoter methylation and DNMT1 expression were observed from normal mucosa to adenoma and adenocarcinoma tissues. Higher DNMT1 expression and lower DACH1 expression were associated with poorer clinical outcomes, including worse tumor differentiation, lymphatic metastasis, and advanced tumor stages. Paired analysis of tissues from the same patient further validated their inverse expression patterns during CRC progression. DNMT1-mediated DACH1 epigenetic silencing plays a critical role in CRC progression, suggesting that the DNMT1-DACH1 regulatory axis may serve as a potential biomarker and therapeutic target in CRC.

KEYWORDS

DNMT1, DACH1, colorectal cancer, promoter methylation, tumor progression

Impact statement

The present study revealed a crucial epigenetic mechanism in colorectal cancer (CRC) progression involving the aberrant regulation of DACH1 by DNMT1 based on the combination of clinical sample analysis with bioinformatic databases. We demonstrated that DACH1 expression progressively decreased from normal colorectal mucosa to adenoma and adenocarcinoma tissues, while its methylation level and DNMT1 expression exhibited the opposite trend. Clinical parameters further highlighted the association of DACH1 and DNMT1 expression with tumor differentiation, lymphatic metastasis, and tumor stage. Our findings suggested that DNMT1-mediated hypermethylation might contribute to the silencing of DACH1, thereby promoting CRC progression. This provided a novel perspective into the epigenetic regulation of tumor suppressor genes in CRC and identified potential therapeutic targets for intervention.

Introduction

Colorectal cancer (CRC) is one of the most commonly diagnosed cancer worldwide and is projected to increase to 3.2 million new cases annually by 2040, with a mortality rate exceeding 50% [1]. This alarming trend underscores its significant threat to global public health. The progression of CRC typically follows a well-established "normal mucosa-adenoma-carcinoma" sequence, which is driven by the dysregulation of tumor suppressor genes and oncogenes, leading to the initiation and progression of malignancy [2]. Under normal physiological conditions, colorectal epithelial cells maintain a delicate balance between proliferation and apoptosis, ensuring mucosal tissue stability. However, disruptions in this balance create a permissive environment for tumor initiation, which is modulated by some key genes [1].

The development of adenomas marks a critical early event in CRC pathogenesis, as adenomas are recognized as precancerous lesions that can progress to carcinomas. Mutations in key genes such as APC and KRAS are frequently observed during this stage [3, 4]. As adenomas progress, tumor cells may acquire additional mutations and accumulate epigenetic changes, facilitating the transition to invasive carcinoma. For instance, the inactivation of the TP53 gene disrupts cell cycle regulation, thereby promoting the development of carcinoma *in situ* [5]. Understanding the molecular mechanisms underlying this progression is essential for the development of effective diagnostic and therapeutic strategies to combat CRC.

Emerging evidence has identified DACH1 as a tumor suppressor gene involved in regulating key processes such as cell proliferation, apoptosis, and invasion across various cancers including breast, prostate, and lung cancers [6–8]. For example, the deletion of the DACH1 gene occurs in up to 18% of human prostate cancer cases, and its loss in mouse prostate cancer models has been shown to enhance prostatic intraepithelial neoplasia and DNA damage [6]. In CRC, previous studies suggest that the loss of DACH1 expression is associated with tumor progression [9, 10]. However, conflicting evidence suggests that DACH1 is highly expressed at all stages of CRC, and increased DACH1 expression was identified as an independent predictor of poor prognosis, highlighting its pro-tumorigenic role through the regulation of BMP signaling [11]. Based on this conflicting evidence, the specific role and regulatory mechanisms of DACH1 expression in CRC require further investigation.

Gene expression during tumor progression is regulated through a variety of mechanisms, among which epigenetic modifications, particularly promoter region DNA methylation, play a pivotal role in regulating gene expression without altering the underlying DNA sequence [12]. Aberrant hypermethylation of promoter CpG islands is a common event in cancer, leading to the silencing of tumor suppressor genes [13]. In CRC, for example, the promoter hypermethylation of PRDM2 and MLH1 is initiated in sessile serrated lesions, which can progress into MLH1-deficient CRC [13]. Additionally, DNA methylation homeostasis is closely related to DNA Methyltransferase 1 (DNMT1), which is a hallmark of various malignancies [14, 15]. Despite overexpression of DNMT1 having correlation with progression, poor prognosis and chemoresistance in CRC [16, 17], whether it exerts this negative regulation through the methylation of DACH1 remains unclear.

As such, our study systematically analyzed the expression patterns of DACH1 and DNMT1 across normal tissues, adenomas, and adenocarcinomas by integrating clinical samples with data from the TCGA database. Our findings revealed the importance of the DNMT1-mediated epigenetic regulation of DACH1 in CRC initiation and progression and clarified its relationship with clinical parameters. Targeting this pathway might represent a promising therapeutic strategy for CRC.

Materials and methods

Ethical statement

The study was conducted in accordance with the Declaration of Helsinki and was approved by the Ethics Committee of Beijing Tongren Hospital. Written informed consent was obtained from all participants before sample collection. Patient information was anonymized to protect confidentiality, and all data were handled following institutional and legal guidelines for patient privacy and research ethics.

Clinical sample collection and grouping

A total of 120 tissue samples were collected from patients who visited the Department of General Surgery at Beijing Tongren Hospital between 2016 and 2022. The samples included 40 cases each of normal colorectal mucosa, colorectal adenoma, and colorectal adenocarcinoma tissues, confirmed by pathological diagnosis. Patients had received radiotherapy or chemotherapy were excluded prior to sample collection. Clinical and pathological data, including age, gender, tumor differentiation degree, lymph node metastasis status, and tumor stage (Dukes staging), were collected and analyzed based on the expression levels of DACH1 and DNMT1.

Criteria for tumor classification and staging

Tumor differentiation degree was evaluated based on the morphology and function of tumor cells to normal tissues. High differentiation indicates cells closely resembling normal cells, retaining partial structure and function, with lower malignancy and better prognosis. Moderate differentiation represents partially disorganized structures and intermediate malignancy. Low differentiation shows severe disorganization, higher malignancy, and worse prognosis. Lymph node metastasis was classified based on regional lymph node involvement. Dukes staging was used to evaluate CRC progression. Dukes A and B represent that tumor confined to mucosa, submucosa or invades muscularis propria without lymph node metastasis, whereas Dukes C and D with lymph node or distant metastases.

Immunohistochemistry (IHC)

Tissue samples were fixed in 10% formalin, embedded in paraffin, and sectioned into 4 μm slices. Sections were deparaffinized with xylene, hydrated through graded ethanol, and subjected to antigen retrieval using sodium citrate buffer under high-pressure heat. Endogenous peroxidase activity was blocked by incubating sections in 3% hydrogen peroxide for 10 min, followed by blocking with 5% bovine serum albumin for 30 min. Sections were incubated overnight at 4°C with primary antibodies anti-DACH1 (1:200; Abcam, Cambridge, UK) and anti-DNMT1 (1:200; Cell Signaling Technology, Danvers, MA, United States). The following day, sections were incubated with biotinylated secondary antibodies (Cell Signaling Technology, 1:200) at room temperature for 30 min. Signal detection was performed using DAB staining, followed by hematoxylin counterstaining, dehydration, clearing, and mounting. DACH1 and DNMT1 expression was assessed independently by two pathologists using a semi-quantitative scoring system based on the proportion of stained cells (0: <5%, 1: 5%–25%, 2: 26%–50%, 3: 51%–75%, 4: >75%) and staining intensity (0: negative, 1: weak, 2: moderate, 3: strong). Total scores ranged from 0 to 7, categorized as negative (–, 0–1), weak (+, 2–3), moderate (++, 4–5), and strong (+++, 6–7).

Bioinformatics analysis

RNA-sequencing data of DACH1 and DNMT1 from 589 CRC patients were obtained from The Cancer Genome Atlas (TCGA) database[1], with DACH1 methylation data (cg26413827; 1st Exon, 5'UTR) derived from Illumina HM27 or HM450 platforms. RNA-sequencing data were used to analyze the mRNA expression levels of DNMT1 and DACH1, while the methylation status of the DACH1 were evaluated by calculating the average Beta values for CpG sites. To investigate the relationship between DACH1 methylation levels and the expression of DACH1 or DNMT1, samples were divided into two groups based on the median mRNA expression levels of DACH1 (low, n = 295; high, n = 294) or DNMT1 (low, n = 295; high, n = 294). The methylation levels of DACH1 were then compared between these two groups to determine any significant differences and assess potential correlations between these mRNA expressions with DACH1 methylation.

Quantitative real-time PCR (qRT-PCR)

Total RNA was extracted from fresh-frozen tissue samples using TRIzol reagent (Invitrogen, Carlsbad, CA, United States) following the manufacturer's instructions. RNA purity and concentration were assessed using a NanoDrop 2000 spectrophotometer (Thermo Fisher Scientific, Waltham, MA, United States). One microgram of total RNA was reverse-transcribed into cDNA using the PrimeScript™ RT reagent Kit (Takara, Shiga, Japan). qRT-PCR was performed on an ABI 7500 Real-Time PCR System (Applied Biosystems, Foster City, CA, United States) using SYBR® Premix Ex Taq™ II (Takara). The primers were used to detect DACH1 (Forward: 5′-AGCAGCAGCGAGTACAAGAA-3′, Reverse: 5′-CTGCTG CTGTTGCTGTTGTT-3′) and DNMT1 (Forward: 5′-GTG CTGCTGCTGCTGCTGTA-3′, Reverse: 5′-ACACACACA CACACACACAC-3′). PCR conditions were set as: 95°C for 30 s, followed by 40 cycles of 95°C for 5 s and 60°C for 30 s. Relative gene expression was calculated using the $2^{-\Delta\Delta CT}$ method, normalized to GAPDH.

1 https://www.cbioportal.org/

Methylation-specific PCR (MSP) and bisulfite sequencing PCR (BSP)

The genomic DNA was extracted from normal mucosa, adenoma, and adenocarcinoma tissues using a standard phenol-chloroform method. The extracted DNA was then bisulfite-converted using the EZ DNA Methylation-Gold™ Kit (Zymo Research, Irvine, CA, United States) following the manufacturer's instructions. Methylation-specific primers for the DACH1 promoter were designed using MethPrimer[2], targeting both methylated and unmethylated CpG sequences. PCR amplification was performed in a 25 μL reaction mixture containing 2 μL bisulfite-treated DNA, 0.2 μM primers, and 12.5 μL 2× Taq PCR Master Mix (Takara, Shiga, Japan). Thermal cycling conditions were as follows: initial denaturation at 95°C for 10 min, followed by 40 cycles of 95°C for 30 se, 58°C for or 56°C for 30 s for methylated primers and unmethylated primers, respectively, and 72°C for 30 s, with a final extension at 72°C for 10 min. The PCR products were cloned into the pGEM-T Easy vector (Promega, Madison, WI, United States) and transformed into *Escherichia coli* DH5α competent cells. Positive clones were selected and plasmid DNA was extracted using the QIAprep Spin Miniprep Kit (Qiagen, Hilden, Germany). The inserted fragments were sequenced using the Sanger sequencing method. Sequencing reactions were performed using the BigDye™ Terminator v3.1 Cycle Sequencing Kit (Thermo Fisher Scientific) following the manufacturer's protocol. The reaction products were purified using a Sephadex™ G-50 column and analyzed on an ABI 3730xl DNA Analyzer (Applied Biosystems). Each CpG site was classified as methylated (black circles) or unmethylated (white circles), and detailed methylation patterns were visualized to create single-molecule methylation maps. The methylation rate was expressed as the ratio of methylation-positive cases.

Luciferase reporter assay

To confirm whether DACH1 methylation regulates the transcriptional activity of its promoter, a luciferase reporter assay was performed using the luciferase reporter vector comprising the pGL3-basic vector (Promega) with the DACH1 promoter sequence containing the binding site. The above vector plasmids were transfected into 293 T cells (ATCC) using Lipofectamine 2000, respectively. After 48 h of transfection, the Dual Luciferase Reporter Gene Assay System kit (Promega) was applied to carry out luciferase assays.

2 http://www.urogene.org/cgi-bin/methprimer/methprimer.cgi

5-Aza-2′-deoxycytidine treatment

HCT116 cells purchased from Procell (Wuhan, China) were treated with a final concentration of 10 μM of 5-aza-2′-deoxycytidine (5-Aza-dC, Sigma-Aldrich, Steinheim, Germany), which is a DNMT1 inhibitor. After 3 days, the treated cells were collected for further detections, including qRT-PCR, western blot, and MSP. The cells treated with PBS served as the control.

Western blot

The total protein was lysed from the cells and subsequently quantified by BCA kit analysis (Thermo Fisher), separated by 10%SDS-PAGE gel electrophoresis, and transferred to PVDF membranes (Millipore Corp, Billerica, MA, United States). Next, the membranes were sealed and then incubated overnight at 4°C with the primary antibody anti-DACH1 (Abcam), and with the secondary antibody for 2 h. Finally, the protein bands were visualized by the ECL Western Blotting Substrate Kit (Abcam). Relative expression of proteins was analyzed using Quantity One software with GAPDH as an internal reference.

Statistical analysis

All data were analyzed using SPSS 22.0 software (IBM Corp., Armonk, NY, United States). Continuous variables were expressed as Mean ± SEM and compared using one-way ANOVA or the Kruskal-Wallis test, followed by Tukey's HSD post-hoc test. Categorical variables were analyzed using chi-square tests. Correlations between parameters were assessed using Pearson or Spearman correlation analysis, with scatterplots generated to visualize trends. Regression analysis was performed to evaluate the degree of correlation. Statistical significance was defined as $p < 0.05$.

Results

DACH1 expression progressively decreased in normal, colorectal adenoma and adenocarcinoma tissues

Forty cases of each type, including normal colorectal mucosa, colorectal adenoma, and colorectal adenocarcinoma tissues, were collected for analysis of DACH1 levels. The expression of DACH1 protein was assessed through IHC. A progressive reduction in DACH1 expression was observed from normal colorectal

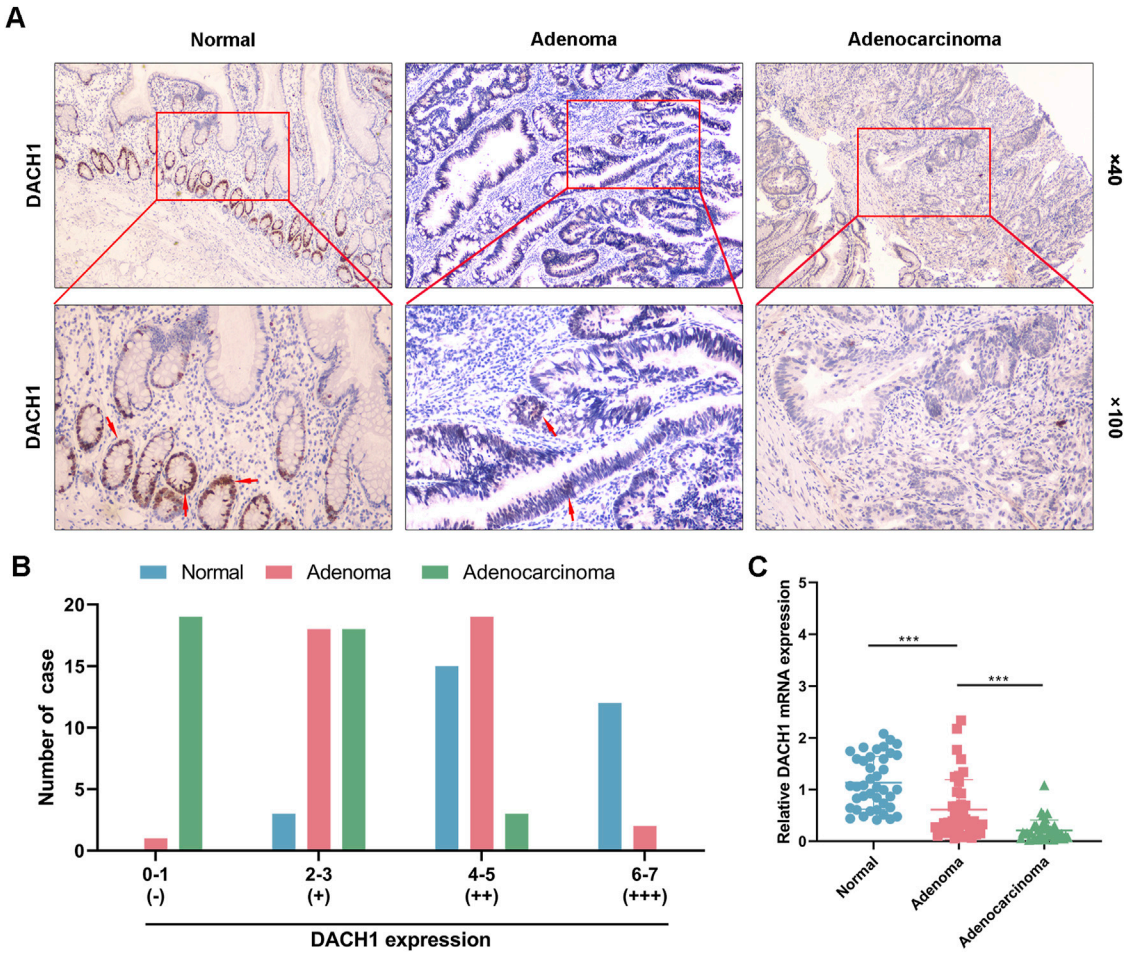

FIGURE 1
DACH1 expression in normal, colorectal adenoma, and adenocarcinoma tissues. Forty cases each of normal colorectal mucosa, colorectal adenoma, and colorectal adenocarcinoma tissues were collected from patients. **(A)** The DACH1 protein expression determined by immunohistochemical analysis in these tissues. Representative images were demonstrated by the magnification of 100 × and 400 ×. **(B)** Immunohistochemical staining intensity evaluated using semi-quantitative scoring for negative (–), weak (+), moderate (++), and high (+++) DACH1 expression across the "normal-adenoma-adenocarcinoma" progression. **(C)** Relative mRNA expression of DACH1 was measured by qRT-PCR. Data are presented as mean ± SEM. ***$p < 0.001$.

mucosa to adenoma and adenocarcinoma tissues. In normal tissues, DACH1 was predominantly localized in the nuclei of epithelial cells, showing strong staining intensity, whereas moderate staining was detected in adenoma tissues, and weak or negligible nuclear staining was evident in adenocarcinoma tissues (Figure 1A). Half-quantification of IHC staining scores revealed a significant decline in the number of cases with high DACH1 expression (+++) across the "normal-adenoma-adenocarcinoma" progression, with its level being negligible in the adenocarcinoma group. Conversely, cases with negative (–) staining were significantly increased in adenocarcinoma tissues compared to normal and adenoma tissues. While weak (+) staining was elevated in both adenoma and adenocarcinoma relative to normal tissues, no significant difference was observed between adenoma and adenocarcinoma cases. The number of cases with moderate (++) staining was markedly reduced in adenocarcinoma compared to both normal and adenoma tissues (Figure 1B). Additionally, the relative mRNA expression of DACH1 followed a similar trend, with the highest levels observed in normal tissues, followed by a significant decrease in adenoma and the lowest levels in adenocarcinoma tissues. Statistical analysis confirmed highly significant differences in DACH1 mRNA expression among these three groups (Figure 1C). These findings indicated a progressive loss of DACH1 expression at both the protein and mRNA levels during the "normal mucosa-adenoma-adenocarcinoma" sequence, suggesting that the downregulation of DACH1 may play a crucial role in the pathogenesis and progression of colorectal cancer.

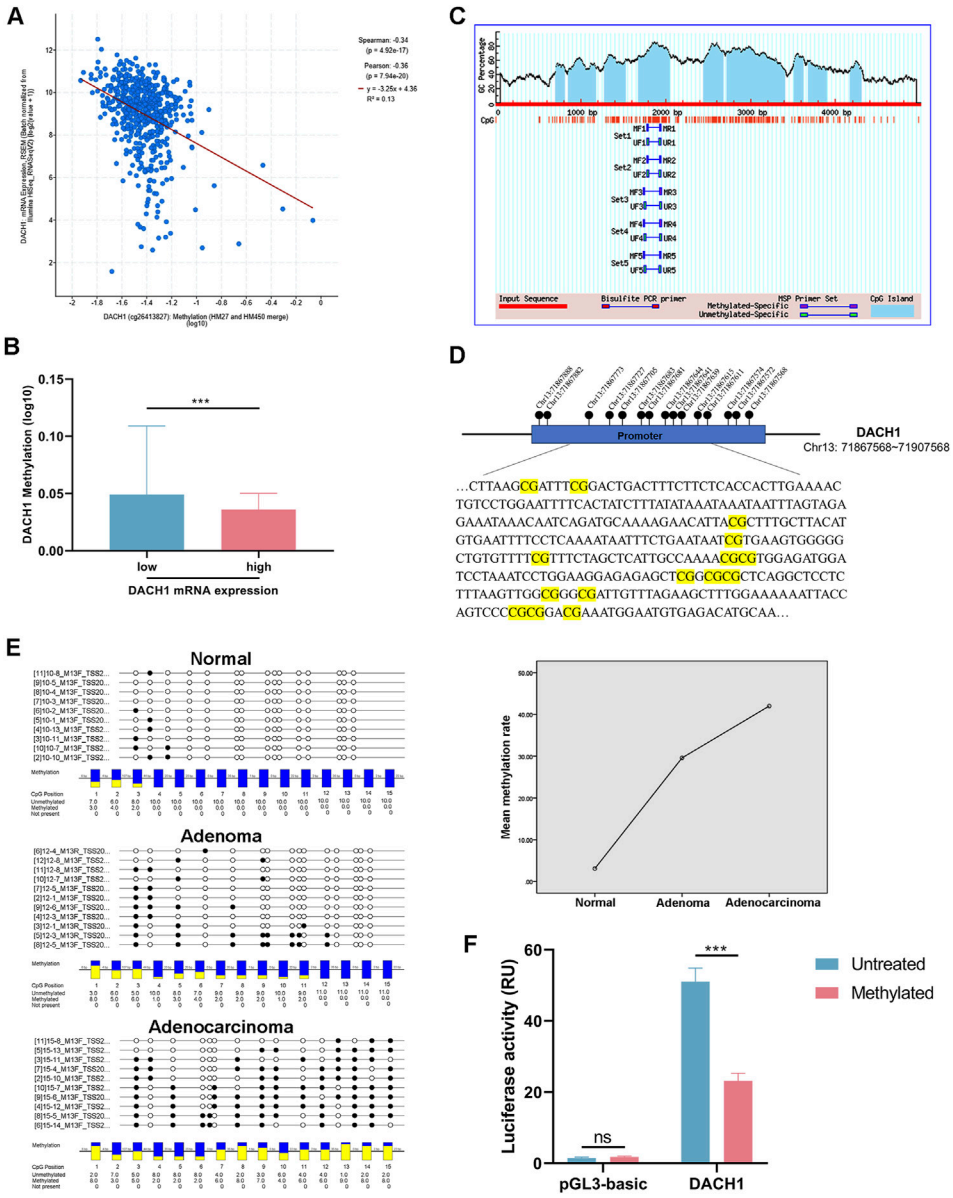

FIGURE 2
Relationship of DACH1 expression and promoter methylation cross colorectal cancer progression. **(A)** Correlation analysis of DACH1 promoter methylation levels and mRNA expression and **(B)** comparison of DACH1 methylation levels between the patients stratified by DACH1 median mRNA expression in colorectal tissues based on the TCGA database. **(C)** Genomic organization of the DACH1 promoter region and visualization of CpG island regions targeted by methylation-specific PCR. **(D)** The schematic diagram of the DACH1 promoter and the location of 15 CpG sites detected in this study. **(E)** Methylation profiling across normal mucosa, adenoma, and adenocarcinoma tissues and quantitative analysis of mean methylation rates across the three stages. **(F)** Luciferase reporter assay confirmed that DACH1 methylation regulates the transcriptional activity of its promoter. Data are presented as mean ± SEM. ***$p < 0.001$.

Promoter hypermethylation of DACH1 contributed to its transcriptional silencing in colorectal tissues

The relationship between DACH1 methylation and transcriptional silencing in colorectal cancer tissues was investigated using methylation data from TCGA (n = 589). A significant negative correlation was identified between the methylation levels of DACH1 CpG sites (cg21343827) and its mRNA expression levels (Pearson correlation coefficient: r = −0.36, $p < 0.001$) (Figure 2A). Using the same data, we divided the samples into two groups

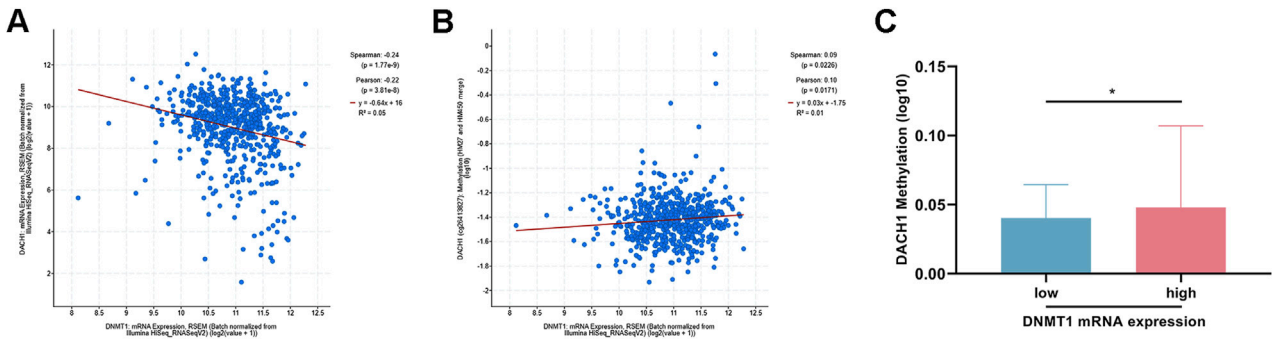

FIGURE 3
Relationship of DNMT1 expression with DACH1 expression and methylation in colorectal cancer. Correlation analysis of DNMT1 and **(A)** DACH1 mRNA expression as well as **(B)** DACH1 promoter methylation levels using TCGA database. **(C)** DACH1 methylation levels in patients divided based on median DNMT1 levels. Data are presented as mean ± SEM. *p < 0.05.

(low and high DACH1 mRNA expression groups) based on the median DACH1 mRNA levels. A comparison of methylation levels revealed significantly higher promoter methylation in patients with low mRNA expression compared to those with high DACH1 expression (Figure 2B). This suggested that increased methylation of the DACH1 is associated with reduced transcriptional activity. To validate these findings, MethPrimer[3] was applied to design primer to target critical CpG island regions within the DACH1 promoter (Figure 2C). The genomic organization of the DACH1 promoter and the specific CpG regions analyzed were visualized (Figure 2D). Based on BSP analysis, detailed methylation profiling across the normal mucosa-adenoma-adenocarcinoma sequence revealed that most CpG sites within the DACH1 promoter were unmethylated in normal mucosa. Moderate increases in methylation were observed in adenoma tissues, while adenocarcinoma tissues exhibited a significant and widespread increase in methylation levels. Quantitative analysis showed a progressive increase in mean methylation rates from normal mucosa to adenoma and adenocarcinoma (Figure 2E). Moreover, the dual-luciferase reporter assay showed that methylation of the DACH1 promoter caused a significant reduction in its transcriptional activity (Figure 2F). These results demonstrate that DACH1 promoter hypermethylation is associated with transcriptional silencing, suggesting that this epigenetic modification may play a pivotal role in the adverse progression of CRC.

DNMT1 expression correlated with DACH1 methylation and expression in colorectal cancer

DNMT1 is a key regulator of DNA methylation. Analysis of TCGA data of CRC revealed a significant negative correlation between DNMT1 and DACH1 mRNA expression levels (Figure 3A). Furthermore, DNMT1 expression was positively correlated with DACH1 promoter methylation levels (Figure 3B). Moreover, patients stratified into two groups based on the median DNMT1 expression level showed consistent results, with higher DNMT1 expression associated with significantly increased DACH1 methylation, while lower DNMT1 expression correlated with reduced methylation (Figure 3C). Furthermore, *in vitro* experiment using a DNMT1 inhibitor (5-Aza-dC) was performed, which indicated that the mRNA, protein, as well as methylation levels of DACH1 in HCT116 cells were significantly reduced after treating with 5-Aza-dC (Figures 4A–C).

The clinical significance of DACH1 and DNMT1 expression levels was also evaluated in CRC patients. No significant differences in either marker was observed between older (≥60 years) and younger patients or between males and females. However, tumor differentiation, lymphatic metastasis, and tumor stage were significantly associated with DACH1 and DNMT1 expression. Poorly differentiated tumors exhibited lower DACH1 expression and higher DNMT1 expression compared to moderately differentiated tumors. Similarly, tumors with lymphatic metastasis showed significantly reduced DACH1 expression and elevated DNMT1 expression compared to non-metastatic cases. Advanced-stage tumors (DUCKS stages C and D) were characterized by markedly lower DACH1 expression and higher DNMT1 expression compared to early-stage tumors (Table 1). These findings suggested that DACH1 downregulation and

3 http://www.urogene.org/methprimer/

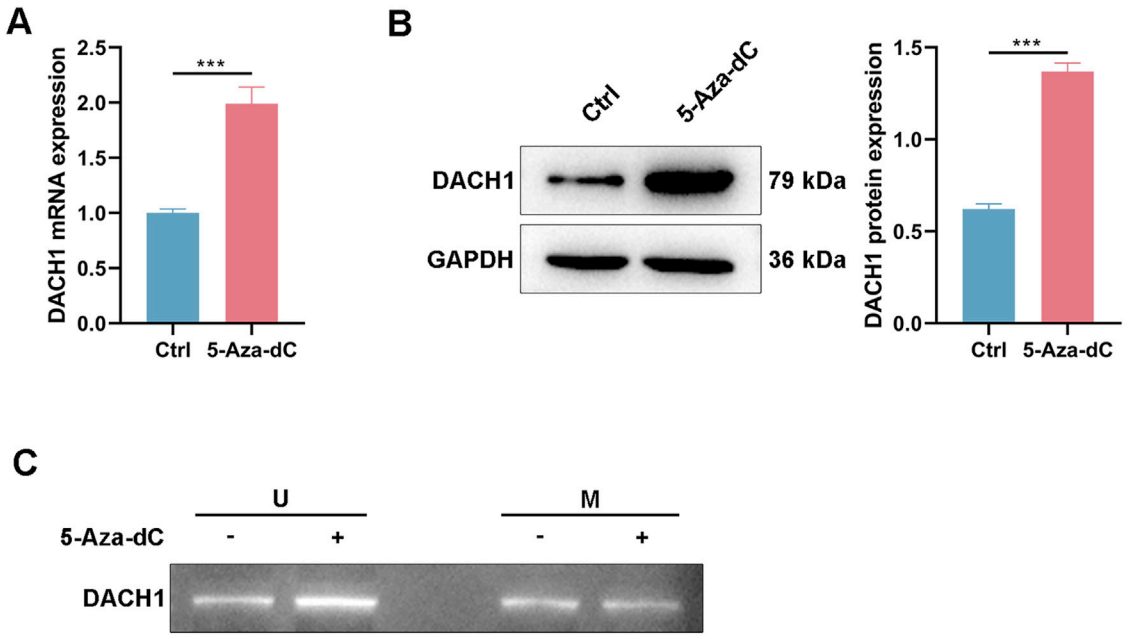

FIGURE 4
DACH1 expression was regulated by DNMT1-mediated methylation *in vitro*. After being exposed to a DNMT1 inhibitor (5-Aza-dC), HCT116 cells were collected for analyzing the **(A)** mRNA, **(B)** protein, and **(C)** methylation levels of DACH1. Data are presented as mean ± SEM. ***p < 0.001.

TABLE 1 Comparison of DNMT1 and DACH1 expression in patients with different clinicopathological parameters.

Clinical parameters	Number of cases	DACH1 expression			DNMT1 expression		
		Low	High	*p* value	Low	High	*p* value
Age				0.525			0.525
<60	22	10	12		10	12	
≥60	18	10	8		10	8	
Gender				0.752			0.342
Male	21	11	10		12	9	
Female	19	9	10		8	11	
Differentiation degree				0.003*			0.022*
High	15	2	13		11	4	
Medium-Low	25	18	7		9	16	
Lymphatic metastasis				0.003*			0.022*
Yes	15	12	3		4	11	
No	25	8	17		16	9	
DUCKS stage				0.001*			0.038*
A, B	25	9	19		17	11	
C, D	15	11	1		3	9	

Note: p*<0.05 indicates statistic differences.

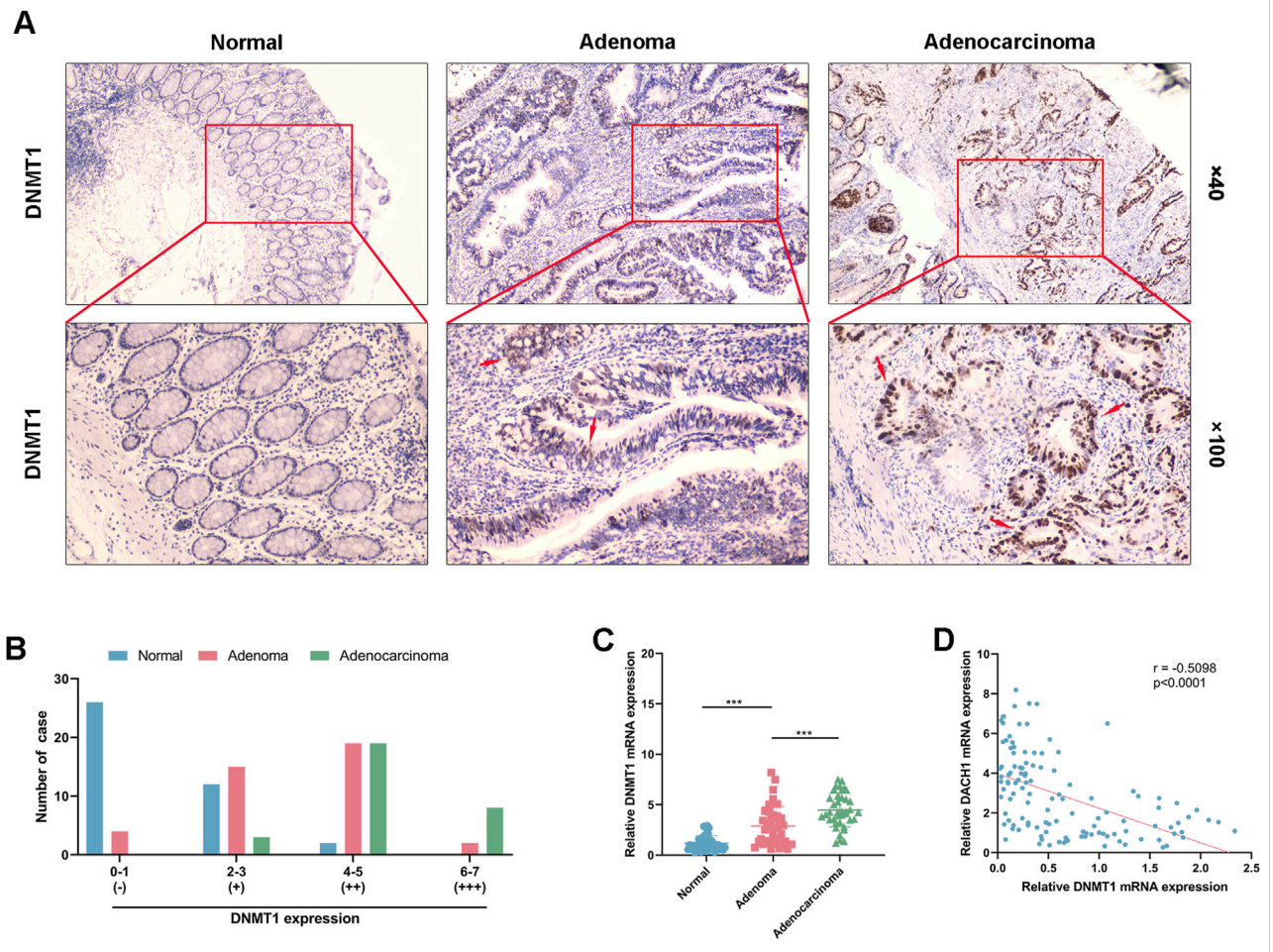

FIGURE 5
DNMT1 expression in colorectal cancer progression. **(A)** Immunohistochemical analysis of DNMT1 protein expression in normal colorectal mucosa, adenoma, and adenocarcinoma tissues of patients (magnifications used were 100 × and 400 ×) and **(B)** semi-quantitative scoring of staining defined as negative (–), weak (+), moderate (++), and high (+++) levels. **(C)** Quantitative PCR analysis of DNMT1 mRNA levels from normal mucosa to adenoma and adenocarcinoma tissues. **(D)** Correlation analysis of DNMT1 and DACH1 mRNA expression conducted by Pearson's correlation analysis. Data are presented as mean ± SEM. ***p < 0.001.

DNMT1 upregulation might be closely associated with tumor progression in CRC. The reciprocal relationship between DNMT1 expression and DACH1 methylation and expression underscored the epigenetic regulation of DACH1 by DNMT1.

DNMT1 expression progressively increased in colorectal cancer progression and negatively correlated with DACH1 expression

To further investigate the role of DNMT1 in CRC progression, its expression was analyzed and compared across normal colorectal mucosa, adenoma, and adenocarcinoma tissues using IHC and PCR. IHC results demonstrated a progressive increase in DNMT1 protein expression along the normal-adenoma-adenocarcinoma sequence (Figure 5A). Semi-quantitative scoring of DNMT1 staining revealed that the proportion of cases with negative staining (–) was highest in normal mucosa and significantly reduced in adenoma and adenocarcinoma tissues, with no cases observed in adenocarcinoma. Weakly positive stained cases (+) demonstrated progressively decreased trend followed normal, adenoma and adenocarcinoma. Moderately positive staining (++) was highest in adenoma, followed by adenocarcinoma, and lowest in normal tissues. Moreover, strongly positive staining (+++) was absent in normal tissues, but significantly more frequent in adenocarcinoma compared to adenoma (Figure 5B). PCR analysis of DNMT1 mRNA expression

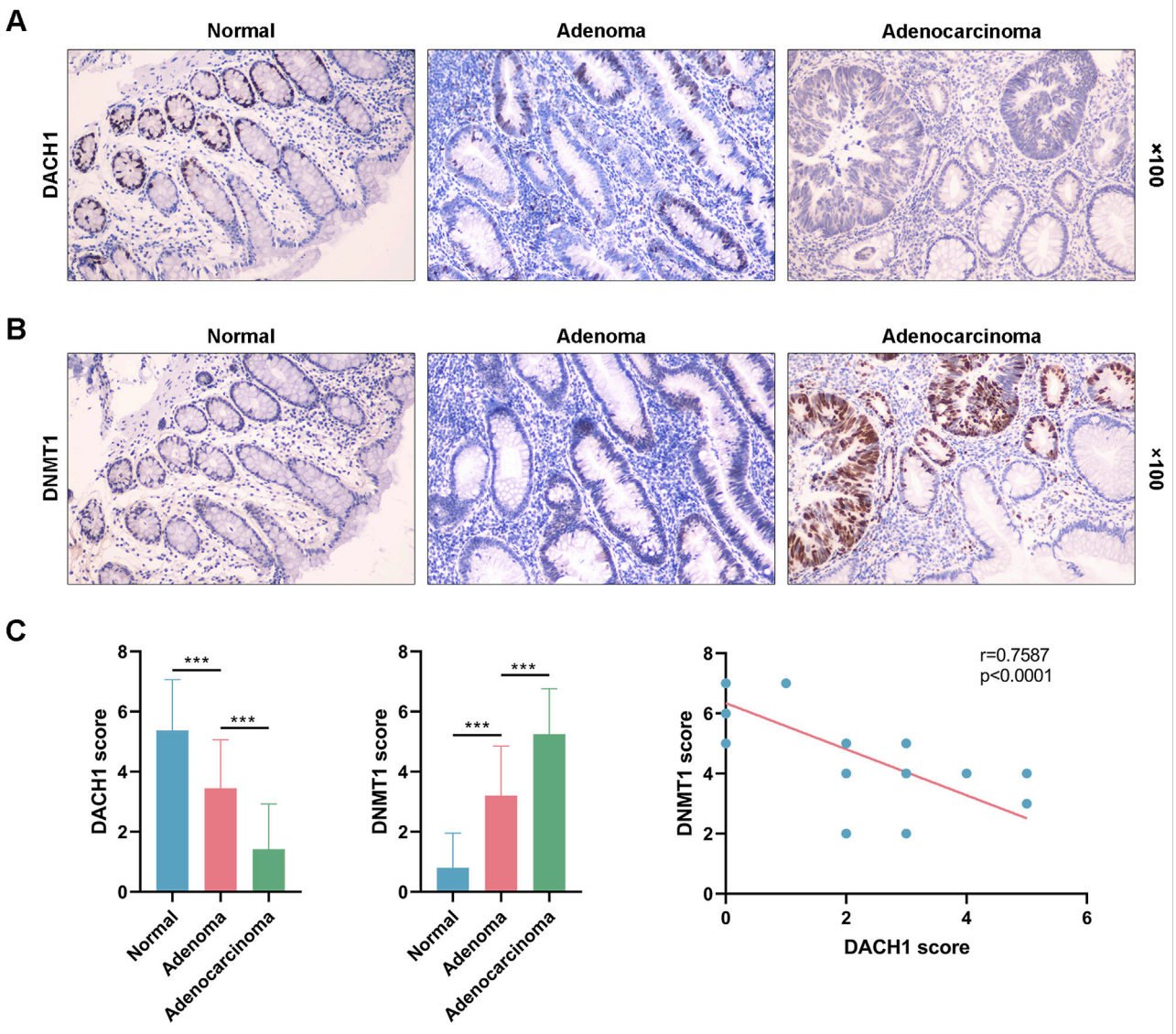

FIGURE 6
DACH1 and DNMT1 protein expression patterns across normal, adenoma, and carcinoma tissues from the same patient. Three types of tissues were collected from a patient to evaluate the protein levels of **(A)** DACH1 and **(B)** DNMT1 by immunohistochemical analysis. The magnifications used were 100 ×. **(C)** The DACH1 and DNMT1 expressions were scored, and a correlation analysis was performed between them.

further confirmed a stepwise increase in expression levels from normal mucosa to adenoma and adenocarcinoma tissues (Figure 5C). Notably, DNMT1 mRNA expression was found to be negatively correlated with DACH1 mRNA expression ($r = -0.5098$, $p < 0.0001$) (Figure 5D), as previously observed in Figure 1C. Overall, DNMT1 expression exhibited a progressive increase at both the protein and mRNA levels during the transition from normal mucosa to adenoma and adenocarcinoma. The inverse correlation between DNMT1 and DACH1 expression highlighted the potential role of DNMT1 in silencing tumor suppressor genes DACH1 through epigenetic mechanisms.

DACH1 and DNMT1 proteins had opposite expression patterns across normal, adenoma, and carcinoma tissues from the same patient

Normal mucosa, adenoma, and carcinoma tissues obtained from the same patient were used to detect the expression of DACH1 and DNMT1 during CRC progression by IHC. DACH1 protein expression was found to decrease progressively from normal to adenoma to carcinoma tissues. Normal mucosa exhibited the highest levels of DACH1 expression, which was markedly reduced

in adenoma and further diminished in carcinoma tissues (Figure 6A). In contrast, DNMT1 protein expression demonstrated an opposite trend, with the lowest expression in normal mucosa, moderate expression in adenoma, and the highest levels in carcinoma tissues (Figure 6B). These expression trends across tissues from the same patient supported the notion that DACH1 downregulation and DNMT1 upregulation play critical roles in CRC progression. Finally, the correlation of expression levels between DACH1 and DNMT1 was plotted, which revealed a potential relationship between DACH1 and DNMT1 in CRC (Figure 6C).

Discussion

The incidence and mortality rates of CRC are steadily increasing, posing a significant threat to human health [18]. The progression of CRC typically follows the normal mucosa-adenoma-carcinoma sequence, investigating the molecular mechanisms underlying which and identifying potential targets for intervention are essential for preventing CRC. In this study, we combined bioinformatics analyses with clinical sample validation to elucidate the expression trends of DACH1 levels, DACH1 promoter methylation, and DNMT1 levels across different stages of CRC progression and our findings revealed that DNMT1-mediated epigenetic silencing of DACH1 plays a pivotal role in driving CRC initiation and progression.

DACH1 was recognized as a tumor suppressor gene in our study, supported by a significant decrease in DACH1 protein and mRNA expression from normal mucosa to adenomas and adenocarcinomas. This was aligning with previous findings linking the loss of DACH1 expression to tumor development and poor prognosis [6, 19]. The silencing of tumor suppressor genes like DACH1 in CRC may result from various mechanisms, including epigenetic regulation such as promoter DNA methylation, aberrant histone modifications, and the involvement of non-coding RNAs [20]. Our findings demonstrated that the progressive decrease in DACH1 expression during CRC progression corresponds with a concurrent increase in promoter methylation, confirming that DNA methylation might be one of a critical mechanism driving DACH1 silencing in this context. This mechanism is not unique to CRC, as CpG island hypermethylation has similarly been shown to silence DACH1 in other cancer types. For instance, the DACH1 methylation rate was illustrated higher levels in non-small cell lung cancer compared to adjacent normal lung tissues and demethylation treatment contributed to decreased migration and invasion of cancer cells [21]. This emphasized the broader significance of this epigenetic regulation in tumor progression.

DNA methylation is regulated by DNMTs, among which DNMT1 is a primary enzyme responsible for maintaining DNA methylation patterns. DNMT1 recognizes hemimethylated CpG dinucleotides with the assistance of the auxiliary factor UHRF1. Using S-adenosylmethionine as a methyl donor, DNMT1 adds methyl groups to cytosines on the newly synthesized DNA strand, preserving the methylation state during DNA replication. [22, 23]. Aberrant overexpression of DNMT1 has been widely reported across various cancers and is frequently associated with hypermethylation and silencing of tumor suppressor gene promoters [24, 25]. For example, DNMT1 was overexpressed in pancreatic ductal adenocarcinoma tissues, with a opposite trend in normal pancreatic tissues and silencing of it demethylated Bax gene promoter, which demonstrated increased mRNA expression [26]. Consistent with this, our present study revealed a significant positive correlation between DNMT1 expression and DACH1 promoter methylation, accompanied by a negative correlation between DNMT1 expression and DACH1 transcription, which also in line with a progressively elevated trend across the CRC progression sequence.

Machine learning based on database analysis has previously predicted numerous critical genes and regulatory axes involved in CRC progression, providing valuable insights into potential therapeutic targets for cancer treatment. Sardari et al. [27] utilized a multivariate machine learning strategy across multiple independent datasets in a recent study and identified genes such as TNS4, SLC7A5, and SCD, which were demonstrated to be associated with CRC. However, these predictions require validation through clinical evidence. Existing studies on gene regulatory mechanisms in CRC primarily focus on database-based predictions or animal models [28–31], with relatively few integrating with clinical sample validation. The strength of our study lies in addressing this gap by combining bioinformatics analyses with multi-layered verification using clinical samples, systematically confirming the expression patterns and regulatory interactions of DACH1 and DNMT1 at critical stages of CRC progression. Specifically, based on the TCGA database, we analyzed RNA sequencing data and DNA methylation profiles from CRC patients. This revealed a significant negative correlation between DACH1 expression and its promoter methylation as well as DNMT1 expression, suggested that the probability of DNMT1 to mediate DACH1 transcriptional silencing by promoting hypermethylation of its promoter. To further confirmation, we collected clinical samples representing normal mucosa, adenomas, and adenocarcinomas tissues. A progressive decrease in DACH1 expression from normal mucosa to adenoma to adenocarcinoma were observed, while DNMT1 expression showed a corresponding increase, demonstrating an inverse relationship in both protein and mRNA levels. BSP analysis further revealed the

hypermethylation of the DACH1 promoter, supporting the hypothesis obtained *in silico*. Additionally, paired analysis of samples from individual patients contributed to eliminating inter-patient variability and clearly demonstrated dynamic changes in molecular expression during the normal mucosa-adenoma-carcinoma sequence within the same patient. The consistent findings with the overall trends observed in the larger cohort reinforced the opposing expression patterns and cooperative regulatory mechanism between DACH1 and DNMT1 during CRC progression.

In addition to elucidating the regulatory axis between DACH1 and DNMT1, our findings demonstrated a strong association between the expression levels of these two factors and clinicopathological features of CRC. Patients with poorly differentiated tumors, advanced stages, or lymphatic metastasis exhibited significantly lower DACH1 expression and higher DNMT1 expression, underscoring the potential of aberrant expression of DACH1 and DNMT1 as molecular biomarkers for the early diagnosis and prognostic evaluation of CRC. From a treatment perspective, DNMT1 inhibitors such as 5-azacytidine have been shown to be able to reverse SPARC promoter hypermethylation and thereby improving therapeutic efficacy [32]. This highlights the potential of epigenetic therapies targeting DNMT1 as a benefit for CRC patients.

The present study also has certain limitations. We primarily relied on the analysis of tissue samples, and while the findings suggest an association between DNMT1 overexpression, DACH1 promoter hypermethylation, and gene silencing, we did not further evaluate these mechanistic links through functional experiments like DNMT1 inhibition or knockdown. Additionally, although we integrated TCGA data with analyses of 120 clinical samples, the relatively small sample size may limit the generalizability of the results. The clinical relevance of DNMT1 and DACH1 requires further validation in larger, multicenter cohorts and preclinical therapeutic studies to provide a more comprehensive understanding of the DNMT1-DACH1 regulatory axis and its potential clinical applications in CRC patients.

Our study revealed the critical role of DNMT1-mediated DACH1 methylation in CRC progression through multi-layered analyses integrating bioinformatics and clinical samples. The progressive increase in DNMT1 expression drives the epigenetic silencing of DACH1 via promoter methylation, facilitating the transition from adenoma to carcinoma. This process is closely associated with clinical tumor differentiation, lymph node metastasis, and DUKES staging. Our findings provided significant evidence supporting the potential of the DNMT1-DACH1 regulatory axis as a biomarker and therapeutic target for CRC patients.

Author contributions

All authors listed have made a substantial, direct, and intellectual contribution to the work and approved it for publication.

Data availability

The original contributions presented in the study are included in the article/Supplementary Material, further inquiries can be directed to the corresponding author.

Ethics statement

The study was conducted in accordance with the Declaration of Helsinki and was approved by the Ethics Committee of Beijing Tongren Hospital. Written informed consent was obtained from all participants before sample collection. The studies were conducted in accordance with the local legislation and institutional requirements. The participants provided their written informed consent to participate in this study.

Funding

The author(s) declare that no financial support was received for the research and/or publication of this article.

Conflict of interest

The author(s) declared no potential conflicts of interest with respect to the research, authorship, and/or publication of this article.

Generative AI statement

The authors declare that no Generative AI was used in the creation of this manuscript.

References

1. Morgan E, Arnold M, Gini A, Lorenzoni V, Cabasag C, Laversanne M, et al. Global burden of colorectal cancer in 2020 and 2040: incidence and mortality estimates from GLOBOCAN. *Gut* (2023) **72**:338–44. doi:10.1136/gutjnl-2022-327736

2. Ganduri V, Rajasekaran K, Duraiyarasan S, Adefuye MA, Manjunatha N. Colorectal carcinoma, cyclooxygenases, and Cox inhibitors. *Cureus* (2022) **14**: e28579. doi:10.7759/cureus.28579

3. Noe O, Filipiak L, Royfman R, Campbell A, Lin L, Hamouda D, et al. Adenomatous polyposis coli in cancer and therapeutic implications. *Oncol Rev* (2021) **15**:534. doi:10.4081/oncol.2021.534

4. Lee HW, Song B, Kim K. Colorectal cancers with a residual adenoma component: clinicopathologic features and KRAS mutation. *Plos one* (2022) **17**: e0273723. doi:10.1371/journal.pone.0273723

5. Naccarati A, Polakova V, Pardini B, Vodickova L, Hemminki K, Kumar R, et al. Mutations and polymorphisms in TP53 gene—an overview on the role in colorectal cancer. *Mutagenesis* (2012) **27**:211–8. doi:10.1093/mutage/ger067

6. Li Z, Jiao X, Robertson AG, Di Sante G, Ashton AW, DiRocco A, et al. The DACH1 gene is frequently deleted in prostate cancer, restrains prostatic intraepithelial neoplasia, decreases DNA damage repair, and predicts therapy responses. *Oncogene* (2023) **42**:1857–73. doi:10.1038/s41388-023-02668-9

7. Zhao B, Zhou R, Ji C, Liu D, Wu T, Xu H, et al. The function of circRNA-0047604 in regulating the tumor suppressor gene DACH1 in breast cancer. *Biomed Res Int* (2022) **2022**:6589651. doi:10.1155/2022/6589651

8. Yu J, Jiang P, Zhao K, Chen Z, Zuo T, Chen B. Role of DACH1 on proliferation, invasion, and apoptosis in human lung adenocarcinoma cells. *Curr Mol Med* (2021) **21**:806–11. doi:10.2174/1566524021666210119094633

9. Wang P. Suppression of DACH1 promotes migration and invasion of colorectal cancer via activating TGF-β-mediated epithelial-mesenchymal transition. *Biochem Biophysical Res Commun* (2015) **460**:314–9. doi:10.1016/j.bbrc.2015.03.032

10. Yan W, Wu K, Herman JG, Brock MV, Fuks F, Yang L, et al. Epigenetic regulation of DACH1, a novel Wnt signaling component in colorectal cancer. *Epigenetics* (2013) **8**:1373–83. doi:10.4161/epi.26781

11. Hu X, Zhang L, Li Y, Ma X, Dai W, Gao X, et al. Organoid modelling identifies that DACH1 functions as a tumour promoter in colorectal cancer by modulating BMP signalling. *EBioMedicine* (2020) **56**:102800. doi:10.1016/j.ebiom.2020.102800

12. Bhootra S, Jill N, Shanmugam G, Rakshit S, Sarkar K. DNA methylation and cancer: transcriptional regulation, prognostic, and therapeutic perspective. *Med Oncol* (2023) **40**:71. doi:10.1007/s12032-022-01943-1

13. Geissler F, Nesic K, Kondrashova O, Dobrovic A, Swisher EM, Scott CL, et al. The role of aberrant DNA methylation in cancer initiation and clinical impacts. *Ther Adv Med Oncol* (2024) **16**:17588359231220511. doi:10.1177/17588359231220511

14. Kerdivel G, Amrouche F, Calmejane M-A, Carallis F, Hamroune J, Hantel C, et al. DNA hypermethylation driven by DNMT1 and DNMT3A favors tumor immune escape contributing to the aggressiveness of adrenocortical carcinoma. *Clin Epigenetics* (2023) **15**:121. doi:10.1186/s13148-023-01534-5

15. Liu Y, Sun Y, Yang J, Wu D, Yu S, Liu J, et al. DNMT1-targeting remodeling global DNA hypomethylation for enhanced tumor suppression and circumvented toxicity in oral squamous cell carcinoma. *Mol Cancer* (2024) **23**:104. doi:10.1186/s12943-024-01993-1

16. Xu X, Nie J, Lu L, Du C, Meng F, Song D. LINC00337 promotes tumor angiogenesis in colorectal cancer by recruiting DNMT1, which suppresses the expression of CNN1. *Cancer Gene Ther* (2021) **28**(12):1285–1297. doi:10.1038/s41417-020-00277-2

17. Zhai P, Zhang H, Li Q, Yang M, Guo Y, Xing C. DNMT1-mediated NR3C1 DNA methylation enables transcription activation of connexin40 and augments angiogenesis during colorectal cancer progression. *Gene* (2024) **892**: 147887. doi:10.1016/j.gene.2023.147887

18. Siegel RL, Wagle NS, Cercek A, Smith RA, Jemal A. Colorectal cancer statistics, 2023. *CA: a Cancer J clinicians* (2023) **73**:233–54. doi:10.3322/caac.21772

19. Riggs MJ, Lin N, Wang C, Piecoro DW, Miller RW, Hampton OA, et al. DACH1 mutation frequency in endometrial cancer is associated with high tumor mutation burden. *PloS one* (2020) **15**:e0244558. doi:10.1371/journal.pone.0244558

20. Yang J, Xu J, Wang W, Zhang B, Yu X, Shi S. Epigenetic regulation in the tumor microenvironment: molecular mechanisms and therapeutic targets. *Signal Transduction Targeted Therapy* (2023) **8**:210. doi:10.1038/s41392-023-01480-x

21. Feng Y, Wang L, Wang M. Alteration of DACH1 methylation patterns in lung cancer contributes to cell proliferation and migration. *Biochem Cell Biol* (2018) **96**: 602–9. doi:10.1139/bcb-2017-0279

22. Song J, Rechkoblit O, Bestor TH, Patel DJ. Structure of DNMT1-DNA complex reveals a role for autoinhibition in maintenance DNA methylation. *science* (2011) **331**:1036–40. doi:10.1126/science.1195380

23. Goyal R, Reinhardt R, Jeltsch A. Accuracy of DNA methylation pattern preservation by the Dnmt1 methyltransferase. *Nucleic Acids Res* (2006) **34**:1182–8. doi:10.1093/nar/gkl002

24. Peng D-F, Kanai Y, Sawada M, Ushijima S, Hiraoka N, Kitazawa S, et al. DNA methylation of multiple tumor-related genes in association with overexpression of DNA methyltransferase 1 (DNMT1) during multistage carcinogenesis of the pancreas. *Carcinogenesis* (2006) **27**:1160–8. doi:10.1093/carcin/bgi361

25. Biniszkiewicz D, Gribnau J, Ramsahoye B, Gaudet F, Eggan K, Humpherys D, et al. Dnmt1 overexpression causes genomic hypermethylation, loss of imprinting, and embryonic lethality. *Mol Cell Biol* (2002) **22**:2124–35. doi:10.1128/mcb.22.7.2124-2135.2002

26. Gao J, Wang L, Xu J, Zheng J, Man X, Wu H, et al. Aberrant DNA methyltransferase expression in pancreatic ductal adenocarcinoma development and progression. *J Exp & Clin Cancer Res* (2013) **32**:86–10. doi:10.1186/1756-9966-32-86

27. Sardari A, Usefi H. Machine learning-based meta-analysis of colorectal cancer and inflammatory bowel disease. *Plos one* (2023) **18**:e0290192. doi:10.1371/journal.pone.0290192

28. Al Mehedi Hasan M, Maniruzzaman M, Shin J. WGCNA and machine learning-based integrative bioinformatics analysis for identifying key genes of colorectal cancer. *IEEE Access* (2024) **12**:144350–63. doi:10.1109/access.2024.3472688

29. Liu C, Yu C, Song G, Fan X, Peng S, Zhang S, et al. Comprehensive analysis of miRNA-mRNA regulatory pairs associated with colorectal cancer and the role in tumor immunity. *BMC genomics* (2023) **24**:724. doi:10.1186/s12864-023-09635-4

30. Neto Í, Rocha J, Gaspar MM, Reis CP. Experimental murine models for colorectal cancer research. *Cancers* (2023) **15**:2570. doi:10.3390/cancers15092570

31. Zhang Q, Luo H, Xun J, Ma Y, Yang L, Zhang L, et al. Targeting PYCR2 inhibits intraperitoneal metastatic tumors of mouse colorectal cancer in a proline-independent approach. *Cancer Sci* (2023) **114**:908–20. doi:10.1111/cas.15635

32. Cheetham S, Tang M, Mesak F, Kennecke H, Owen D, Tai I. SPARC promoter hypermethylation in colorectal cancers can be reversed by 5-Aza-2′ deoxycytidine to increase SPARC expression and improve therapy response. *Br J Cancer* (2008) **98**: 1810–9. doi:10.1038/sj.bjc.6604377

EBM Experimental Biology and Medicine

TYPE Original Research
PUBLISHED 06 May 2025
DOI 10.3389/ebm.2025.10509

OPEN ACCESS

*CORRESPONDENCE
Lijie Zhang,
cyzlj8383@163.com

RECEIVED 21 January 2025
ACCEPTED 23 April 2025
PUBLISHED 06 May 2025

CITATION
Jiang S, Zhao S, Zhao Q, Wang Y, Zhang W, Feng Y and Zhang L (2025) Vaccination with synthetic long peptide and CpG 2395 in AddaVax induces potent anti-tumor effects.
Exp. Biol. Med. 250:10509.
doi: 10.3389/ebm.2025.10509

Vaccination with synthetic long peptide and CpG 2395 in AddaVax induces potent anti-tumor effects

Shanshan Jiang[1], Shuqi Zhao[1], Qiaojiajie Zhao[1], Yinfang Wang[1], Weihua Zhang[2], Yangmeng Feng[3] and Lijie Zhang[1]*

[1]Institute of Hematological Research, Shaanxi Provincial People's Hospital, Xi'an, China, [2]Department of Hematology, Shaanxi Provincial People's Hospital, Xi'an, China, [3]Central laboratory, Shaanxi Provincial People's Hospital, Xi'an, China

Abstract

Cancer/testis antigen HCA587, also known as MAGE-C2, highly expressed in a wide range of malignant tumors with unique immunological characteristics, serves as a potential target for tumor immunotherapy. Synthetic long peptides from HCA587 (HCA587 SLP) were proved to be highly immunogenic and promising in the application of cancer vaccine composed of Freud's adjuvant (FA) and CpG 1826, whereas, scarce $CD8^+$ T cell response may limit their anti-tumor effects during previous research. In this study, notwithstanding the multiple potential of IFN-α in immune modulation, there was no evidence of IFN-α in enhancing the immune response elicited by HCA587 SLP vaccine (HCA587 SLP + FA + CpG 1826). Given the unpleasant side-effects of Freud's adjuvant, then we applied AddaVax as a substitute for Freud's adjuvant, and we demonstrated that HCA587 SLP, formulated with AddaVax and CpG 2395, could induce more robust immune response in comparison with combined use of AddaVax and CpG 1826 through ELISpot assay. Furthermore, both IFN-γ-secreting $CD4^+$ T cell and $CD8^+$ T cell responses could be elicited by HCA587 SLP in combination with AddaVax and CpG 2395, and $CD8^+$ T cell response was most obviously observed under the condition of 10-h inhibition of cytokine secretion by brefeldin A post 10-h stimulation with HCA587 SLP, suggesting that cross presentation of exogenous long peptides to $CD8^+$ T cells may require more time than direct presentation to $CD4^+$ T cells. This vaccine formulation also conferred protection against challenge with HCA587-expressing B16 melanoma presented by delayed tumor growth and prolonged survival compared. This formulation of HCA587 SLP vaccine holds promise for the treatment of patients with cancer in future clinical trials.

KEYWORDS

AddaVax, synthetic long peptides, vaccine, anti-tumor effects, CpG 2395

Impact statement

Synthetic long peptide (SLP) vaccines have shown great potential in cancer treatment. However, lack of CD8+ T cell responses restricted their anti-tumor effects. It is well known that CD8+ T cells are the major "killer" in anti-tumor immunity. Therefore, efficient CD8+ T cell responses are the key to maximize the antitumor potential of SLP vaccine. In this study, we applied AddaVax and CpG 2395 as adjuvants to enhance the SLP-specific CD8+ T cell responses and improve the anti-tumor effects. This vaccine formula also appeared to be safer than Freud's adjuvants by avoiding the unpleasant side-effects such as tubercle and fester. Our research demonstrated the emulsion of SLP and CpG 2395 in AddaVax as a more effective and safer vaccine combination to combat the tumors.

Introduction

Cancer vaccines aim to stimulate the patient's adaptive immune system against specific tumor antigens in order to make tumors under control, and induce the long-term memory to prevent the tumor relapse [1–3]. The priority of successful cancer vaccines is to pinpoint the optimal target tumor antigen. Cancer/testis antigen HCA587, also known as MAGE-C2, is widely expressed in cancers including melanoma, hepatocellular carcinoma, bladder cancer, lung cancer, sarcoma, etc., but not normal tissues except testis [4, 5]. HCA587 protein vaccine has been proved to induce humoral and cellular immune responses efficiently, and confer protection in prophylactic and therapeutic animal models during our previous study [6]. All these findings make HCA587 an excellent target antigen for cancer immunotherapy.

Synthetic long peptides (SLP) contain multiple epitopes for presentation on MHC Ⅰ and MHC Ⅱ capable of inducing both $CD4^+$ and $CD8^+$ T cell responses. SLP also allows for administration to patients independent of their HLA types and avoiding immune tolerance through antigen presentation on non-professional antigen presenting cells (APCs) [7]. SLP is better processed by dendritic cells (DC) than protein, thus leads to enhanced $CD8^+$ T cell responses [8]. Moreover, usage of SLP can induce T-cell responses to subdominant epitopes of tumor antigen, thus exerting more broad biological activity against intact tumor cells. All these above mentioned properties endow SLP with an edge in the vaccine field.

Given the advantages of the synthetic long peptide as cancer vaccine, we tested the capacity of HCA587 SLP to stimulate HCA587-specific immune responses and antitumor effects in animal tumor model. Our previous results indicated that HCA587 SLP combined with CFA and CpG 1826 could elicit Th1-type immune response and decrease the tumor incidence, but no protection against developed HCA587-expressing tumors was observed compared to the adjuvant group [9]. The possible reason may lie in the dominating Th1 immune response barely composed of $CD8^+$ T cells producing IFN-γ.

As far as we know, $CD8^+$ T cells are the major "killer" in anti-tumor immunity, therefore, in order to maximize the antitumor potential of SLP vaccine-induced $CD8^+$ T cell response, the optimal adjuvants are in the need for vaccine development.

Many researches had suggested that IFN-α could enhance the cross-priming activity of DC through up-regulation of MHC class Ⅰ and co-stimulatory molecules, thereby eliciting more robust $CD8^+$ T cell response [10–12]. The multiple functions of IFN-α, including both direct and indirect anti-tumor effects, have made it suitable for the treatment of a number of cancers [13–15].

Compared to the paraffin oil used in Freund's adjuvants, Squalene is a kind of oil more readily metabolized. AddaVax is a squalene-based oil-in-water nano-emulsion, which can elicit both cellular (Th1) and humoral (Th2) immune responses, showing as a great potential adjuvant. Except for the depot effect and enhancement of antigen persistence at the injection site, this class of adjuvants can act through recruitment and activation of antigen presenting cells, and direct stimulation of cytokine and chemokine production by macrophages and granulocytes [16–18]. It was reported that peptide vaccines assembled with AddaVax and IFN-α-inducer could bring protection against tumor [19, 20].

Many reports from our and other research centers demonstrated that CpG has proved strong immune-stimulatory effects. It can be classified into three classes, CpG-A, CpG-B, and CpG-C based on their distinct chemical and biophysical properties. CpG-A was shown to be potent inducer of IFN-α production from pDCs, while CpG-B is a strong B cell stimulator. CpG-C (such as CpG 2395 or ODN 2395), which combine the effects of CpG-A and CpG-B, are potent inducers of IFN-α from pDC and strong B cell activators, proving to be more powerful adjuvant in cancer vaccine development [21–24].

In this study, we immunized the C57BL/6 mice with the emulsion of HCA587 SLP and CpG 2395 (source of endogenous IFN-α) with AddaVax to detect the vaccine-induced immune response and applied this emulsion to tumor-bearing mice to investigate anti-tumor effects in the therapeutic animal model.

Materials and methods

Mice and cell lines

6 to 8-week-old C57BL/6 mice were obtained from the Laboratory Animal Center of Xi'an jiao tong University. Mice were housed under standard pathogen-free conditions. All animal studies were approved by the Animal Care and Use Committees of Xi'an jiao tong University Health Science Center. Tumor cell line B16-HCA587 was generated by transfection of melanoma B16 cells of C57BL/6 origin by full-

length HCA587 cDNA sequence as described previously. The tumor cells were maintained in DMEM with 10% heat-inactivated fetal bovine serum (Invitrogen).

Antibodies and cytokines

Fluorescence labeled antibodies specific for CD4 and CD8, IFN-γ and Granzyme B were obtained from Biolegend. In all experiments, control mAbs of the respective IgG isotypes were included. rm-IFNα was purchased from pbl assay science.

Synthetic long peptides (SLP) and adjuvants

The peptides (13 peptides of 25–35 amino acids long with an overlapping of 14 amino acids) representing the HCA587 protein from amino acids 136 to 373, which harbors most of the published MHC class and epitopes were synthesized at the Ontores Biotechnologies Co. (HangZhou). All peptides were >90% pure as indicated by reverse High-performance Liquid Chromatography. Flu peptide STSADQQSLYQNAD (209-212) was used as a control peptide.

Squalene-based oil-in-water adjuvant AddaVax and ODN 2395 VacciGrade™ (5′-tcgtcgttttcggcgc:gcgccg-3′) were purchased from Invivogen. Complete Freund's Adjuvant (CFA) and Incomplete Freund's Adjuvant (IFA) were purchased from Sigma-Aldrich. All-phosphorothioate modified CpG oligonucleotide (CpG ODN) 1826 (5′ –tccatg acgttcctgacgtt-3′) was synthesized by the Shanghai Sangon Biological Engineering & Technology and Service.

Immunization procedures

C57BL/6 mice were immunized subcutaneously (s.c.) with 100 μL mixture of SLP (20 μg each peptide), 20 μg ODN 2395 VacciGrade™(CpG 2395) or CpG 1826 and AddaVax; or with synthetic long peptide pool (20 μg each peptide) at the volume of 100 μL admixed with 100 μL CFA/IFA in the presence of 20 μg CpG 1826 (subcutaneous injection next to the immunization site), rmIFN-α was administered s. c. twice a week at the dose of 2500 IU each mouse. Each animal received two immunizations at a 3-week interval. For the vaccination procedures involving Freund's Adjuvants (FA), IFA was used for the second immunization. Controls were set up by immunizing age-matched mice with adjuvants alone. 8 days after second immunization, the mice were euthanized and the splenocytes were harvested for the following experiments.

IFN-γ ELISPOT assay

After lysing RBCs, splenocytes were resuspended and seeded at a density of 5×10^5 cells per well in a 96-well nitrocellulose plates (MAHA N4550; Millipore) coated with anti-IFN-γ capture Abs (Mabtech), in the presence of HCA587-derived SLP (1.25 μg/mL each peptide). Flu peptide was used as a negative control for HCA587 SLP. After incubation for 20 h at 37°C, cells were removed, and the plates were washed 5 times with PBS, then incubated with a biotinylated anti-mouse IFN-γ detecting Ab (1:1000, 100 μL/well) for 2 h and streptavidin-alkaline phosphatase (1:1000, 100 μL/well) for 1 h at room temperature. After incubation, the dark violet spots were developed by the addition of substrate solution (BCIP/NBT-plus) (100μL/well). The spots displayed on the plate membranes were automatically counted with the ELISPOT reader.

Intracellular cytokine assay and flow cytometry

Splenocytes were resuspended and seeded at a density of 5×10^6 cells per well in a 24-well plates, in the presence of HCA587-derived SLP (1.25 μg/mL each peptide). For blocking the intracellular cytokine secretion, brefeldin A (5 μg/mL; Biolegend) was added to the cell culture after 3-h or 10-h stimulation with HCA587 SLP, and further cultured for 10 h. Simultaneous addition of brefeldin A and HCA587 SLP to the cell culture was also tested.

The cells were first stained with fluorescence labeled anti-mouse CD4 and CD8 antibodies, then fixed and permeabilized (Biolegend) according to the manufacturer's instructions, followed by staining with fluorescence-labeled antibodies against IFN-γ, Granzyme B, or isotype-matched control antibodies. Data were collected using a Beckman Coulter cytometer and analyzed using Kaluza software 2.1.

Evaluation of the anti-tumor effects of HCA587 SLP adjuvanted with CpG 2395 and AddaVax *in vivo*

The effect of HCA587 SLP vaccination (mixture of HCA587 SLP and CpG 2395, AddaVax) on tumor growth and survival was evaluated in therapeutic mode. Groups of C57BL/6 mice (n = 8–11) were inoculated with 2×10^4 B16-HCA587 tumor cells, the day after tumor challenge, they received the HCA587 SLP vaccination treatment (HCA587 SLP + AddaVax + CpG 2395) or just adjuvant control treatment (AddaVax + CpG 2395) according to the

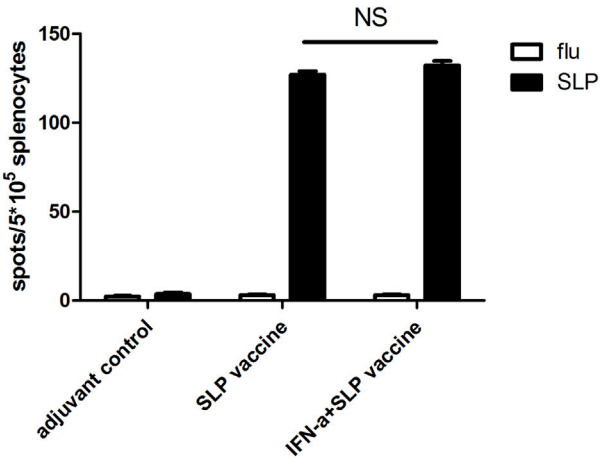

FIGURE 1
IFN-α could barely improve the immune response induced by SLP vaccine (HCA587 + FA + CpG1826) further. 6-to-8-week female C57BL/6 mice were vaccinated with SLP vaccine (HCA587 + FA + CpG1826) according to a prime-boost procedure (day 0 and day 21), for "INF-α + SLP vaccine" group, recombinant IFN-α (rmIFN-α) was given subcutaneously (s.c.) twice a week at the dose of 2500 IU each mouse. 8 days after the boost vaccination, mice were sacrificed and splenocytes were re-stimulated with HCA587 SLP (1.25 μg/mL each peptide) or irrelevant flu peptide (10 μg/mL) for 20 h. IFN-γ-producing cells were detected by ELISPOT assay. Data were presented as mean ± SD. NS, $P > 0.05$.

immunization procedures as above mentioned. Mouse survival was monitored daily, and the tumor length and width were measured every 2–3 days with a caliper, and calculated using the following formula: (length × width^2)/2.

Statistical analyses

All analysis and graphics were done using GraphPad Prism, version 5 for PC (GraphPad Software, San Diego, CA). The statistical significance of differential findings was determined using Student's *t*-test. Differences in the survival of mice were analyzed using the Kaplan-Meier method, and groups were compared using the log-rank test. Statistical significance was based on a value of $P < 0.05$.

Results

The local administration of rmIFN-α could not further improve the immune response elicited by the HCA587 SLP adjuvanted with FA and CpG1826

Our previous study found that HCA587 SLP vaccine (HCA587+FA + CpG 1826) elicited Th1 immune response, which presented limited effects in reducing the tumor growth and prolonging the survival of tumor-bearing mice. IFN-α has been proved to possess pleiotropic properties, including inhibition of proliferation and angiogenesis and induction of apoptosis [13]. Besides these, IFN-α also exerts immunomodulatory effects such as up-regulation of MHC class I, enhancement of maturation and activation of dendritic cells, thus cross-priming CD8$^+$ T cell response, which make it an appropriate candidate to combine with cancer vaccines [11, 12]. To verify whether IFN-α could enhance the immune response elicited by the HCA587 SLP vaccine, we immunized C57BL/6 mice with the recombinant HCA587 SLP formulated with FA and CpG1826, and IFN-α was delivered at the vaccine site twice per week for 4 weeks. Ten days after the second immunization, splenocytes were prepared and analyzed for the presence of HCA587 SLP-specific, IFN-γ-secreting cells using an ELISPOT assay. As depicted in Figure 1, addition of rmIFN-α could barely enhance the HCA587 SLP specific immune response intensity induced by the HCA587 SLP vaccine.

HCA587 SLP in combination with AddaVax and CpG 2395 (ODN 2395) induce the strong cellular immune response

Apart from the inefficiency of rmIFN-α addition in improving HCA587 SLP vaccine invFA + CpG 1826)-elicited immune responses, skin ulcers of vaccinated mice in HCA587 SLP vaccine were frequently observed. This unexpected side effect may be caused by the combined usage of CFA and rmIFN-α, which induced excessive inflammation. AddaVax, a squalene-based oil-in-water nano-emulsion, is more readily metabolized compared to the paraffin oil used in Freund's adjuvants. AddaVax can elicit both cellular (Th1) and humoral (Th2) immune responses through the activation of the innate immune system such as recruitment and activation of antigen presenting cells, cytokine and chemokine production of innate immune cells. All of these advantages indicated AddaVax as a great potential adjuvant. So we vaccinated C57BL/6 mice with HCA587 SLP emulsified with AddaVax in combination with different types of CpG (CpG 1826 and CpG 2395), thus testified the immune response through ELISPOT assay. As shown in Figure 2, specific cellular immune responses were induced by both types of CpG upon co-application of AddaVax with HCA587 SLP, moreover, a much enhanced cellular response was observed in CpG 2395 group than CpG 1826 group. Thereby the following experiments would adopt the combination of HCA587 SLP with CpG 2395 and AddaVax as the vaccine in the therapeutic model.

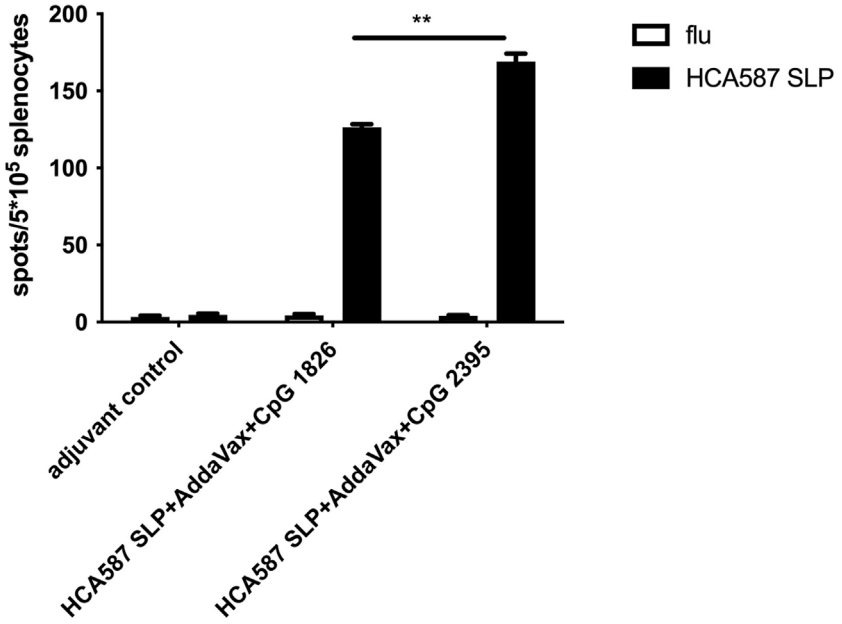

FIGURE 2
Immunization with HCA587 SLP in combination with AddaVax and CpG induces antigen-specific cellular immune responses. 6-to-8-week female C57BL/6 mice were immunized with HCA587 SLP emulsified in AddaVax with CpG 2395 (20 μg) or CPG 1826 (20 μg) at the base of tail twice 3 weeks away. 8 days after the boost vaccination, mice were sacrificed and splenocytes were re-stimulated with HCA587 SLP (1.25 μg/mL each peptide) or irrelevant flu peptide (10 μg/mL) for 20 h. IFN-γ-producing cells were detected by ELISPOT assay. Data were presented as mean ± SD. **, $P < 0.01$, HCA587 SLP + AddaVax + CpG 2395 in comparison with HCA587 SLP + AddaVax + CpG 1826.

HCA587 SLP adjuvanted with AddaVax and CpG 2395 could induce both CD4$^+$ and CD8$^+$ T cell responses

To further verify the efficient production of CD4$^+$ T-cell and CD8$^+$ T cell responses by HCA587 SLP in combination with AddaVax and CpG 2395, splenocytes from SLP vaccinated mice were re-stimulated with HCA587 SLP *ex vivo* under different conditions, such as simultaneous incubation of SLP and BFA for 6 h, addition of BFA to the cultured splenocytes post 3-h or 10-h stimulation with HCA587 SLP, and 10 h after BFA administration, all the splenocytes were analyzed for the T-cell markers CD4 and CD8 and IFN-γ secretion by multiparameter flow cytometry. As depicted in Figure 3, specific CD4$^+$ T-cell responses could be induced independent of the time points of BFA addition, albeit the IFN-γ secreting CD4$^+$ T-cells were less upon the simultaneous BFA addition with HCA587 SLP stimulation. However, CD8$^+$ T cell responses were most robust when the splenocytes were incubated with HCA587 SLP for 10 h, and then blockade of IFN-γ secretion by BFA for 10 h further. The cause for this discrepancy may lie in that SLP has to be ingested by DC firstly, trimmed to fit into the MHC Ⅰ, and then cross-presented to and primed CD8$^+$ T cells, whereas SLP could interact with MHC Ⅱ directly in the endosome, thus displayed at cell surface to activate CD4$^+$ T-cells.

HCA587 SLP combined with AddaVax and CpG 2395 generates antitumor effect in mice challenged with HCA587-expressing tumor cells

The therapeutic tumor model was performed to determine the whether the CD4$^+$ and CD8$^+$ T cell responses induced by HCA587 SLP immunization with AddaVax and CpG 2395 could translate into anti-tumor effect *in vivo*. B16-HCA587 cells, stably expressing HCA587, were established as described in previous study and adopted for subsequent studies.

C57BL/6 mice were inoculated with 2 × 10^4 B16-HCA587 cells and immunized 1 day later with the HCA587 SLP in combination with AddaVax and CpG 2395 (HCA587 SLP + AddaVax + CpG 2395) or adjuvant control (AddaVax + CpG 2395). Compared with adjuvant control, HCA587 SLP vaccinated with AddaVax and CpG 2395 conferred efficient protection against tumor, as demonstrated by the retarded tumor growth (Figure 4A) and prolonged survival of the tumor-bearing mice (Figure 4B). These results indicated that the vaccination of HCA587 SLP in combination with AddaVax and CpG 2395 could provide sufficient anti-tumor effects in our studies.

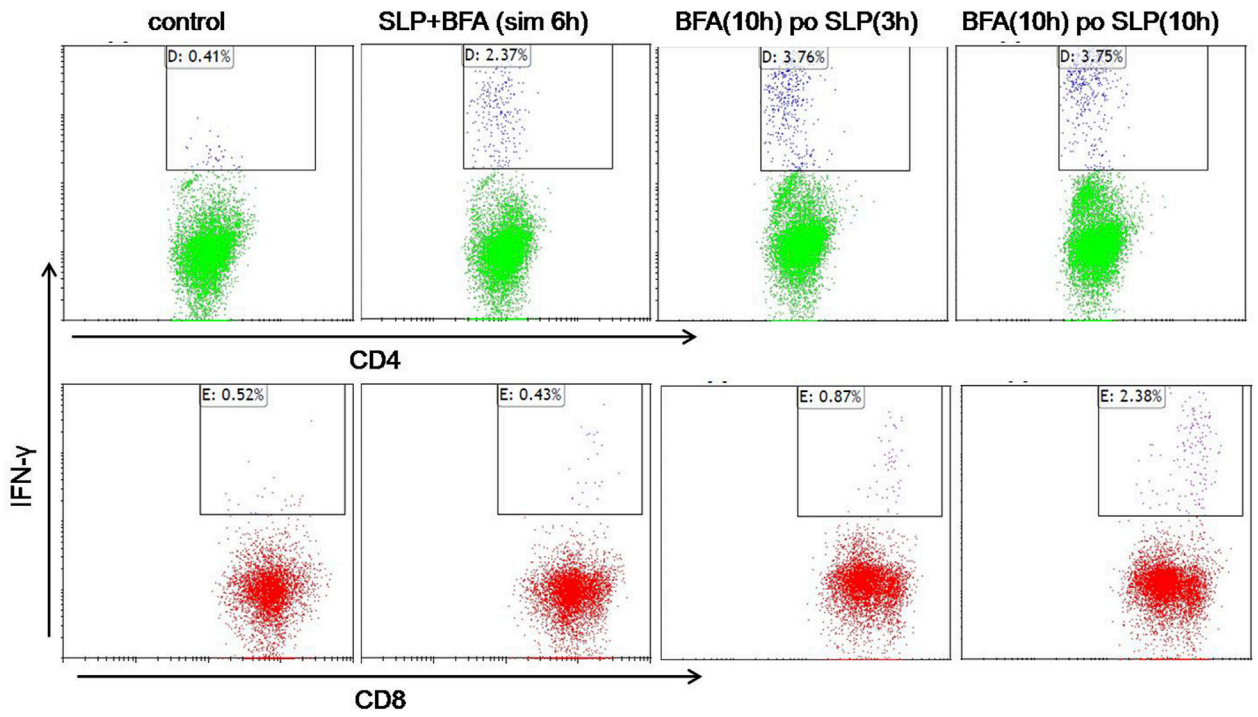

FIGURE 3
HCA587-specific CD4$^+$ T cells and CD8$^+$ T cells are induced by HCA587 SLP in combination with AddaVax and CpG 2395. 6-to-8-week female C57BL/6 mice were immunized with the emulsified combination of HCA587 SLP and CpG 2395 with AddaVax at the base of tail twice 3 weeks away. 8 days after the boost vaccination, the splenocytes of mice were stimulated *ex vivo* with HCA587 SLP (1.25 μg/ml each peptide) for ICCS. "BFA(10 h) po SLP(3 h)", brefeldin A (5 μg/mL) was added to the cell culture after 3-h stimulation with HCA587 SLP, and further cultured for 10 h. "BFA(10 h) po SLP(10 h)," brefeldin A (5 μg/mL) was added to the cell culture post 10-h stimulation with HCA587 SLP, and further cultured for 10 h. "SLP + BFA (sim 6 h)," simultaneous application of brefeldin A and HCA587 SLP was exerted to the splenocytes. The upper right quadrant displayed the positive cytokine-secreting cell population. IgG isotype staining served as control in flow cytometry.

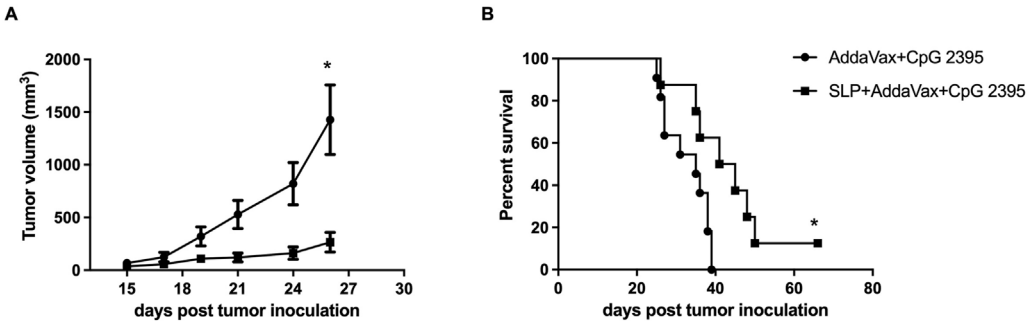

FIGURE 4
Therapeutic vaccination with HCA587 SLP assembled in AddaVax and CpG 2395 confers protection against HCA587-expressing tumors. 6-to-8-week female C57BL/6 mice were inoculated with 2 × 10^4 B16-HCA587 cells, 1 day post tumor inoculation, one group of them were vaccinated with HCA587 SLP + AddaVax + CpG 2395; the other group received the treatment of AddaVax + CpG 2395 (adjuvant control). Mouse survival was monitored daily, and the tumor length and width were measured every 2–3 days with a caliper, and calculated using the following formula: (length × width^2)/2. **(A)** Tumor size (n = 8–12 per group). Points represented mean of tumor volumes; bars represented SE. **(B)** Survival curve of tumor-bearing mice. *, $P < 0.05$.

Discussion

HCA587, one kind of cancer/testis antigens, possesses strong immunogenicity and has been confirmed to exert efficient anti-tumor effects during previous research, making it an ideal candidate for specific cancer immunity. There are many advantages for synthetic long peptide in the cancer vaccine development. Besides the speed of manufacturing, purity and safety, SLPs contain epitopes that are recognized by helper ($CD4^+$) and cytotoxic ($CD8^+$) T cells and, in contrast to short peptides, may need to be processed and presented to T cells by professional antigen-presenting cells [25, 26].

In our previous study, synthetic long peptides (14 peptides of 25–35 amino acids long with an overlapping of 14 amino acids) representing the HCA587 protein from amino acids 136 to 373, were applied to the immunization experiment and therapeutic model in the mode of emulsion with FA and CpG 1826. Albeit the specific IFN-γ-producing $CD4^+$ T cell response can be induced, but no sufficient protection was observed against developed HCA587-expressing tumors, which may be due to the deficiency of vaccine-elicited $CD8^+$ T cell response. Pleiotropic functions of IFN-α, especially enhancement of immune responses, make it an optimal component in cancer vaccine preparation. We applied rmIFN-α in combination with the HCA587 SLP vaccine (HCA587 SLP + FA + CpG 1826) in C57BL/6 mice, thus the cellular immune responses were detected through IFNγ-secreting ELISPOT assay. To our surprise, the application of rmIFN-α did not improve the intensity of HCA57 SLP-specific immune response. Besides that, given the adverse side-effects caused by the vaccine formulation, the local administration of rmIFN-α may be inappropriate for further research.

AddaVax is a squalene-based oil-in-water nano-emulsion, proved to be more powerful in eliciting both cellular and humoral immune responses than water-in-oil emulsion such as Freud's adjuvant, which is more adept at inducing humoral immunity. CpG 2395, belonging to CpG-C, displays its potent in inducing IFN-α production from pDC and activating B cells. The combined use of AddaVax and CpG 2395 could multiply their strengths in recruitment and activation of antigen presenting cells, thus enhancement of cellular immune responses. The encouraging research findings by Maynard et al. about HPV17 E6 synthetic long peptide vaccine formulated with CpG and AddaVax has brought us huge confidence in utilization of AddaVax and CpG 2395 for HCA587 SLP vaccination [20]. By applying the emulsion of HCA587 SLP and CpG 2395 with AddaVax, the SLP-specific IFN-γ-secreting $CD4^+$ and $CD8^+$ T cell responses were verified through ELISPOT and intracellular cytokine assay (ICCS). And during our ICCS experiment, we encountered an interesting phenomenon, the manifestation of IFN-γ secreted by $CD8^+$ T cells depending on when to apply BFA, which is an inhibitor of protein trafficking from endoplasmic reticulum (ER) to Golgi apparatus often used in intracellular cytokine assay [27]. Untimely BFA addition may block the transport of SLP-derived peptide-MHCl complex to the cell surface, which led to less primed IFN-γ-producing $CD8^+$ T cells, just as scarce IFN-γ-secreting $CD8^+$ T cells upon simultaneous incubation of BFA and SLP with splenocytes. The cross-priming of $CD8^+$ T cells taking more procedures and longer time than activation of $CD4^+$ T cells.

HCA587 SLP in combination with AddaVax and CpG 2395 provided sufficient protection against B16-HCA587 challenge in C57BL/6 mice, demonstrated by the decreased tumor growth and prolonged survival compared to the adjuvant group. After 55 days post tumor inoculation, there was only one tumor-bearing mouse alive, which received the HCA587 SLP combined with AddaVax and CpG 2395 treatment. To probe whether the SLP-specific immune response was the key to efficient anti-tumor effects, the splenocytes of this mouse were re-stimulated with SLP and the secretion of IFN-γ and Granzyme B were detected through ICCS, and finally robust production of Granzyme B in $CD8^+$ T cells was monitored, whereas IFN-γ-secreting $CD8^+$ T cells were rarely noticed (in supplementary data). Granzyme B is a serine-protease released by $CD8^+$ T cells and natural killer cells during the cellular immune response and represents one of the two dominant mechanisms by which cytotoxic T cells mediate cancer cell death. Larimer et al. reported that Granzyme B PET Imaging could serve as a predictive biomarker of cancer immunotherapy Response [28].

In summary, the present study demonstrates that HCA587 SLP in combination with AddaVax and CpG 2395 can induce robust $CD4^+$ T cell and $CD8^+$ T cell responses and potent antitumor immunity in the mouse. This data supports a potential clinical application of this HCA587-SLP combination with AddaVax and CpG 2395 in the treatment of HCA587-expressing cancer patients.

Author contributions

SJ, SZ, YW, and YF conducted the experiments; QZ and WZ analyzed the data; LZ wrote the manuscript and contributed to the funding acquisition. All authors contributed to the article and approved the submitted version.

Data availability

The original contributions presented in the study are included in the article/supplementary material, further inquiries can be directed to the corresponding author.

Ethics statement

The animal study was approved by Ethics Committee of Shaanxi Provincial People's Hospital and Ethics Committee of Xi'an Jiaotong University (2018-379). The study was conducted in accordance with the local legislation and institutional requirements.

Funding

The author(s) declare that financial support was received for the research and/or publication of this article. This work was supported by the National Natural Science Foundation of China (grant number 81801647); the Natural Science Foundation of Shaanxi Province (grant number 2022JQ-944); and Talent Support Program of Shaanxi Provincial People's Hospital (grant number 2022BJ-03, 2022JY-55 and 2022JY-56).

Acknowledgments

We appreciated the Shaanxi Engineering Research Center of Cell Immunology and the Shaanxi Provincial Key Laboratory of Infection and Immune Diseases for providing the experiment platform.

Conflict of interest

The author(s) declared no potential conflicts of interest with respect to the research, authorship, and/or publication of this article.

Generative AI statement

The authors declare that no Generative AI was used in the creation of this manuscript.

References

1. Drew L. How does a cancer vaccine work? *Nature* (2024) **627**(8005):S34–S35. doi:10.1038/d41586-024-00841-y

2. Liu J, Fu MY, Wang MN, Wan DD, Wei YQ, Wei XW. Cancer vaccines as promising immuno-therapeutics: platforms and current progress. *J Hematol Oncol* (2022) **15**(1):28. doi:10.1186/s13045-022-01247-x

3. Saxena M, van der Burg SH, Melief CJM, Bhardwaj N. Therapeutic cancer vaccines. *Nat Rev Cancer* (2021) **21**(6):360–78. doi:10.1038/s41568-021-00346-0

4. Simpson AJ, Caballero OL, Jungbluth A, Chen YT, Old LJ. Cancer/testis antigens, gametogenesis and cancer. *Nat Rev Cancer* (2005) **5**(8):615–25. doi:10.1038/nrc1669

5. Li B, Qian XP, Pang XW, Zou WZ, Wang YP, Wu HY, et al. HCA587 antigen expression in normal tissues and cancers: correlation with tumor differentiation in hepatocellular carcinoma. *Lab Invest* (2003) **83**(8):1185–92. doi:10.1097/01.lab.0000080605.73839.96

6. Chen JJ, Zhang LJ, Wen WG, Hao JQ, Zeng PM, Qian XP, et al. Induction of HCA587-specific antitumor immunity with HCA587 protein formulated with CpG and ISCOM in mice. *PLoS One* (2012) **7**(10):e47219. doi:10.1371/journal.pone.0047219

7. Khazaie K, Bonertz A, Beckhove P. Current developments with peptide-based human tumor vaccines. *Curr Opin Oncol* (2009) **21**(6):524–30. doi:10.1097/cco.0b013e328331a78e

8. Rosalia RA, Quakkelaar ED, Redeker A, Khan S, Camps M, Drijfhout JW, et al. Dendritic cells process synthetic long peptides better than whole protein, improving antigen presentation and T-cell activation. *Eur J Immunol* (2013) **43**(10):2554–65. doi:10.1002/eji.201343324

9. Zhang LJ, Chen JJ, Song X, Wen WG, Li Y, Zhang Y, et al. Cancer/testis antigen HCA587-derived long peptide vaccine generates potent immunologic responses and antitumor effects in mouse model. *Oncol Res* (2014) **21**(4):193–200. doi:10.3727/096504014x13887748696789

10. Prell RA, Li B, Lin JM, VanRoey M, Jooss K. Administration of IFN-alpha enhances the efficacy of a granulocyte macrophage colony stimulating factor-secreting tumor cell vaccine. *Cancer Res* (2005) **65**(6):2449–56. doi:10.1158/0008-5472.can-04-1975

11. Le Bon A, Etchart N, Rossmann C, Ashton M, Hou S, Gewert D, et al. Cross-priming of $CD8^+$ T cells stimulated by virus-induced type I interferon. *Nat Immunol* (2003) **4**(10):1009–15. doi:10.1038/ni978

12. Fuertes MB, Kacha AK, Kline J, Woo SR, Kranz DM, Murphy KM, et al. Host type I IFN signals are required for antitumor CD8+ T cell responses through CD8α+ dendritic cells. *J Exp Med* (2011) **208**(10):2005–16. doi:10.1084/jem.20101159

13. Borden EC. Interferons α and β in cancer: therapeutic opportunities from new insights. *Nat Rev Drug Discov* (2019) **18**(3):219–34. doi:10.1038/s41573-018-0011-2

14. Hu B, Yu MC, Ma XL, Sun JL, Liu CL, Wang CY, et al. IFNα potentiates anti-PD-1 efficacy by remodeling glucose metabolism in the hepatocellular carcinoma microenvironment. *Cancer Discov* (2022) **12**(7):1718–41. doi:10.1158/2159-8290.cd-21-1022

15. Fairchild PJ, Davies TJ. Boosting antitumour immunity through targeted delivery of interferon-α. *Trends Mol Med* (2019) **25**(11):935–7. doi:10.1016/j.molmed.2019.09.001

16. Mbow ML, De Gregorio E, Valiante NM, Rappuoli R. New adjuvants for human vaccines. *Curr Opin Immunol* (2010) **22**(3):411–6. doi:10.1016/j.coi.2010.04.004

17. Calabro S, Tritto E, Pezzotti A, Taccone M, Muzzi A, Bertholet S, et al. The adjuvant effect of MF59 is due to the oil-in-water emulsion formulation, none of the individual components induce a comparable adjuvant effect. *Vaccine* (2013) **31**(33):3363–9. doi:10.1016/j.vaccine.2013.05.007

18. Schetters STT, Kruijssen LJW, Crommentuijn MHW, Kalay H, Haan JMM, Kooyk Y. Immunological dynamics after subcutaneous immunization with a squalene-based oil-in-water adjuvant. *FASEB J* (2020) **34**(9):12406–18. doi:10.1096/fj.202000848r

19. Delitto D, Zabransky DJ, Chen F, Thompson ED, Zimmerman JW, Armstrong TD, et al. Implantation of a neoantigen-targeted hydrogel vaccine prevents recurrence of pancreatic adenocarcinoma after incomplete resection. *Oncoimmunology* (2021) **10**(1):2001159. doi:10.1080/2162402x.2021.2001159

20. Maynard SK, Marshall JD, MacGill RS, Yu L, Cann JA, Cheng LI, et al. Vaccination with synthetic long peptide formulated with CpG in an oil-in-water emulsion induces robust E7-specific CD8 T cell responses and TC-1 tumor eradication. *BMC Cancer* (2019) **19**(1):540. doi:10.1186/s12885-019-5725-y

21. Jurk M, Schulte B, Kritzler A, Noll B, Uhlmann E, Wader T, et al. C-Class CpG ODN: sequence requirements and characterization of immunostimulatory activities on mRNA level. *Immunobiology* (2004) **209**(1-2):141–54. doi:10.1016/j.imbio.2004.02.006

22. Abel K, Wang Y, Fritts L, Sanchez E, Chung E, Fitzgerald-Bocarsly P, et al. Deoxycytidyl-deoxyguanosine oligonucleotide classes A, B, and C induce distinct cytokine gene expression patterns in rhesus monkey peripheral blood mononuclear cells and distinct alpha interferon responses in TLR9-expressing rhesus monkey plasmacytoid dendritic cells. *Clin Vaccin Immunol* (2005) **12**(5):606–21. doi:10.1128/cdli.12.5.606-621.2005

23. Dorn A, Kippenberger S. Clinical application of CpG-, non-CpG-, and antisense oligodeoxynucleotides as immunomodulators. *Curr Opin Mol Ther* (2008) **10**(1):10–20. doi:10.1159/000088065

24. Vollmer J, Weeratna R, Payette P, Jurk M, Schetter C, Laucht M, et al. Characterization of three CpG oligodeoxynucleotide classes with distinct immunostimulatory activities. *Eur J Immunol* (2004) **34**(1):251–62. doi:10.1002/eji.200324032

25. Corradin G, Kajava AV, Verdini A. Long synthetic peptides for the production of vaccines and drugs: a technological platform coming of age. *Sci Transl Med* (2010) **2**(50):50rv3. doi:10.1126/scitranslmed.3001387

26. Chen XT, Yang J, Wang LF, Liu BR. Personalized neoantigen vaccination with synthetic long peptides: recent advances and future perspectives. *Theranostics* (2020) **10**(13):6011–23. doi:10.7150/thno.38742

27. Chardin P, McCormick F. Brefeldin A: the advantage of being uncompetitive. *Cell* (1999) **97**(2):153–5. doi:10.1016/s0092-8674(00)80724-2

28. Larimer BM, Wehrenberg-Klee E, Dubois F, Mehta A, Kalomeris T, Flaherty K, et al. Granzyme B PET imaging as a predictive biomarker of immunotherapy response. *Cancer Res* (2017) **77**(9):2318–27. doi:10.1158/0008-5472.can-16-3346

EBM Experimental Biology and Medicine

TYPE Mini Review
PUBLISHED 28 April 2025
DOI 10.3389/ebm.2025.10490

OPEN ACCESS

*CORRESPONDENCE
Ying Kong,
kongying1502@csu.edu.cn

RECEIVED 04 January 2025
ACCEPTED 11 April 2025
PUBLISHED 28 April 2025

CITATION
Sun Y, Luo Z, Fu Y, Ngo T, Wang W, Wang Y and Kong Y (2025) Primary cilia and inflammatory response: unveiling new mechanisms in osteoarthritis progression.
Exp. Biol. Med. 250:10490.
doi: 10.3389/ebm.2025.10490

Primary cilia and inflammatory response: unveiling new mechanisms in osteoarthritis progression

Yuyan Sun, Ziyu Luo, Yuanyuan Fu, ThaiNamanh Ngo, Wen Wang, Yuanrong Wang and Ying Kong*

Department of Rehabilitation, The Second Xiangya Hospital, Central South University, Changsha, China

Abstract

Osteoarthritis (OA) is a common degenerative joint disease that can lead to chronic pain and disability. The pathogenesis of OA involves chronic low-grade inflammation, characterized by the degradation of chondrocytes, inflammation of the synovium, and systemic low-grade inflammation. This inflammatory response accelerates the progression of OA and contributes to pain and functional impairment. Primary cilia play a crucial role in cellular signal transduction and the maintenance of cartilage matrix homeostasis, and their dysfunction is closely linked to inflammatory responses. Given these roles, primary cilia may significantly contribute to the pathogenesis of OA. This review explores inflammation-associated signaling pathways in OA, including NF-κB, MAPK, JAK/STAT, and PI3K/AKT/mTOR signaling. In addition, we place particular emphasis on cilia-mediated inflammatory modulation in OA. Primary cilia mediate chondrocyte responses to mechanical loading and inflammatory cytokines via pathways including NF-κB, MAPK, TRPV4, and Hedgehog signaling. Notably, alterations in the length and incidence of primary cilia in chondrocytes during OA further underscore their potential role in disease pathogenesis. The identification of biomarkers and therapeutic targets related to primary cilia and inflammatory pathways offers new potential for the treatment and management of OA.

KEYWORDS

osteoarthritis, primary cilia, inflammatory responses, chondrocytes, inflammatory signaling pathways

Impact statement

This review is crucial for the field of osteoarthritis research as it unveils the critical role of primary cilia in the inflammatory pathways of osteoarthritis, a previously under explored area. By investigating the complex molecular mechanisms linking primary cilia and inflammation signaling, the review provides new insights into how primary cilia

TABLE 1 Comparison of different types of joint inflammations.

Disease	Osteoarthritis (OA)	Rheumatoid arthritis (RA)	Psoriatic arthritis (PsA)	Gouty arthritis (GA)	Ankylosing spondylitis (AS)
Nature of Disease	Degenerative joint disease with chronic low-grade inflammation	Chronic inflammatory autoimmune disease	Chronic inflammatory autoimmune disease	Autoimmune and metabolic disease with acute inflammation	Chronic inflammatory autoimmune disease, spondyloarthritis
Mechanism of Inflammation	Joint damage or overuse triggers an immune response, leading to local tissue damage, failed tissue repair, and low-grade inflammation within the joint	Persistent autoimmune response causes synovial inflammation, with elevated pro-inflammatory cytokines (e.g., IL-6, TNF-α) and autoantibodies [e.g., Rheumatoid factor (RF), Anti-citrullinated protein antibodies (ACPA)]	Interaction of genetic susceptibility and environmental triggers leads to dysregulation of immune-inflammatory pathways	Elevated serum uric acid levels lead to deposition of monosodium urate crystals in joint tissues, activating an inflammatory response	Genetic factors (e.g., HLA-B27) and autoimmune response, involving Th17-related inflammatory signaling
Inflammatory Cell Infiltration	Macrophages, mast cells	T cells, B cells, macrophages, fibroblasts	Macrophages, T cells, neutrophils, dendritic cells	Lymphocytes, dendritic cells, macrophages, neutrophils, mast cells	Macrophages, neutrophils, mast cells
Inflammatory Markers	IL-1β, TNF-α, IL-6, MMPs, C-reactive protein (CRP)	CRP, Erythrocyte sedimentation rate (ESR), RF, ACPA, IL-6, TNF-α, IFN-γ, Th17A	IL-17, IL-23	IL-1β, TNF-α, IL-6	IL-23, IL-17
Affected Sites	Weight-bearing joints (knees, hips, spine, distal interphalangeal joints of the hand)	Hands, arms, knees	Asymmetric involvement of large joints, monoarticular or oligoarticular, enthesitis, and dactylitis	Monoarticular or polyarticular, commonly affecting the big toe	Sacroiliac joints, spine, hip joints, knee joints
Disease Progression	Cartilage degeneration, osteophyte formation, joint capsule thickening, synovial inflammation	Chronic synovial joint inflammation, pannus formation, bone erosion, and joint destruction	Skin manifestations often precede joint symptoms	Acute attacks with symptom-free intervals	Chronic back pain and stiffness, potentially progressing to spinal ankylosis
Treatment Strategies	Nonsteroidal anti-inflammatory drugs (NSAIDs), physical therapy, analgesics, steroids, hyaluronic acid	Disease-modifying antirheumatic drugs (DMARDs), NSAIDs, immunosuppressive corticosteroids, physical therapy	NSAIDs, biologics, anti-TNF-α agents, anti-IL-17 agents, anti-IL-12/IL-23, skin treatments	Colchicine, NSAIDs, corticosteroids, IL-1β inhibitors, urate-lowering drugs	Physical therapy, NSAIDs, TNF inhibitors, IL-17 inhibitors, JAK inhibitors
References	Robinson WH et al. (2016) [6]	Lin YJ et al. (2020) [7] Scott DL et al. (2010) [8]	Porta S et al. (2021) [9] Talotta R et al. (2019) [10]	Liu et al. (2023) [11] Cabău G et al. (2020) [12]	Wei et al. (2025) [13] Voruganti A et al. (2020) [14]

contribute to chronic inflammation and cartilage degradation. These findings may prove valuable for the early diagnosis and targeted treatment of osteoarthritis.

Introduction

Osteoarthritis (OA) is a prevalent chronic joint disease characterized by functional impairment, pain, cartilage degeneration, synovial inflammation, and structural alterations in the subchondral bone, including sclerosis, osteophyte formation, and cystic lesions [1]. As a leading cause of disability and chronic pain globally, OA affects over 500 million people (7% of the world's population), with a particularly high incidence in the elderly and women [2, 3]. This condition significantly diminishes mobility, physical function, and quality of life in older adults [4]. Despite its widespread impact, the treatment of OA remains challenging, primarily due to the limited understanding of its pathogenesis and the mechanisms underlying its progression [5]. Therefore, there is an urgent need for in-depth research into the key signaling pathways and molecular mechanisms involved in OA, along with the identification of potential biomarkers and therapeutic targets for its various stages.

OA was traditionally regarded as a non-inflammatory joint disease, but recent studies have highlighted the critical role of inflammatory responses in its pathogenesis [6]. Unlike the acute inflammation observed in autoimmune diseases like rheumatoid arthritis (RA), OA is characterized by low-grade, chronic inflammation [4]. Table 1 presents a comparison of osteoarthritis with other types of joint inflammations. A hallmark of the pathological process of OA is synovitis, which involves synovial hyperplasia and the infiltration of inflammatory cells into the synovium. These immune cells

release pro-inflammatory factors such as interleukin-1β (IL-1β), tumor necrosis factor-α (TNF-α), and nitric oxide (NO). This inflammatory factors subsequently activate matrix metalloproteinases (MMPs) and aggrecanases, further accelerating cartilage degradation. Ultimately, these processes lead to joint pain and functional impairment [6, 15]. Synovial fluid serves as a multi-functional mediator between the synovium and articular cartilage, and the inflammatory microenvironment of the synovial fluid plays a pivotal role in regulating OA pathogenesis [16]. OA synovial fluid not only drives macrophage polarization toward the pro-inflammatory M1 phenotype [17] but also upregulate catabolic enzymes matrix metalloproteinases (MMPs) [16]. Additionally, mast cells—one of the dominant infiltrating immune cell populations in OA synovium—contribute to synovitis progression and osteophyte formation through the release of pro-inflammatory mediators [18]. In addition to local joint inflammation, systemic inflammation also plays a significant role in the pathogenesis of OA [6]. For instance, obesity, a known risk factor for OA, not only increases the mechanical load on the joints but also triggers systemic low-grade inflammation. This inflammation is mediated by inflammatory factors released by adipose tissue, such as adipokines and other pro-inflammatory cytokines, which further promote the onset of OA [6, 15, 19, 20]. Therefore, inflammation accelerates the progression of OA by fostering chondrocyte degradation, synovial inflammation, and systemic low-grade inflammation, thereby causing pain and functional impairment in patients.

Primary cilia are microtubule-based structures that extend from the surface of cells. They are widely distributed across various cell types, including chondrocytes, synovial cells, and other joint tissue cells, and play an important role in sensing and transmitting mechanical and chemical signals in these cells [21]. Growing evidence indicates that primary cilia are essential for chondrocyte signal transduction and the maintenance of cartilage matrix homeostasis, particularly in the pathogenesis of OA [21]. The direction, length, and number of cilia in chondrocytes are closely linked to OA progression, and their dysfunction may contribute to inflammatory responses and cartilage degeneration [22, 23]. Consequently, regulating primary cilia and their associated signaling pathways not only enhances our understanding of OA pathogenesis but also offers potential therapeutic targets for treatment.

In recent years, there has been increasing attention on the role of primary cilia in the inflammatory signaling processes of OA. This review, therefore, focuses on the involvement of primary cilia in OA-related inflammation. It examines the inflammatory signaling pathways in which primary cilia are involved, as well as the bidirectional regulatory mechanisms between inflammation and primary cilia. The goal of this review is to elucidate the potential roles and mechanisms of primary cilia in OA inflammation. We hope that this article will offer new insights for the treatment of OA.

Inflammatory signaling pathways in osteoarthritis

In OA, sustained chronic inflammation is associated with the degradation of articular cartilage and synovial hyperplasia, promoting joint degeneration and triggering pain responses [24]. These inflammatory reactions are mediated by a series of cytokines, chemokines, and enzymes [25]. Below are several key inflammatory signaling pathways closely associated with OA. The major signaling pathways that regulate inflammation in OA cartilage include NF-κB, JAK/STAT, MAPK, and PI3K/AKT/mTOR, among others [25, 26] (Figure 1).

NF-κB signaling pathway

NF-κB is a family of transcription factors that likely plays a critical role in various biological processes, including immune responses, inflammation, cell differentiation, as well as cell proliferation and apoptosis [27]. NF-κB activation occurs mainly through two pathways: the classical and non-classical pathways. In the classical pathway, various immune mediators, such as pro-inflammatory cytokines (e.g., TNF-α and IL-1β), activate the IKK complex (IKKα/β/γ), leading to the phosphorylation and degradation of IκB proteins. This process releases NF-κB dimers (e.g., p65/p50/RelB), which translocate to the nucleus and initiate the transcription of target genes. This process is rapid and reversible [28, 29]. In contrast, the non-classical pathway primarily involves IKKα activation, which leads to the production of p52 and RelB, activating target gene transcription. This pathway is slower and more sustained [30].

In the pathogenesis of OA, NF-κB is a transcription factor extensively involved in the joint inflammation and tissue-destruction processes [5]. Mechanical receptors on the cell membrane of chondrocytes, cytokine receptors, TNFR, and TLRs, activated by pro-inflammatory mediators, mechanical stress, or fibronectin fragments, induce NF-κB signaling [31]. NF-κB signaling promotes the secretion of various degradative enzymes, such as MMPs (including MMP1, MMP9, MMP13) and a disintegrin and metalloproteinases with thrombospondin motifs (ADAMTS, e.g., ADAMTS5), which lead to cartilage degradation [29]. Moreover, NF-κB mediates the production of catabolic cytokines and chemokines, including TNF-α, IL-1β, IL-6, receptor activator of NF-κB ligand (RANKL), and IL-8. This increases the production of MMPs, reduces the synthesis of collagen and proteoglycans, and enhances NF-κB activation through a positive feedback loop [32]. Additionally, NF-κB promotes joint damage by inducing the synthesis of pro-inflammatory molecules such as nitric oxide (NO), cyclooxygenase-2 (COX-2), nitric oxide synthase (NOS), and prostaglandin E2 (PGE2), thereby contributing to cartilage inflammation, the production of catabolic factors, and chondrocyte apoptosis [33, 34]. Furthermore, the NF-κB

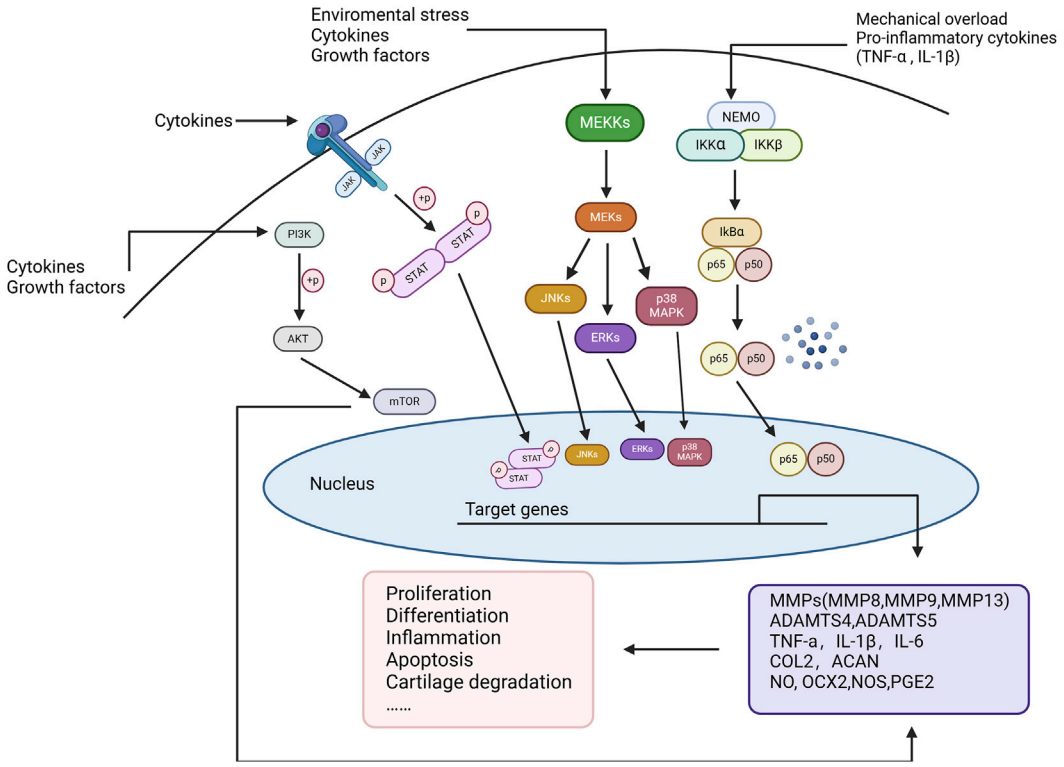

FIGURE 1
Key inflammatory signaling pathways in OA. Environmental stress, mechanical overload, and pro-inflammatory cytokines (such as TNF-α and IL-1β) activate multiple signaling pathways, including NF-κB, MAPK, JAK/STAT, and PI3K/AKT/mTOR, to regulate cellular inflammatory responses. These pathways, through multi-level phosphorylation cascades, ultimately translocate into the nucleus to regulate the expression of key genes associated with OA progression, such as matrix metalloproteinases (MMPs), ADAMTS enzymes, TNF-α, IL-1β, and IL-6. This process induces cellular proliferation, differentiation, inflammation, apoptosis, and cartilage degradation, playing a pivotal role in OA pathogenesis.

pathway interacts with other signaling pathways, such as Wnt, to collectively drive the inflammatory response and tissue degeneration in OA [35].

MAPK signaling pathway

Mitogen-activated protein kinases (MAPKs) are a group of serine/threonine protein kinases found in eukaryotes [36]. MAPK signaling is activated by extracellular stimuli such as pro-inflammatory cytokines, growth factors, and oxidative stress. This signaling transduces the extracellular signal into the nucleus via a phosphorylation cascade, regulating various cellular processes [37], such as inflammation responses, catabolism, and degradation of the extracellular matrix, that can have a crucial role in OA development [38]. The extracellular signal-regulated kinase (ERK), c-Jun N-terminal kinase (JNK), and p38 MAPK are the most studied MAPK family members involved in OA pathogenesis. Each cascade consists of at least three enzymes to activate the signaling pathway (MAPKK, MAPK kinase, and MAPK) [39]. Under inflammatory conditions, phosphorylation levels of ERK1, JNK, and p38 MAPK are upregulated. This upregulation stimulates downstream transcription factors, thereby promoting the production of inflammatory cytokines and the progression of inflammatory responses [38]. Inflammatory factors like IL-1 can activate the MAPK signaling pathways, subsequently promoting the expression and activity of MMPs and leading to the degradation of the cartilage [40]. Recent studies have confirmed that both JNK and p38 MAPK signaling pathways are associated with chondrocyte apoptosis in OA [41], while the p38 MAPK and ERK1/2 pathways are closely linked to the cross-talk between bone and cartilage [42, 43].

JAK/STAT signaling pathway

The JAK/STAT signaling pathway consists of three components: Janus kinases (JAKs), signal transducer and activator of transcription proteins (STATs), and tyrosine kinase-associated receptors [44]. This pathway regulates cell proliferation, differentiation, apoptosis, and inflammation

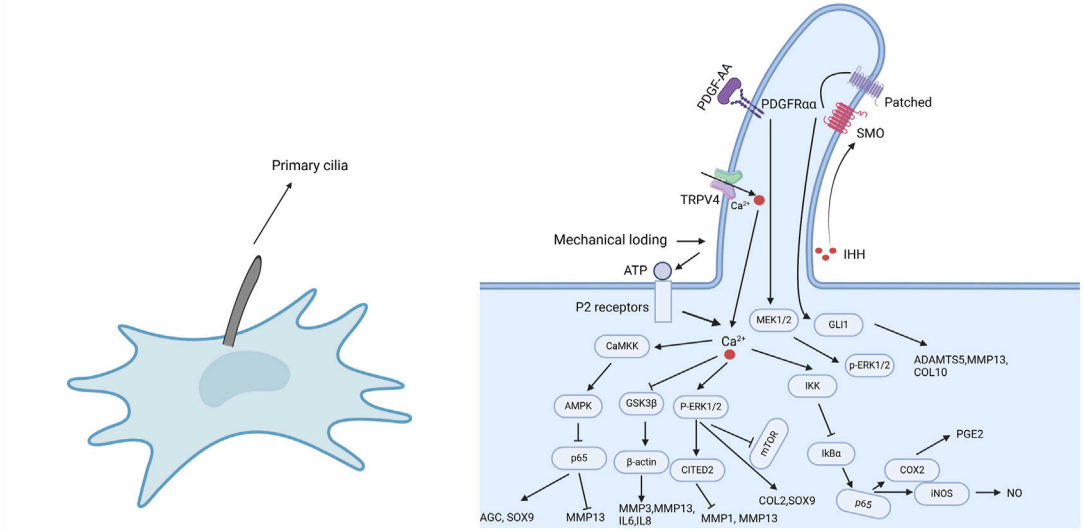

FIGURE 2
The role of primary cilia in inflammatory responses. As cellular sensory organelles, primary cilia regulate multiple signaling pathways, including NF-κB, MAPK, TRPV4, and Hedgehog pathways. Mechanical loading or external stimuli trigger Ca^{2+} influx through TRPV4 channels, activating a cascade of signaling events, such as the CaMKK-AMPK-NF-κB axis to regulate inflammation, the GSK3β pathway to influence cytoskeletal dynamics, and the P-ERK1/2 pathway to suppress the overexpression of inflammatory factors. Additionally, primary cilia modulate IHH and PDGFRα signaling, contributing to the regulation of MMPs, ADAMTS enzymes, and inflammation-related factors. These signaling pathways work in concert to regulate cartilage homeostasis, inflammatory responses, and the pathological progression of osteoarthritis.

[39, 44]. In the pathogenesis of OA, pro-inflammatory cytokines such as IL-1β, IL-6, and TNF-α bind to cell membrane receptors, activating JAK kinases, which in turn phosphorylate STAT transcription factors [45]. The phosphorylated STATs dimerize and translocate to the nucleus, where they bind to promoter regions of target genes to regulate gene expression [44], promoting synovial and cartilage inflammation, as well as the degeneration of cartilage [45]. For example, IL-1β and IL-6 activate JAK/STAT3 signaling in chondrocytes, inducing the expression of MMPs like MMP-13, directly contributing to cartilage matrix degradation and exacerbating cartilage damage [46, 47]. Simultaneously, the JAK/STAT pathway can induce the production of pro-inflammatory factors, such as IL-6, thereby creating a vicious cycle that intensifies synovial inflammation and promotes OA progression [48]. The JAK/STAT signaling pathway also regulates factors such as ELP2 [49] and RANKL [50], which are involved in the differentiation of osteoblasts and osteoclasts. This pathway also induces pathological angiogenesis in subchondral bone through HIF-α/VEGF pathways [51] and factors like EGFL7 [52], thereby exacerbating joint pathological changes.

PI3K/AKT/mTOR signaling pathway

The PI3K/AKT/mTOR signaling pathway consists of PI3K, AKT, and mTOR. When insulin, glucose, and various growth factors and cytokines stimulate the cell membrane, PI3K is activated. PI3K catalyzes the phosphorylation of phosphatidylinositol-4,5-bisphosphate (PIP2) to produce phosphatidylinositol-3,4,5-trisphosphate (PIP3), which activates the downstream AKT protein [53]. The downstream effector of PI3K, mTOR, also functions as a regulator of pro-inflammatory responses in the synovium [53]. In OA pathology, chondrocytes and synovial cells excessively produce inflammatory mediators such as IL-1β and NO [32]. Stimulation by cytokines like IL-1β rapidly phosphorylates PI3K and AKT, leading to the abnormal activation of the PI3K/AKT pathway [54]. This activation increases the production of MMPs by chondrocytes through multiple downstream target proteins [55]. Additionally, protein kinase A (PKA)/AKT can activate NF-κB by affecting the upstream IκB kinase, leading to the phosphorylation and nuclear translocation of NF-κB p65. The interaction between PI3K/AKT and NF-κB enhances the release of inflammatory factor [53].

TABLE 2 Inflammatory signaling pathways involving primary cilia.

Study	Cell and tissue	Intervention	Ion channel	Results
Wann AK et al. (2014) [58]	Primary murine articular chondrocytes	IFT88 conditional knockout	NF-kB	Primary cilia influence the NF-κB signaling pathway by regulating IKK activity
Meng et al. (2023) [59]	Primary bovine articular chondrocytes	YAP	NF-kB	Activation of YAP inhibits the IL-1β-induced NF-κB signaling pathway and the release of downstream molecules, such as NO and PGE2, by regulating IKK activity
Hattori et al. (2021) [60]	Primary bovine articular chondrocytes	TRPV4 agonist (GSK1016790 A)	TRPV4 NF-kB	GSK101 increased AMPK phosphorylation and reduced IL-1β-induced NF-κB phosphorylation, reversing the increase in MMP-13 expression and the decrease in AGC and SOX9 expression
Fu et al. (2021) [61]	Primary bovine articular chondrocytes	TRPV4 agonist (GSK1016790 A), TRPV4 antagonist (GSK205)	TRPV4	GSK101 inhibited IL-1β-mediated NO release, while GSK205 promoted IL-1β-mediated release of NO and PGE2
O'Conor CJ et al. (2014) [62]	Primary porcine articular chondrocytes	TRPV4 agonist (GSK1016790 A), TRPV4 antagonist (GSK205)	TRPV4	GSK101 reduced the expression of NOS2 and ADAMTS5 genes, while enhancing the expression of COL2 and s-GAG
Takeda et al. (2021) [63]	ATDC5 mouse chondrogenic cell	TRPV4 agonist (GSK1016790A), TRPV4 antagonist (HC-067047)	TRPV4	GSK101 inhibited the compression load-induced mRNA levels of ADAMTS4 and IL-1R, whereas TRPV4 antagonists enhanced the mRNA levels of ADAMTS4 and IL-1R
Agarwal et al. (2021) [64]	Primary human articular chondrocytes	TRPV4 agonist (GSK101), TRPV4 antagonist (GSK205)	TRPV4	GSK101 increased the phosphorylation of GSK3β, promoting the expression of matrix metalloproteinases MMP3 and MMP13, as well as the inflammatory factors IL-6 and IL-8
Sun et al. (2022) [65]	Human synovium tissue SD rats RAW264.7 cells	TRPV4 agonist (GSK1016790A), TRPV4 antagonist (HC-067047)	TRPV4	The infiltration of M1 synovial macrophages and the expression of TRPV4 are significantly increased in OA synovium. The TRPV4 inhibitor HC067074 can alleviate the progression of OA in rats and significantly reduce the M1 polarization of synovial macrophages
Shen et al. (2023) [66]	Primary rat chondrocytes	TRPV4 antagonist	TRPV4	After TRPV4 inhibition, the expression of TRPV4, MMP-13, ADAMTS-5, and NOS2 mRNA in chondrocytes under inflammatory conditions significantly decreased, while the expression of COL2 and ACAN mRNA increased
Subramanian et al. (2017) [67]	Primary bovine articular chondrocytes	Chloral hydrat	MAPK	In deciliated chondrocytes, the expression of phosphorylated ERK1/2 is reduced
He et al. (2016) [68]	Primary human articular chondrocyte, C28/I2 chondrocytes, C57BL/6 mice	IFT88 siRNA	MAPK	Knockout of IFT88 reduced the mechanical load-induced expression of CITED2 and upregulated MMPs
Xiang et al. (2019) [69]	chondrocytic cell line ATDC5, primary rat chondrocytes	Icariin	MAPK	Icariin enhances ERK phosphorylation and increases the expression of COL2 and SOX9 by promoting primary cilia assembly and IFT88 expression, thereby maintaining the chondrocyte phenotype
Thompson et al. (2016) [70]	Primary bovine articular chondrocytes, Wistar rats	LiCL	Hedgehog	LiCl inhibits the Hedgehog signaling pathway, a process associated with the increase in primary cilia length
Ma et al. (2012) [71]	Primary human and bovine articular chondrocytes	IL-1β	Wnt/β-catenin NF-κB	The Wnt/β-catenin signaling pathway counteracts IL-1β-induced NF-κB-mediated MMPs expression through a negative feedback loop
Hdud et al. (2014) [72]	Primary equine articular chondrocytes	Osmotic pressure	TRPV4 MAPK	The expression of TRPV4 and BKCa channels is sensitive to changes in osmotic pressure, and these changes may involve the activation of ERK and p38

Primary cilium-mediated inflammatory signaling regulation

Primary cilia participate in a variety of cellular signaling pathways, with the most commonly involved being Hedgehog, Wnt, platelet-derived growth factor (PDGF), transforming growth factor-β (TGF-β), and mechanotransduction [23, 56]. Abnormalities or dysfunction of primary cilia negatively impact cartilage homeostasis, promoting abnormal cartilage remodeling and early-onset OA [57]. Recent studies have shown that primary cilia play a role in the inflammatory processes of OA [23], interacting with several inflammatory signaling pathways, including NF-κB, TRPV4 (Transient Receptor Potential Vanilloid 4), MAPK, and Hedgehog pathways (Figure 2). These inflammatory pathways are involved in the expression of inflammatory factors and the initiation of inflammatory responses, critically affecting the onset and progression of OA. Below, we will describe in detail the relationships between these signaling pathways and primary cilia (Table 2).

NF-κB signaling pathway

IL-1β activates a wide range of intracellular inflammatory signaling, largely regulated through either NF-κB signaling, or mitogen activated kinase (MAP) activates or combinations of both. In OA models, damage or dysfunction of primary cilia is often associated with inhibition of the NF-κB pathway [73]. Numerous studies have shown that changes in ciliary proteins, such as IFT88, lead to alterations in the cytoskeletal structure. Since NF-κB relies on an active, dynein-dependent cytoskeletal transport system, it is particularly susceptible to the activation of cytokine-induced pathways [58]. Research by Wann et al. [58, 73]. Revealed how primary cilia influence inflammatory signaling via the NF-κB pathway. The disruption of primary cilia is associated with specific molecular events in the IL-1β-induced NF-κB pathway, leading to the inhibition of COX2 (cyclooxygenase-2) and iNOS (inducible nitric oxide synthase) protein expression [73]. Moreover, although IKK (IκB kinase) activation remains unaffected in cilia-deficient cells, the reduction in IκB phosphorylation delays and decreases IκB degradation, thus affecting the nuclear translocation and binding of NF-κB p65 [58]. Rose BJ et al. [57] also identified the potential key role of heat shock protein 27 (hsp27), which is linked to IKK activity and may be crucial for the regulation of the NF-κB pathway in primary cilia. Meng et al. [59] further demonstrated that YAP signaling regulates NF-κB pathway activation by inhibiting primary cilium expression, thereby blocking IL-1β-induced cartilage matrix degradation and exerting anti-inflammatory effects. However, dysfunction or loss of primary cilia can impair the ability of YAP to regulate the NF-κB pathway.

In conclusion, the disruption of the ciliary protein IFT88 and the loss of primary cilia alter the NF-κB-dependent response to inflammatory signals [58]. Therefore, ciliary proteins in the peripheral cytoplasm may represent a novel component in inflammatory signaling encoding, making them an exciting target for exploring methods to restore physiological inflammation signals in disease processes.

TRPV4 signaling pathway

Mechanical stimuli have anti-inflammatory effects in many tissues [23]. TRPV4, located on the ciliary membrane [74], is one of the primary ion channels that senses mechanical stimuli through primary cilia, detecting mechanical forces in the joint, such as compression, stretching, or fluid shear stress [21]. While TRPV4 channels are widely distributed on the cell membrane of chondrocytes and not limited to primary cilia, the integrity of primary ciliary structure and function appears to play a significant role in TRPV4-mediated calcium responses [75]. Hattori et al. [60] demonstrated that activation of TRPV4 protects joint cartilage through the CaMKK/AMPK/NF-κB signaling pathway. Activation of TRPV4 inhibits the increase in MMP-13 expression induced by IL-1β and the decrease in AGC and SOX9 expression, alleviating cartilage degeneration and inflammation. Similarly, Fu et al. [61] showed that mechanical stimulation activates TRPV4 channels, enhancing HDAC6 expression and ciliary length, thereby mitigating IL-1β-induced NO release, inflammatory responses and cartilage degradation, which positively influences cartilage health. Furthermore, activation of TRPV4 channels in chondrocytes under dynamic compression load promotes anabolic processes and suppresses inflammation [62]. TRPV4 agonists suppress the expression of ADAMTS4 and IL-1 receptor (IL-1R) induced by compressive loading, while TRPV4 antagonists exhibit the opposite effect [63]. These findings suggest that activation of the TRPV4 pathway holds therapeutic potential for inhibiting pro-inflammatory signaling and preventing cartilage degradation in OA.

Other studies, however, have shown that activation of the TRPV4 channel exacerbates the progression of osteoarthritis. Activation of the TRPV4 ion channel increases intracellular calcium levels, which regulate the phosphorylation of GSK3β and inhibit its activity, impairing the ability of chondrocytes to sense the viscoelasticity of the extracellular matrix (ECM) [64]. Furthermore, inactivated GSK3β has been shown to upregulate several transcription factors, including β-catenin, c-Jun, and NF-κB. This upregulation promotes inflammatory responses and cartilage degradation [64, 76]. Sun et al. discovered that M1 synovial macrophage infiltration and TRPV4 expression were significantly increased in OA synovium. Conversely, TRPV4 inhibitors markedly reduced M1 polarization of synovial macrophages, thereby alleviating OA progression, potentially through the ROS/NLRP3 pathway [65]. Additionally, TRPV4 inhibitors downregulate the expression of genes associated with chondrocyte degeneration. In chondrocytes under inflammatory conditions, treatment with TRPV4 inhibitors

leads to increased expression of ACAN and COL2, while reducing the expression of MMP13, ADAMTS5, and NOS2 [66].

The role of TRPV4 may be closely related to the timing of its activation, the physiological state of chondrocytes, and the stage of disease progression. Further studies are needed to explore the mechanistic details of TRPV4 and develop precise strategies to regulate its activity in OA treatment to optimize therapeutic outcomes. Overall, these findings highlight the significant role of primary cilia in regulating chondrocyte inflammatory responses via TRPV4 channels.

MAPK signaling pathway

Deciliated chondrocytes exhibit lower basal expression levels of phosphorylated ERK1/2, suggesting that primary cilia may participate in signal transduction through the MAPK/ERK signaling pathway [67]. Studies have shown that under moderate mechanical stimulation, primary cilia, acting as cellular mechanosensors, activate the expression of CITED2 via the ERK1/2 phosphorylation. Such activation downregulates the transcription and expression of matrix-degrading enzymes MMP-1 and MMP-13,thereby exerting an anti-catabolic effect [68]. Additionally, drugs like Icariin [69] and bFGF [77] activate the ERK pathway by enhancing IFT88 expression, inducing the expression of SOX9 and COL2 genes, and promoting cartilage matrix secretion, thereby stimulating chondrocyte proliferation and differentiation while inhibiting inflammatory factors such as MMP3 and MMP9. Xiang et al. [78] showed that after sensing mechanical signals, primary cilia can activate the ERK pathway, further inhibiting the downstream mTOR signaling axis, which not only regulates chondrocyte autophagic activity but also alleviates cartilage degeneration by modulating the expression of inflammatory mediators. The platelet-derived growth factor receptor (PDGFRα), a G-protein-coupled receptor located on primary cilia, activates through binding with PDGF ligands, inducing cellular responses via the downstream MEK/ERK signaling cascade [79].

Hedgehog signaling pathway

The Hedgehog signaling pathway consists of ligands like Sonic Hedgehog (Shh), Indian Hedgehog (Ihh), and Desert Hedgehog (Dhh), and receptors such as Patched (Ptc) and Smoothened (Smo). In the absence of Hedgehog ligands, Ptc inhibits Smo, but upon ligand binding to Ptc, this inhibition is relieved, activating downstream Gli transcription factors and influencing target gene expression [70, 80]. Hedgehog signaling plays a vital role in regulating cell proliferation, differentiation, and tissue morphogenesis [80, 81].

Numerous studies have demonstrated that Hedgehog signaling in chondrocytes requires primary cilia [82], and deletion of IFT88 disrupts primary cilia-mediated Hedgehog signaling [83]. IFT88 maintains the threshold level of Hh signaling under physiological mechanical loading, thereby regulating chondrocyte mineralization [83]. Thompson et al. [84] showed that mechanical loading activates primary cilia-mediated Hedgehog signaling in chondrocytes and promotes ADAMTS-5 expression, emphasizing the close link between primary ciliary length and Hedgehog signaling. This further underscores the importance of primary ciliary structure in Hedgehog signaling transduction and cartilage health. Hedgehog-related genes play key roles in regulating extracellular matrix and inflammatory responses and are involved in the pathogenesis of OA. Yang et al. [85] showed that upregulation of Ihh expression promotes chondrocyte hypertrophy and increases the expression of hypertrophic markers such as collagen X and MMP-13, further promoting cartilage matrix degradation and OA progression. In articular cartilage, IL-1β-induced ciliary elongation may also affect cilia function including mechanotransduction and Hedgehog signaling [86]. In their investigation of the potential of LiCl treatment for OA, Thompson et al. [80] found that LiCl significantly inhibited the Hedgehog signaling pathway, a process directly related to changes in ciliary length. Previous reports have shown that LiCl can suppress IL-1β-induced NF-κB signaling [87]. These studies suggest that LiCl may modulate ciliary length to influence the Hedgehog pathway, thereby playing a role in the regulation of inflammatory signaling.

In summary, the activation and transmission of Hedgehog signaling depend on the structure and function of primary cilia, and changes in primary cilia may be influenced by inflammatory factors like IL-1β. This interaction may play a role in various pathological processes, including the onset and progression of OA.

Cross-regulation of signaling pathways

Primary cilia also engage in cross-regulation with various signaling pathways. According to a review by Pala et al. [88], primary cilia are involved in regulating several signaling pathways, including Hedgehog, Wnt, PDGFR, Notch, and TGF-β. The interactions between these pathways may jointly influence the regulation of inflammation. For example, the interaction between Wnt/β-catenin and NF-κB signaling has been well-documented [89]. Wnt/β-catenin not only reduces the basal expression levels of MMP1, MMP3, and MMP13 but also inhibits NF-κB-induced upregulation of MMPs in human chondrocytes [71, 90]. This indicates that the Wnt/β-catenin pathway can antagonize NF-κB signaling and exert a protective effect. Similarly, activation of TRPV4 can inhibit IL-1β-induced cartilage degeneration and inflammatory responses by activating the CaMKK/AMPK pathway and suppressing NF-κB activation. This process plays a key role in cartilage degradation and the progression of osteoarthritis [60]. Additionally, when

chondrocytes are exposed to hypotonic conditions, the expression of TRPV4 channel proteins rapidly increases, triggering a MAPK cascade that leads to ERK1/2 phosphorylation, and in turn, ERK1/2 phosphorylation regulates the endogenous expression of TRPV4 channels. These two processes may interact with each other in a feedback loop [72]. Furthermore, the natural isoflavone glycoside ononin alleviates IL-1β-induced reductions in chondrocyte viability by concurrently downregulating MAPK and NF-κB signaling pathways. Ononin also mitigates the overexpression of inflammatory factors TNF-α and IL-6 and reverses extracellular matrix degradation by inhibiting MMP-13 expression and promoting COL2 expression, thereby improving chondrocyte inflammation [38].

These findings collectively demonstrate the complexity and diversity of the inflammatory response in osteoarthritis. The cross-regulation of multiple signaling pathways involving primary cilia profoundly influences the inflammatory processes associated with osteoarthritis.

Mechanisms of inflammatory damage to primary ciliary function

Primary cilia are involved in modulating inflammatory responses in chondrocytes. When chondrocytes are stimulated by inflammatory cytokines like IL-1β, primary cilia may regulate their function by adjusting ciliary length, a process potentially controlled by IFT protein activity [74]. Primary cilia and IFT (intraflagellar transport) are key in inflammatory signal transduction [86]. IL-1 is one of the most important inflammatory mediators in the formation and progression of OA [23]. Research by Wann et al. [86] showed that exposure to IL-1 for 3 hours increased primary ciliary length by 50% in chondrocytes. This elongation occurs via a protein kinase A (PKA)-dependent mechanism. Furthermore, IL-1-treated chondrocytes exhibited increased release of typical inflammatory mediators such as NO and PGE2. However, in cells with IFT88 mutations leading to ciliary structural loss, the IL-1-induced inflammatory response was significantly diminished, and the progression of OA was correspondingly reduced. These findings suggest that primary cilia are involved in regulating intracellular inflammatory responses.

Histone deacetylase 6 (HDAC6) is a major driver of ciliary disassembly. HDAC6 can induce ciliary disassembly through the deacetylation of α-tubulin and cortactin [91]. Fu [92] and Zhang's studies [93] indicated that inhibiting HDAC6 promotes microtubule assembly and active elongation, improving the IL-1β-induced inflammatory response. They proposed that the inflammatory environment promotes passive elongation of primary cilia to enhance their mechanotransduction effects, enabling chondrocytes to adapt optimally to inflammation. In contrast, when HDAC6 is inhibited, primary cilia actively elongate to improve mechanotransduction and adjust to their most favorable state.

In summary, primary cilia play a significant role in mediating inflammatory responses through morphological and functional changes. Interestingly, the elongation of primary cilia in response to IL-1 requires the accumulation of hypoxia-inducible factor-2α (HIF-2α) in the cilia [94]. Research by Yang et al. [95] showed that upregulation of HIF-2α promotes OA progression by mediating primary ciliary loss. Another study by Fu et al. [96] also indicated IL-1β-induced elongation of primary cilia in chondrocytes. However, other studies have reported a decrease in the incidence of primary cilia in chondrocytes following IL-1β treatment [75].

Impact of primary cilia on synovitis

Primary cilia serve as sensors to detect changes in the osmotic pressure or chemical composition of synovial fluid and act as signaling transducers to regulate intracellular signaling pathways in chondrocytes [97]. In osteoarthritis, synovial inflammation is a key factor in joint destruction. Fibroblast-like synovial cells (FLS), the main cellular component of the synovium, may promote OA progression by producing pro-inflammatory mediators, such as inflammatory cytokines, nitric oxide (NO), and prostaglandin E2 (PGE2) [98]. FLS respond to the secretion of inflammatory factors by secreting cytokines into the synovial fluid, making them essential components in maintaining the articular cartilage environment [99]. Research by Yuan et al. [100] showed that during inflammatory arthritis, both the length and incidence of cilia in FLS were increased, a change that could enhance the transduction of inflammatory signals to regulate cell function, thereby triggering joint swelling and cartilage damage. Similarly, Estell et al. [99] found that IL-1α significantly increased the average length and incidence of primary cilia in FLS under OA conditions. FLS can sense and respond to mechanical and chemical stimuli in the joint, and changes in their function are associated with OA progression.

Conclusions and perspectives

Inflammation is an integral factor in the pathogenesis of osteoarthritis. Various molecules released by chondrocytes, synovial cells, and immune cells, including cytokines, chemokines, and MMPs, are involved in maintaining cartilage homeostasis [25]. At the same time, the expression of these molecules is regulated by signaling pathways such as NFκB, MAPK, PI3K/AKT, prostaglandins, and nitric oxide [25]. Primary cilia, as sensory organelles, have the ability to detect and regulate physical and chemical signals, making them important mechanoreceptors [74, 101]. There is a close relationship between inflammatory responses, mechanical

loading, and cartilage homeostasis [102]. Therefore, targeting the receptors of inflammatory mediators and the mechanotransduction mechanisms of chondrocytes primary cilia may be an effective strategy for directly controlling chondrocyte responses to pathological loads or disease progression [102].

Despite existing research revealing the potential role of primary cilia in inflammatory responses in osteoarthritis, many scientific questions remain unresolved. For example, it is still unclear how primary cilia mediate bidirectional regulation of chondrocyte degradation and regeneration, how primary cilia act as a bridge between different signaling pathways, and how to modulate the function of primary cilia to suppress inflammation and repair cartilage. In conclusion, primary cilia play an important role in the inflammatory response of osteoarthritis and may represent a novel therapeutic target for treating osteoarthritis in the future.

Author contributions

YS designed and wrote the manuscript. ZL, YF, TN, WW and YW revised the manuscript. YS and ZL designed and drew the figures. YK supervised and revised the manuscript. All authors contributed to the article and approved the submitted version.

Funding

The author(s) declare that financial support was received for the research and/or publication of this article. This work was supported by the Natural Science Foundation of China (grant number 82060418).

Conflict of interest

The author(s) declared no potential conflicts of interest with respect to the research, authorship, and/or publication of this article.

Generative AI statement

The authors declare that no Generative AI was used in the creation of this manuscript.

References

1. Martel-Pelletier J, Barr AJ, Cicuttini FM, Conaghan PG, Cooper C, Goldring MB, et al. Osteoarthritis. *Nat Rev Dis Primers* (2016) **2**:16072. doi:10.1038/nrdp.2016.72

2. Hunter DJ, March L, Chew M. Osteoarthritis in 2020 and beyond: a lancet commission. *The Lancet* (2020) **396**(10264):1711–2. doi:10.1016/S0140-6736(20)32230-3

3. Long H, Liu Q, Yin H, Wang K, Diao N, Zhang Y, et al. Prevalence trends of site-specific osteoarthritis from 1990 to 2019: findings from the global burden of disease study 2019. *Arthritis and Rheumatol* (2022) **74**(7):1172–83. doi:10.1002/art.42089

4. Steinmetz JD, Culbreth GT, Haile LM, Rafferty Q, Lo J, Fukutaki KG, et al. Global, regional, and national burden of osteoarthritis, 1990-2020 and projections to 2050: a systematic analysis for the Global Burden of Disease Study 2021. *The Lancet Rheumatol* (2023) **5**(9):e508–e522. doi:10.1016/S2665-9913(23)00163-7

5. Yao Q, Wu X, Tao C, Gong W, Chen M, Qu M, et al. Osteoarthritis: pathogenic signaling pathways and therapeutic targets. *Signal Transduction Targeted Ther* (2023) **8**(1):56. doi:10.1038/s41392-023-01330-w

6. Robinson WH, Lepus CM, Wang Q, Raghu H, Mao R, Lindstrom TM, et al. Low-grade inflammation as a key mediator of the pathogenesis of osteoarthritis. *Nat Rev Rheumatol* (2016) **12**(10):580–92. doi:10.1038/nrrheum.2016.136

7. Lin YJ, Anzaghe M, Schülke S. Update on the pathomechanism, diagnosis, and treatment options for rheumatoid arthritis. *Cells* (2020) **9**(4):880. doi:10.3390/cells9040880

8. Scott DL, Wolfe F, Huizinga TW. Rheumatoid arthritis. *The Lancet* (2010) **376**(9746):1094–108. doi:10.1016/S0140-6736(10)60826-4

9. Porta S, Otero-Losada M, Kölliker Frers RA, Cosentino V, Kerzberg E, Capani F. Adipokines, cardiovascular risk, and therapeutic management in obesity and psoriatic arthritis. *Front Immunol* (2021) **11**:590749. doi:10.3389/fimmu.2020.590749

10. Talotta R, Atzeni F, Sarzi-Puttini P, Masala IF. Psoriatic arthritis: from pathogenesis to pharmacologic management. *Pharmacol Res* (2019) **148**:104394. doi:10.1016/j.phrs.2019.104394

11. Liu W, Peng J, Wu Y, Ye Z, Zong Z, Wu R, et al. Immune and inflammatory mechanisms and therapeutic targets of gout: an update. *Int Immunopharmacology* (2023) **121**:110466. doi:10.1016/j.intimp.2023.110466

12. Cabău G, Crișan TO, Klück V, Popp RA, Joosten LAB. Urate-induced immune programming: consequences for gouty arthritis and hyperuricemia. *Immunol Rev* (2020) **294**(1):92–105. doi:10.1111/imr.12833

13. Wei Y, Zhang S, Shao F, Sun Y. Ankylosing spondylitis: from pathogenesis to therapy. *Int Immunopharmacology* (2025) **145**:113709. doi:10.1016/j.intimp.2024.113709

14. Voruganti A, Bowness P. New developments in our understanding of ankylosing spondylitis pathogenesis. *Immunology* (2020) **161**(2):94–102. doi:10.1111/imm.13242

15. Goldring MB, Otero M. Inflammation in osteoarthritis. *Curr Opin Rheumatol* (2011) **23**(5):471–8. doi:10.1097/BOR.0b013e328349c2b1

16. Ingale D, Kulkarni P, Electricwala A, Moghe A, Kamyab S, Jagtap S, et al. Synovium-synovial fluid Axis in osteoarthritis pathology: a key regulator of the cartilage degradation process. *Genes (Basel)* (2021) **12**(7):989. doi:10.3390/genes12070989

17. Kulkarni P, Srivastava V, Tootsi K, Electricwala A, Kharat A, Bhonde R, et al. Synovial fluid in knee osteoarthritis extends proinflammatory niche for macrophage polarization. *Cells* (2022) **11**(24):4115. doi:10.3390/cells11244115

18. Kulkarni P, Harsulkar A, Märtson AG, Suutre S, Märtson A, Koks S. Mast cells differentiated in synovial fluid and resident in osteophytes exalt the inflammatory pathology of osteoarthritis. *Int J Mol Sci* (2022) **23**(1):541. doi:10.3390/ijms23010541

19. Berenbaum F, Eymard F, Houard X. Osteoarthritis, inflammation and obesity. *Curr Opin Rheumatol* (2013) **25**(1):114–8. doi:10.1097/BOR.0b013e32835a9414

20. Zhang Z, Xing X, Hensley G, Chang L, Liao W, Abu-Amer Y, et al. Resistin induces expression of proinflammatory cytokines and chemokines in human articular chondrocytes via transcription and messenger RNA stabilization. *Arthritis and Rheum* (2010) **62**(7):1993–2003. doi:10.1002/art.27473

21. Zhang Y, Tawiah GK, Wu X, Zhang Y, Wang X, Wei X, et al. Primary cilium-mediated mechanotransduction in cartilage chondrocytes. *Exp Biol Med (Maywood)* (2023) **248**(15):1279–87. doi:10.1177/15353702231199079

22. Zhou H, Wu S, Ling H, Zhang C, Kong Y. Primary cilia: a cellular regulator of articular cartilage degeneration. *Stem Cells Int* (2022) **2022**:2560441–11. doi:10.1155/2022/2560441

23. Li X, Guo S, Su Y, Lu J, Hang D, Cao S, et al. Role of primary cilia in skeletal disorders. *Stem Cells Int* (2022) **2022**:1–12. doi:10.1155/2022/6063423

24. Scanzello CR. Role of low-grade inflammation in osteoarthritis. *Curr Opin Rheumatol* (2017) **29**(1):79–85. doi:10.1097/BOR.0000000000000353

25. Chow YY, Chin KY. The role of inflammation in the pathogenesis of osteoarthritis. *Mediators Inflamm* (2020) **2020**:8293921–19. doi:10.1155/2020/8293921

26. Zhou Q, Ren Q, Jiao L, Huang J, Yi J, Chen J, et al. The potential roles of JAK/STAT signaling in the progression of osteoarthritis. *Front Endocrinol (Lausanne)* (2022) **13**:1069057. doi:10.3389/fendo.2022.1069057

27. Hayden MS, Ghosh S. NF-κB, the first quarter-century: remarkable progress and outstanding questions. *Genes Dev* (2012) **26**(3):203–34. doi:10.1101/gad.183434.111

28. Oliver KM, Garvey JF, Ng CT, Veale DJ, Fearon U, Cummins EP, et al. Hypoxia activates NF-κB–Dependent gene expression through the canonical signaling pathway. *Antioxid and Redox Signaling* (2009) **11**(9):2057–64. doi:10.1089/ars.2008.2400

29. Choi MC, Jo J, Park J, Kang HK, Park Y. NF-κB signaling pathways in osteoarthritic cartilage destruction. *Cells* (2019) **8**(7):734. doi:10.3390/cells8070734

30. Sun SC. The non-canonical NF-κB pathway in immunity and inflammation. *Nat Rev Immunol* (2017) **17**(9):545–58. doi:10.1038/nri.2017.52

31. Yasuda T. Activation of Akt leading to NF-κB up-regulation in chondrocytes stimulated with fibronectin fragment. *Biomed Res* (2011) **32**(3):209–15. doi:10.2220/biomedres.32.209

32. Kapoor M, Martel-Pelletier J, Lajeunesse D, Pelletier JP, Fahmi H. Role of proinflammatory cytokines in the pathophysiology of osteoarthritis. *Nat Rev Rheumatol* (2011) **7**(1):33–42. doi:10.1038/nrrheum.2010.196

33. Ulivi V, Giannoni P, Gentili C, Cancedda R, Descalzi F. p38/NF-κB-dependent expression of COX-2 during differentiation and inflammatory response of chondrocytes. *J Cell Biochem* (2008) **104**(4):1393–406. doi:10.1002/jcb.21717

34. Marcu KB, Otero M, Olivotto E, Borzi RM, Goldring MB. NF-kappaB signaling: multiple angles to target OA. *Curr Drug Targets* (2010) **11**(5):599–613. doi:10.2174/138945010791011938

35. Ge XP, Gan YH, Zhang CG, Zhou CY, Ma KT, Meng JH, et al. Requirement of the NF-κB pathway for induction of Wnt-5A by interleukin-1β in condylar chondrocytes of the temporomandibular joint: functional crosstalk between the Wnt-5A and NF-κB signaling pathways. *Osteoarthritis and Cartilage* (2011) **19**(1):111–7. doi:10.1016/j.joca.2010.10.016

36. Lan CN, Cai WJ, Shi J, Yi ZJ. MAPK inhibitors protect against early-stage osteoarthritis by activating autophagy. *Mol Med Rep* (2021) **24**(6):829. doi:10.3892/mmr.2021.12469

37. Zhou X, Cao H, Yuan Y, Wu W. Biochemical signals mediate the crosstalk between cartilage and bone in osteoarthritis. *Biomed Res Int* (2020) **2020**:5720360. doi:10.1155/2020/5720360

38. Xu F, Zhao LJ, Liao T, Li ZC, Wang LL, Lin PY, et al. Ononin ameliorates inflammation and cartilage degradation in rat chondrocytes with IL-1β-induced osteoarthritis by downregulating the MAPK and NF-κB pathways. *BMC Complement Med Ther* (2022) **22**(1):25. doi:10.1186/s12906-022-03504-5

39. Nailwal NP, Doshi GM. Role of intracellular signaling pathways and their inhibitors in the treatment of inflammation. *Inflammopharmacology* (2021) **29**(3):617–40. doi:10.1007/s10787-021-00813-y

40. Mengshol JA, Vincenti MP, Coon CI, Barchowsky A, Brinckerhoff CE. Interleukin-1 induction of collagenase 3 (matrix metalloproteinase 13) gene expression in chondrocytes requires p38, c-jun N-terminal kinase, and nuclear factor κB: differential regulation of collagenase 1 and collagenase 3. *Arthritis and Rheum* (2000) **43**(4):801–11. doi:10.1002/1529-0131(200004)43:4<801::AID-ANR10>3.0.CO;2-4

41. Zhong M, Carney DH, Jo H, Boyan BD, Schwartz Z. Inorganic phosphate induces mammalian growth plate chondrocyte apoptosis in a mitochondrial pathway involving nitric oxide and JNK MAP kinase. *Calcif Tissue Int* (2011) **88**(2):96–108. doi:10.1007/s00223-010-9433-5

42. Prasadam I, Friis T, Shi W, van Gennip S, Crawford R, Xiao Y. Osteoarthritic cartilage chondrocytes alter subchondral bone osteoblast differentiation via MAPK signalling pathway involving ERK1/2. *Bone* (2010) **46**(1):226–35. doi:10.1016/j.bone.2009.10.014

43. Prasadam I, van Gennip S, Friis T, Shi W, Crawford R, Xiao Y. ERK-1/2 and p38 in the regulation of hypertrophic changes of normal articular cartilage chondrocytes induced by osteoarthritic subchondral osteoblasts. *Arthritis and Rheum* (2010) **62**(5):1349–60. doi:10.1002/art.27397

44. Leonard WJ, O'Shea JJ. Jaks and STATs: biological implications. *Annu Rev Immunol* (1998) **16**:293–322. doi:10.1146/annurev.immunol.16.1.293

45. Malemud CJ. Negative regulators of JAK/STAT signaling in rheumatoid arthritis and osteoarthritis. *Int J Mol Sci* (2017) **18**(3):484. doi:10.3390/ijms18030484

46. Lim H, Kim HP. Matrix metalloproteinase-13 expression in IL-1β-treated chondrocytes by activation of the p38 MAPK/c-Fos/AP-1 and JAK/STAT pathways. *Arch Pharm Res* (2011) **34**(1):109–17. doi:10.1007/s12272-011-0113-4

47. Aida Y, Honda K, Tanigawa S, Nakayama G, Matsumura H, Suzuki N, et al. IL-6 and soluble IL-6 receptor stimulate the production of MMPs and their inhibitors via JAK-STAT and ERK-MAPK signalling in human chondrocytes. *Cell Biol Int* (2012) **36**(4):367–76. doi:10.1042/CBI20110150

48. Yang P, Tan J, Yuan Z, Meng G, Bi L, Liu J. Expression profile of cytokines and chemokines in osteoarthritis patients: proinflammatory roles for CXCL8 and CXCL11 to chondrocytes. *Int Immunopharmacology* (2016) **40**:16–23. doi:10.1016/j.intimp.2016.08.005

49. Xu CP, Sun HT, Yang YJ, Cui Z, Wang J, Yu B, et al. ELP2 negatively regulates osteoblastic differentiation impaired by tumor necrosis factor α in MC3T3-E1 cells through STAT3 activation. *J Cell Physiol* (2019) **234**(10):18075–85. doi:10.1002/jcp.28440

50. Li CH, Zhao JX, Sun L, Yao Z, Deng X, Liu R, et al. AG490 inhibits NFATc1 expression and STAT3 activation during RANKL induced osteoclastogenesis. *Biochem Biophysical Res Commun* (2013) **435**(4):533–9. doi:10.1016/j.bbrc.2013.04.084

51. Giatromanolaki A, Sivridis E, Maltezos E, Athanassou N, Papazoglou D, Gatter KC, et al. Upregulated hypoxia inducible factor-1α and -2α pathway in rheumatoid arthritis and osteoarthritis. *Arthritis Res Ther* (2003) **5**(4):R193–R201. doi:10.1186/ar756

52. Chim SM, Kuek V, Chow ST, Lim BS, Tickner J, Zhao J, et al. EGFL7 is expressed in bone microenvironment and promotes angiogenesis via ERK, STAT3, and integrin signaling cascades. *J Cell Physiol* (2015) **230**(1):82–94. doi:10.1002/jcp.24684

53. Sun K, Luo J, Guo J, Yao X, Jing X, Guo F. The PI3K/AKT/mTOR signaling pathway in osteoarthritis: a narrative review. *Osteoarthritis and Cartilage* (2020) **28**(4):400–9. doi:10.1016/j.joca.2020.02.027

54. Xie L, Xie H, Chen C, Tao Z, Zhang C, Cai L. Inhibiting the PI3K/AKT/NF-κB signal pathway with nobiletin for attenuating the development of osteoarthritis: *in vitro* and *in vivo* studies. *Food Funct* (2019) **10**(4):2161–75. doi:10.1039/c8fo01786g

55. Chen J, Crawford R, Xiao Y. Vertical inhibition of the PI3K/Akt/mTOR pathway for the treatment of osteoarthritis. *J Cell Biochem* (2013) **114**(2):245–9. doi:10.1002/jcb.24362

56. Leu T, Denda J, Wrobeln A, Fandrey J. Hypoxia-inducible factor-2alpha affects the MEK/ERK signaling pathway via primary cilia in connection with the intraflagellar transport protein 88 homolog. *Mol Cell Biol* (2023) **43**(4):174–83. doi:10.1080/10985549.2023.2198931

57. Rose BJ, Kooyman DL, Porter J, Woolstenhulme J, Hanson R, Woodbury R, et al. NF-κB activation in osteoarthritis occurs independent of primary cilia associated proteins HSP27 and IKK activity. *The FASEB J* (2020) **34**(1):1. doi:10.1096/fasebj.2020.34.s1.06919

58. Mc Fie M, Koneva L, Collins I, Coveney CR, Clube AM, Chanalaris A, et al. Ciliary proteins specify the cell inflammatory response by tuning NFκB signalling, independently of primary cilia. *J Cell Sci* (2020) **133**(13):jcs239871. doi:10.1242/jcs.239871

59. Meng H, Fu S, Ferreira MB, Hou Y, Pearce O, Gavara N, et al. YAP activation inhibits inflammatory signalling and cartilage breakdown associated with reduced primary cilia expression. *Osteoarthritis and Cartilage* (2023) **31**(5):600–12. doi:10.1016/j.joca.2022.11.001

60. Hattori K, Takahashi N, Terabe K, Ohashi Y, Kishimoto K, Yokota Y, et al. Activation of transient receptor potential vanilloid 4 protects articular cartilage against inflammatory responses via CaMKK/AMPK/NF-κB signaling pathway. *Sci Rep* (2021) **11**(1):15508. doi:10.1038/s41598-021-94938-3

61. Fu S, Meng H, Inamdar S, Das B, Gupta H, Wang W, et al. Activation of TRPV4 by mechanical, osmotic or pharmaceutical stimulation is anti-inflammatory blocking IL-1β mediated articular cartilage matrix destruction. *Osteoarthritis and Cartilage* (2021) **29**(1):89–99. doi:10.1016/j.joca.2020.08.002

62. O'Conor CJ, Leddy HA, Benefield HC, Liedtke WB, Guilak F. TRPV4-mediated mechanotransduction regulates the metabolic response of chondrocytes to dynamic loading. *Proc Natl Acad Sci U S A.* (2014) **111**(4):1316–21. doi:10.1073/pnas.1319569111

63. Takeda Y, Niki Y, Fukuhara Y, Fukuda Y, Udagawa K, Shimoda M, et al. Compressive mechanical stress enhances susceptibility to interleukin-1 by increasing interleukin-1 receptor expression in 3D-cultured ATDC5 cells. *BMC Musculoskelet Disord* (2021) **22**(1):238. doi:10.1186/s12891-021-04095-x

64. Agarwal P, Lee HP, Smeriglio P, Grandi F, Goodman S, Chaudhuri O, et al. A dysfunctional TRPV4-GSK3β pathway prevents osteoarthritic chondrocytes from sensing changes in extracellular matrix viscoelasticity. *Nat Biomed Eng* (2021) **5**(12):1472–84. doi:10.1038/s41551-021-00691-3

65. Sun H, Sun Z, Xu X, Lv Z, Li J, Wu R, et al. Blocking TRPV4 ameliorates osteoarthritis by inhibiting M1 macrophage polarization via the ROS/NLRP3 signaling pathway. *Antioxidants (Basel)* (2022) **11**(12):2315. doi:10.3390/antiox11122315

66. Shen X, Zhang H, Chen DT, Cao YL. Preliminary study of TRPV4 affects chondrocyte degeneration. *Zhongguo Gu Shang* (2023) **36**(10):990–5. doi:10.12200/j.issn.1003-0034.2023.10.015

67. Subramanian A, Budhiraja G, Sahu N. Chondrocyte primary cilium is mechanosensitive and responds to low-intensity-ultrasound by altering its length and orientation. *The Int J Biochem and Cell Biol* (2017) **91**(Pt A):60–4. doi:10.1016/j.biocel.2017.08.018

68. He Z, Leong DJ, Zhuo Z, Majeska R, Cardoso L, Spray D, et al. Strain-induced mechanotransduction through primary cilia, extracellular ATP, purinergic calcium signaling, and ERK1/2 transactivates CITED2 and downregulates MMP-1 and MMP-13 gene expression in chondrocytes. *Osteoarthritis and Cartilage* (2016) **24**(5):892–901. doi:10.1016/j.joca.2015.11.015

69. Xiang W, Zhang J, Wang R, Wang L, Wang S, Wu Y, et al. Role of IFT88 in icariin-regulated maintenance of the chondrocyte phenotype. *Mol Med Rep* (2018) **17**(4):4999–5006. doi:10.3892/mmr.2018.8486

70. Thompson CL, Wiles A, Poole CA, Knight MM. Lithium chloride modulates chondrocyte primary cilia and inhibits Hedgehog signaling. *FASEB J* (2016) **30**(2):716–26. doi:10.1096/fj.15-274944

71. Ma B, van Blitterswijk CA, Karperien M. A Wnt/β-catenin negative feedback loop inhibits interleukin-1-induced matrix metalloproteinase expression in human articular chondrocytes. *Arthritis and Rheum* (2012) **64**(8):2589–600. doi:10.1002/art.34425

72. Hdud IM, Mobasheri A, Loughna PT. Effect of osmotic stress on the expression of TRPV4 and BKCa channels and possible interaction with ERK1/2 and p38 in cultured equine chondrocytes. *Am J Physiology-Cell Physiol* (2014) **306**(11):C1050–C1057. doi:10.1152/ajpcell.00287.2013

73. Wann AK, Chapple JP, Knight MM. The primary cilium influences interleukin-1β-induced NFκB signalling by regulating IKK activity. *Cell Signal* (2014) **26**(8):1735–42. doi:10.1016/j.cellsig.2014.04.004

74. Tao F, Jiang T, Tao H, Cao H, Xiang W. Primary cilia: versatile regulator in cartilage development. *Cell Prolif* (2020) **53**(3):e12765. doi:10.1111/cpr.12765

75. Wu S, Zhou H, Ling H, Sun Y, Luo Z, Ngo T, et al. LIPUS regulates the progression of knee osteoarthritis in mice through primary cilia-mediated TRPV4 channels. *Apoptosis* (2024) **29**(5-6):785–98. doi:10.1007/s10495-024-01950-9

76. Han S. Osteoarthritis year in review 2022: biology. *Osteoarthritis and Cartilage* (2022) **30**(12):1575–82. doi:10.1016/j.joca.2022.09.003

77. Zhan D, Xiang W, Guo F, Ma Y. Basic fibroblast growth factor increases IFT88 expression in chondrocytes. *Mol Med Rep* (2017) **16**(5):6590–9. doi:10.3892/mmr.2017.7449

78. Xiang W, Jiang T, Hao X, Wang R, Yao X, Sun K, et al. Primary cilia and autophagy interaction is involved in mechanical stress mediated cartilage development via ERK/mTOR axis. *Life Sci* (2019) **218**:308–13. doi:10.1016/j.lfs.2019.01.001

79. Christensen ST, Pedersen SF, Satir P, Veland IR, Schneider L. The primary cilium coordinates signaling pathways in cell cycle control and migration during development and tissue repair. *Curr Top Developmental Biol* (2008) **85**:261–301. doi:10.1016/S0070-2153(08)00810-7

80. Thompson CL, Patel R, Kelly TA, Wann AKT, Hung CT, Chapple JP, et al. Hedgehog signalling does not stimulate cartilage catabolism and is inhibited by Interleukin-1β. *Arthritis Res Ther* (2015) **17**:373. doi:10.1186/s13075-015-0891-z

81. Rux D, Helbig K, Han B, Cortese C, Koyama E, Han L, et al. Primary cilia direct murine articular cartilage tidemark patterning through hedgehog signaling and ambulatory load. *Journal of Bone and Mineral Research* (2022) **37**(6):1097–116. doi:10.1002/jbmr.4506

82. Thompson CL, Plant JC, Wann AK, Bishop C, Novak P, Mitchison H, et al. Chondrocyte expansion is associated with loss of primary cilia and disrupted hedgehog signalling. *Eur Cells Mater* (2017) **34**:128–41. doi:10.22203/eCM.v034a09

83. Coveney CR, Zhu L, Miotla-Zarebska J, Stott B, Parisi I, Batchelor V, et al. Role of ciliary protein intraflagellar transport protein 88 in the regulation of cartilage thickness and osteoarthritis development in mice. *Arthritis Rheumatol* (2022) **74**(1):49–59. doi:10.1002/art.41894

84. Thompson CL, Chapple JP, Knight MM. Primary cilia disassembly down-regulates mechanosensitive hedgehog signalling: a feedback mechanism controlling ADAMTS-5 expression in chondrocytes. *Osteoarthritis and Cartilage* (2014) **22**(3):490–8. doi:10.1016/j.joca.2013.12.016

85. Yang Z, Song L. Correlation between Indian hedgehog and damage degree of knee osteoarthritis cartilage. *Zhonghua Yi Xue Za Zhi* (2014) **94**(31):2434–7. doi:10.3760/cma.j.issn.0376-2491.2014.31.010

86. Wann AK, Knight MM. Primary cilia elongation in response to interleukin-1 mediates the inflammatory response. *Cell Mol Life Sci* (2012) **69**(17):2967–77. doi:10.1007/s00018-012-0980-y

87. Minashima T, Zhang Y, Lee Y, Kirsch T. Lithium protects against cartilage degradation in osteoarthritis. *Arthritis and Rheumatol* (2014) **66**(5):1228–36. doi:10.1002/art.38373

88. Pala R, Alomari N, Nauli SM. Primary cilium-dependent signaling mechanisms. *Int J Mol Sci* (2017) **18**(11):2272. doi:10.3390/ijms18112272

89. Du Q, Geller DA. Cross-regulation between Wnt and NF-κB signaling pathways. *Forum Immunopathological Dis Ther* (2010) **1**:155–81. doi:10.1615/forumimmundisther.v1.i3.10

90. Feng J, Zhang Q, Pu F, Zhu Z, Lu K, Lu WW, et al. Signalling interaction between β-catenin and other signalling molecules during osteoarthritis development. *Cell Prolif* (2024) **57**(6):e13600. doi:10.1111/cpr.13600

91. Ran J, Yang Y, Li D, Liu M, Zhou J. Deacetylation of α-tubulin and cortactin is required for HDAC6 to trigger ciliary disassembly. *Sci Rep* (2015) **5**:12917. doi:10.1038/srep12917

92. Fu S, Thompson CL, Ali A, Wang W, Chapple J, Mitchison H, et al. Mechanical loading inhibits cartilage inflammatory signalling via an HDAC6 and IFT-dependent mechanism regulating primary cilia elongation. *Osteoarthritis and Cartilage* (2019) **27**(7):1064–74. doi:10.1016/j.joca.2019.03.003

93. Zhang Y, Tawiah GK, Zhang Y, Wang X, Wei X, Chen W, et al. HDAC6 inhibition regulates substrate stiffness-mediated inflammation signaling in chondrocytes. *Acta Biochim Biophys Sinica* (2023) **55**(12):1987–98. doi:10.3724/abbs.2023144

94. Wann AK, Thompson CL, Chapple JP, Knight MM. Interleukin-1β sequesters hypoxia inducible factor 2α to the primary cilium. *Cilia* (2013) **2**(1):17. doi:10.1186/2046-2530-2-17

95. Yang Q, Zhou Y, Cai P, Fu W, Wang J, Wei Q, et al. Up-regulated HIF-2α contributes to the Osteoarthritis development through mediating the primary cilia loss. *Int Immunopharmacology* (2019) **75**:105762. doi:10.1016/j.intimp.2019.105762

96. Fu S, Meng H, Freer F, Kwon J, Shelton JC, Knight MM. Sub-toxic levels of Co2+ are anti-inflammatory and protect cartilage from degradation caused by IL-1β. *Clin Biomech* (2020) **79**:104924. doi:10.1016/j.clinbiomech.2019.12.006

97. Relucenti M, Miglietta S, Covelli E, Familiari P, Battaglione E, Familiari G, et al. Ciliated cell observation by SEM on the surface of human incudo-malleolar-joint articular cartilage: are they a new chondrocyte phenotype? *Acta Oto-Laryngologica* (2019) **139**(5):439–43. doi:10.1080/00016489.2019.1575520

98. Han D, Fang Y, Tan X, Jiang H, Gong X, Wang X, et al. The emerging role of fibroblast-like synoviocytes-mediated synovitis in osteoarthritis: an update. *J Cell Mol Med* (2020) **24**(17):9518–32. doi:10.1111/jcmm.15669

99. Estell EG, Murphy LA, Silverstein AM, Tan AR, Shah RP, Ateshian GA, et al. Fibroblast-like synoviocyte mechanosensitivity to fluid shear is modulated by interleukin-1α. *J Biomech* (2017) **60**:91–9. doi:10.1016/j.jbiomech.2017.06.011

100. Yuan G, Yang ST, Yang S. Regulator of G protein signaling 12 drives inflammatory arthritis by activating synovial fibroblasts through MYCBP2/KIF2A signaling. *Mol Ther - Nucleic Acids* (2023) **31**:197–210. doi:10.1016/j.omtn.2022.12.017

101. Muhammad H, Rais Y, Miosge N, Ornan EM. The primary cilium as a dual sensor of mechanochemical signals in chondrocytes. *Cell Mol Life Sci* (2012) **69**(13):2101–7. doi:10.1007/s00018-011-0911-3

102. Sanchez-Adams J, Leddy HA, McNulty AL, O'Conor CJ, Guilak F. The mechanobiology of articular cartilage: bearing the burden of osteoarthritis. *Curr Rheumatol Rep* (2014) **16**(10):451. doi:10.1007/s11926-014-0451-6

EBM Experimental Biology and Medicine

TYPE Original Research
PUBLISHED 25 April 2025
DOI 10.3389/ebm.2025.10349

OPEN ACCESS

*CORRESPONDENCE
Guojun Zeng,
zengguojun@wchscu.cn

†These authors have contributed equally to this work and share first authorship

RECEIVED 15 October 2024
ACCEPTED 15 April 2025
PUBLISHED 25 April 2025

CITATION
Zhao X, Huang H, Zeng G, Shi Q, Zhu P, Zhang L, Li L, Liu L, Huang N, Liu W and Yu K (2025) Research on the online service mechanism of internet hospital in infectious disease prevention and control.
Exp. Biol. Med. 250:10349.
doi: 10.3389/ebm.2025.10349

Research on the online service mechanism of internet hospital in infectious disease prevention and control

Xin Zhao[1†], Haitao Huang[2†], Guojun Zeng[3,4*], Qingke Shi[5], Peijia Zhu[6], Longhao Zhang[7], Lei Li[8], Lunxu Liu[9], Nan Huang[10], Wenguang Liu[2] and Kexin Yu[2]

[1]Emergency Office, West China Hospital, Sichuan University, Chengdu, China, [2]Department of Computer Application, Chengdu College of University of Electronic Science and Technology of China, Chengdu, China, [3]Division of Vascular Surgery, Department of General Surgery, West China Hospital, Sichuan University, Chengdu, China, [4]Department of Vascular Surgery, The People's Hospital of Leshan, Leshan, China, [5]Information Center, West China Hospital, Sichuan University, Chengdu, China, [6]Department of Science and Technology, West China Hospital, Sichuan University, Chengdu, China, [7]Double First-Class Construction Office, West China Hospital, Sichuan University, Chengdu, China, [8]Department of Clinical Research Management, West China Hospital, Sichuan University, Chengdu, China, [9]Department of Thoracic Surgery, and President's Office, West China Hospital, Sichuan University, Chengdu, China, [10]Department of Dermatology and Venerology, West China Hospital, Sichuan University, Chengdu, China

Abstract

Infectious diseases can sometimes lead to pandemics, often transmitted through public and social gatherings, including in-person hospital visits. Consequently, there is an urgent need for innovative approaches to prevent their spread. Taking COVID-19 as an example, we have explored a remote, contactless hospital online model that offers the public online medical consultations, professional psychological counseling, and chronic disease management consultations, thereby mitigating the risk of new transmissions resulting from hospital visits. This model was implemented, validated, and practiced at West China Hospital in China from 29 January 2020, to 12 March 2020. It was also applicable to other infectious diseases, such as influenza A. In this research, we utilized the hospital's internet platform, supplemented by telephone services, to offer the following to the public: 1) General medical education and consultation related to epidemics and psychological anxiety; 2) Online screening for at-risk populations; 3) Online prescription and medication delivery services for patients with chronic diseases. Consequently, over a period of more than 1 month, the online epidemic platform completed a total of 32,755 cases, including 8,783 internet consultations and 1,082 telephone consultations for the public, as well as 22,890 internet consultations for chronic disease patients. Among these, 289 high-risk individuals were identified, with 3 cases confirmed as COVID-19 during follow-up diagnoses, while no infections were detected in the remaining individuals. In conclusion, this innovative medical model serves as a significant supplement to existing healthcare systems and has the potential to be expanded to other hospitals and other infectious diseases. It is particularly

beneficial in scenarios where medical resources are limited, populations are under quarantine, and there is a large demand for medical services and anxiety management during infectious disease pandemics.

KEYWORDS

internet hospital, online service, infectious disease, prevention, control internet hospital

Impact statement

To the best of our knowledge, this is the first online hospital strategy and implementation scheme executed in China during an infectious disease pandemic. This strategy leveraged the pre-established infrastructure of the hospital's internet hospital, integrating clinicians, pharmacies, IT engineers, and logistics companies to serve a population of approximately 15 million people in the surrounding areas. Besides, the online clinical screening and prescription services for chronic disease patients significantly reduced the human-to-human transmission of infectious diseases, while also alleviating psychological stress for both clinicians and the public. The experience of chronic disease patients in seeking medical care became more convenient than before. Overall, since this is a novel clinical model, there is a greater need for the public to have more understanding and trust in this system, with a view to better application during major infectious disease outbreaks.

Introduction

Infectious diseases can sometimes pose global challenges, as exemplified by the novel coronavirus pneumonia (NCP) pathogen (COVID-19) [1, 2]. Symptoms include fever, fatigue, and dry cough, with additional symptoms such as difficulty breathing appearing later [3–5]. Different variants may present with different symptoms. At times, an epidemic can escalate rapidly into an outbreak, becoming a global public health challenge [6]. In epidemic prevention and control, it is crucial to identify the source of transmission, reduce population movement, and expedite the screening of at-risk individuals. Some individuals contracted the virus during medical visits, and healthcare workers were infected while interacting with undiagnosed or diagnosed patients [7, 8]. More concerning is that infections can also occur between asymptomatic contacts. A non-contact, remote online consultation model in hospitals can reduce population movement and lower the risk of human-to-human transmission, making it a viable approach to achieving this goal.

Our hospital's internet hospital began operations at the end of 2018, providing a technical platform to support online consultations for infectious diseases. In the event of an infectious disease outbreak, we facilitated prevention and control efforts through online consultations via the internet hospital. The public received medical advice related to diseases and professional psychological counseling for anxiety, fear, and paranoia induced by infectious diseases through online and telephone consultations. High-risk individuals were screened, and the needs of chronic disease patients for regular medical visits were met. The number of patients visiting the hospital decreased, reducing the potential for cross-infection. Under the circumstances, panic and despair were alleviated possibly. This study was approved by the hospital's ethics committee.

Materials and methods

Overall design of the hospital's online strategy

The online and telephone prevention and control plan was based on the internet hospital platform, which involved the following tasks: 1) Dynamic online training for healthcare personnel; 2) Scientific education on infectious diseases and online consultations; 3) Screening of high-risk populations; 4) Online consultations, prescriptions, and home delivery of medications for chronic disease patients. The hospital's IT department issued CA certificates to all doctors participating in online consultations and provided training on online operations. The pharmacist team reviewed the online electronic prescription process. A logistics company was responsible for medication delivery, and the medical internet service team handled medication consultations. The overall process of the hospital's online model is shown in the diagram (Figure 1). During this process, some patients avoided hospital visits, thus reducing the likelihood of exposure.

Online consultations via internet hospital during the epidemic

Through online consultations provided by the internet hospital, high-risk individuals were screened based on the diagnostic guidelines issued by the National Health Commission of China. The services included scientific education, epidemic-related consultations, and psychological services. The online screening of the population could be conducted using AI-assisted self-assessment, utilizing an

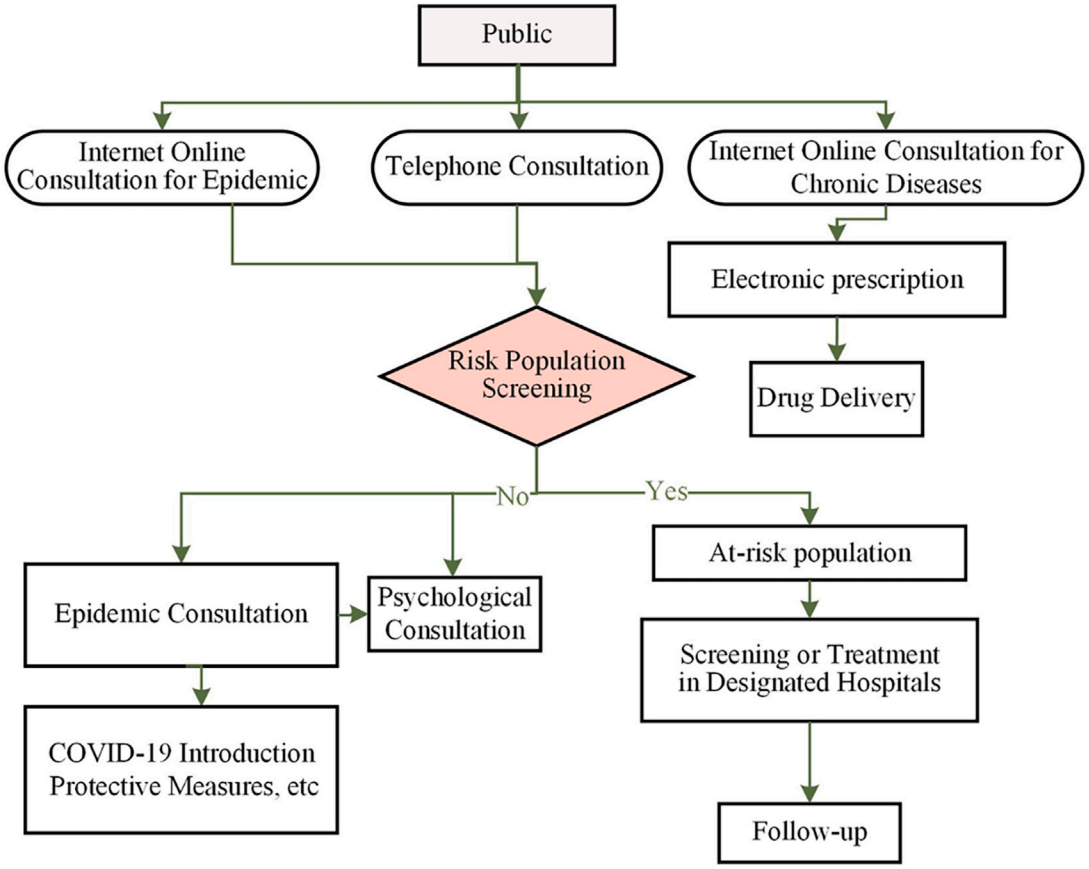

FIGURE 1
The work flow of online mode for epidemic management. The on-line project working team is divided into four groups, administrative group, Information group, Consultation group and Follow-up group.

information collection system where patients could autonomously gather symptom data through multimodal inputs, including text, voice, and images. Patients described their symptoms and experiences, and the system automatically analyzed the uploaded data to rank suspected cases, generating a list of suspected patients based on confidence levels [9–11]. If necessary, individuals with suspected cases were advised to visit designated hospitals for diagnosis or follow-up treatment.

A knowledge base, containing professional medical guidelines and research content, was constructed to store various disease-related information and support scientific education. A team consisting of medical experts, IT specialists, and data managers was established to update, review, and maintain the Clinical Decision Support System (CDSS) knowledge base. Regular updates ensured that the latest clinical research findings and guidelines were promptly integrated into the system. The scientific education provided included introductions to infectious diseases, protective measures, mask-wearing methods, disinfection, and handwashing techniques. For those experiencing anxiety and stress due to the epidemic, a team of professional psychologists offered psychological counseling services. The process of online consultation during the epidemic is illustrated in a diagram (Figure 2). For patients with a clear epidemiological history, we provided one-on-one guidance to direct them to the nearest location for nucleic acid testing and quarantine patients with positive testing results.

Pre-consultation medical history collection

Patients were free to describe their symptoms and sensations using voice, text, or a combination of both. The system analyzed the patient's condition and automatically provided a ranked list of suspected diseases along with confidence levels. Patients could also choose to further specify their symptoms with additional options, such as selecting the affected body part, to describe their condition in more detail, thereby receiving more accurate department recommendations. Based on these recommendations, patients could choose to continue with either online or in-person consultations until the consultation was completed.

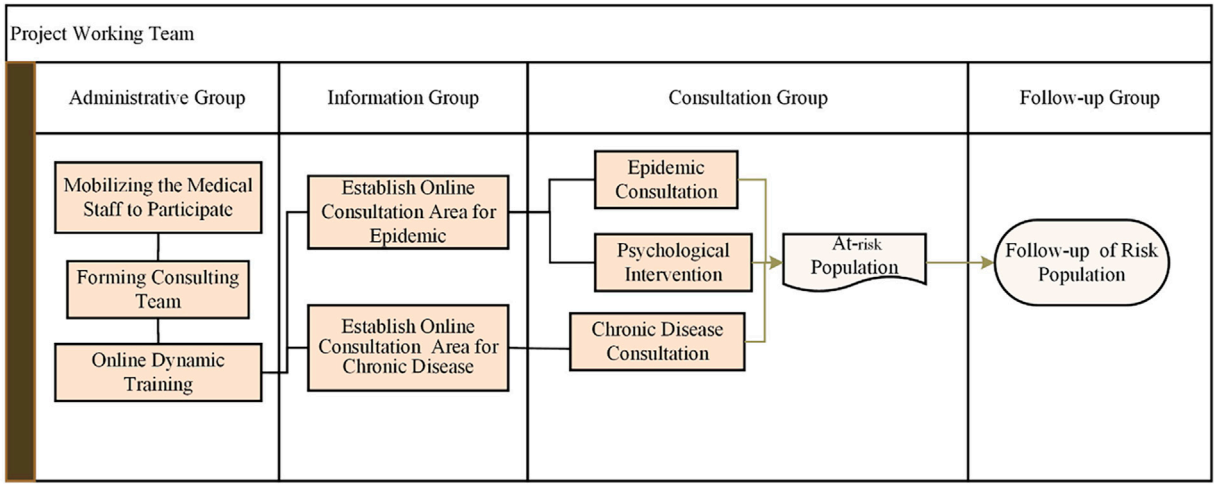

FIGURE 2
Online model consultation operation process. The on-line consultation includes two main activities, consultation for epidemic and consultation for chronic diseases. Scientific education, psychological consultation, and chronic diseases prescriptions are achieved online, meanwhile the persons at risk are screened.

Knowledge base construction

The intelligent triage system required a knowledge base to store information about hospital departments, doctors' availability for online and offline consultations, disease manifestations, and disease names. In this study, the disease knowledge base was derived from professional medical guidelines and textbooks, integrated with a large number of outpatient medical records, and confirmed by authoritative experts in the field.

Online consultations and medication delivery for chronic disease patients

Chronic disease patients are those who require long-term medication and regular hospital visits for prescription refills. To avoid cross-infection during the epidemic, chronic disease patients described their recent health status to doctors via the online consultation platform. Each department established its own project team and developed corresponding follow-up procedures. A multidisciplinary team (MDT) outpatient clinic was set up as a central hub for chronic disease patients. The system pre-sorted the patient's condition based on pre-visit online data collection and consultation content. For patients with unclear diagnoses, the MDT treatment team jointly discussed and made decisions, categorizing chronic disease patients and directing them to the appropriate specialized department, thereby improving diagnostic efficiency. If the patient's condition was stable and showed no significant changes, the doctor would send an electronic prescription to the pharmacy department. After the pharmacist approved the prescription, the patient could pay online, and the delivery company would deliver the medication to the patient's home. During the epidemic, registration fees were waived. According to the department's follow-up procedures, doctors could track the patient's condition and make adjustment to treatment and medication as needed at various follow-up points [12].

Departmental project teams

Each department established its own project team as needed and assigned team members with specific roles (administrator, disease manager, and management assistant). The follow-up process for each disease was then developed, with each follow-up process containing multiple follow-up points, which were visually displayed using a timeline to show the patient's status changes after enrollment.

MDT outpatient clinic

Inter-hospital MDT patients often require comprehensive treatment involving multiple disciplines. To facilitate this, our hospital established a green channel for post-consultation MDT patients, allowing appointments for follow-up consultations to be made during the consultation, or transferring the patient to the relevant specialist within the team with a single click. This helps patients receive timely consultations and enables the team of doctors to follow up on the patient's condition and adjust medication plans as needed. If the patient requires hospitalization, MDT office staff can stamp the admission certificate with a major disease green channel seal, helping patients gain quick admission and thereby improving patient satisfaction.

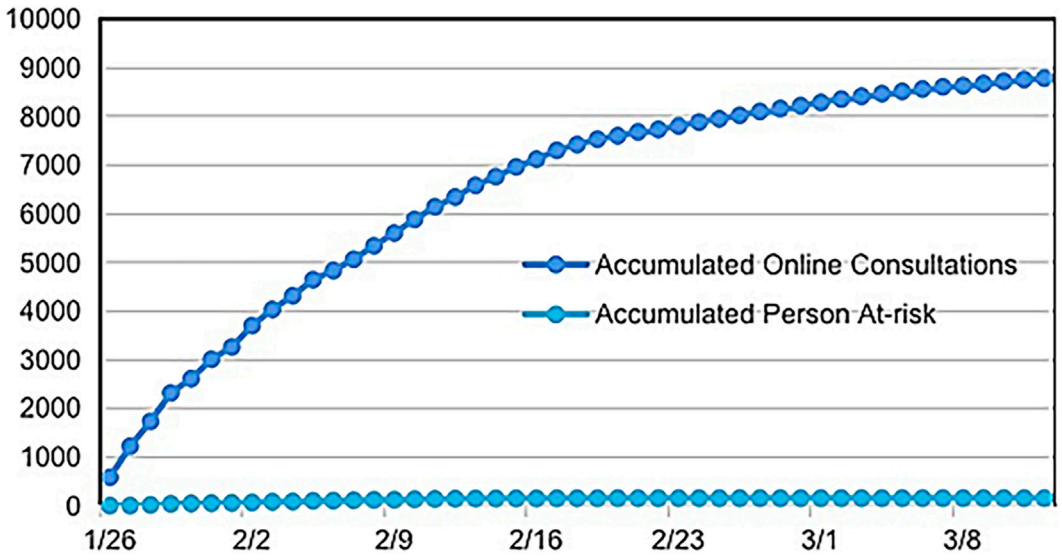

FIGURE 3
Data of internet online consultation for population in the epidemic from 29 January 2020, to 12 March 2020.

Telephone consultations

Since the first recorded medical telephone consultation in 1879, telephone consultations have become a key component of modern patient-centered healthcare systems. Today, more than a quarter of nursing consultations are conducted via telephone. To ensure that people of all ages could participate in epidemic consultations, we established telephone consultation services. Each department utilized machine learning to analyze large amounts of patient data and consultation records, predicting potential trends in issues or changes in user needs, and making timely adjustments to service strategies while preparing the necessary medical resources in advance. Considering that some elderly people might not be familiar with smartphones or the internet, they could call the hospital hotline, and the system would transfer their calls to the mobile phones of doctors in the epidemic consultation group. These consultations included high-risk population screening, scientific education, epidemic situation updates, and psychological counseling.

Results

As of 12 March 2020, a total of 485 healthcare workers had participated in online training and engaged in online consultations and follow-up work. Sixteen training materials were utilized, covering information about COVID-19, including the "Diagnosis and Treatment Protocol for Novel Coronavirus Pneumonia" issued by the National Health Commission of China (currently updated to the seventh edition) and recommendations from the Chinese Center for Disease Control and Prevention. Training sessions were provided once daily, allowing healthcare workers to learn online. Criteria for identifying potential suspected COVID-19 cases were established based on individual epidemiological histories and clinical symptoms. In summary, the screening process involved asking the following questions: 1) Whether the individual had lived in or traveled to Hubei Province within 14 days prior to the consultation; 2) Whether the individual had been in contact with a COVID-19 patient reported in the epidemic reporting internet system in the past 14 days; 3) Whether the individual had been in contact with someone from Hubei Province who had a fever or difficulty breathing in the past 14 days; 4) Whether the individual had a fever or difficulty breathing; 5) Whether the individual had CT imaging similar to COVID-19 infection; 6) Whether the individual had lymphopenia. As of 12 March 2020, 205 doctors conducted 8,783 online consultations through the epidemic internet platform, averaging 187 online consultations per day, and identified 154 potential high-risk suspected cases (Figure 3).

Telephone consultations began on 29 January 2020. As of 12 March 2020, a total of 1,082 telephone consultations had been conducted, with an average of 23 calls per day, identifying 135 potential high-risk suspected COVID-19 cases. As of 12 March 2020, a total of 289 potential COVID-19 risk patients were identified through online and telephone consultations, including one patient who had been diagnosed at the hospital but participated in online consultations. All high-risk patients were followed up daily, and they were guided to visit designated hospitals for further screening or diagnosis. During

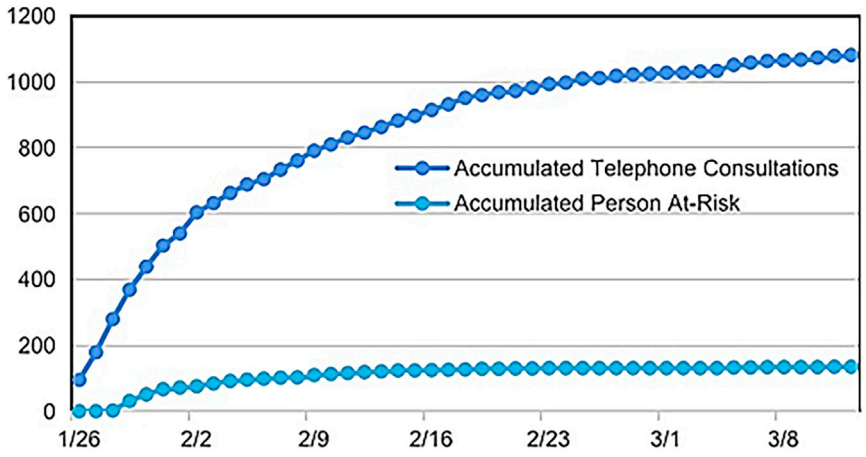

FIGURE 4
Data of telephone consultation for population in the epidemic from 29 January 2020, to 12 March 2020.

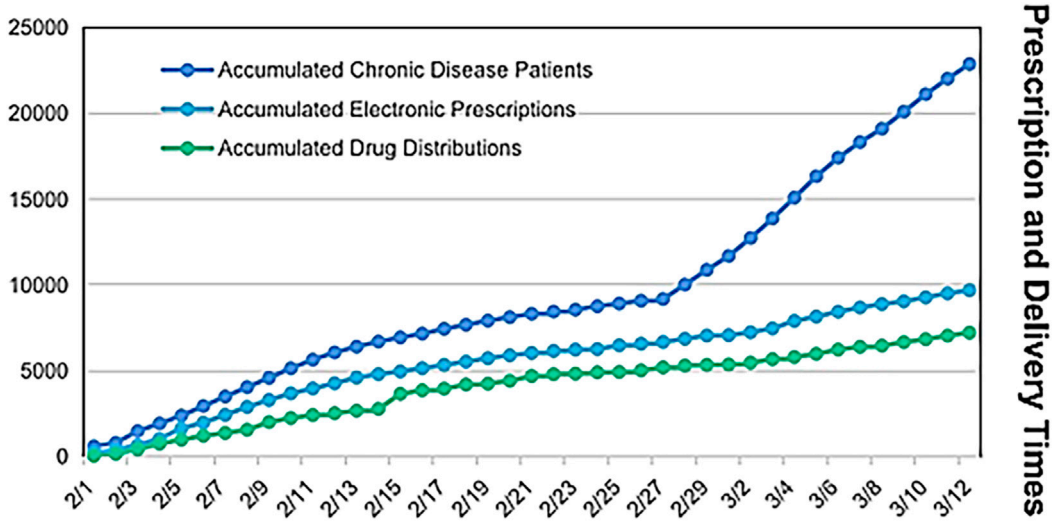

FIGURE 5
Online consultation, prescriptions and medicine distributions for chronic patients in the epidemic from 29 January 2020, to 12 March 2020.

the follow-up period, three suspected COVID-19 patients were diagnosed and treated at designated hospitals. The four confirmed patients were in stable condition. No infections were detected in the other patients during follow-up. (Figure 4).

As of 12 March 2020, 22,890 online consultations for chronic disease patients had been conducted, resulting in 9,690 electronic prescriptions and 7,218 medication delivery orders. The average daily consultation volume for chronic disease patients was 558 cases, with an average of 236 valid electronic prescriptions and 176 medication deliveries per day. During the epidemic, chronic disease patients were exempted from registration fees and delivery charges through the online consultation and medication delivery platform (Figure 5).

Discussion

We have reported a pioneering case of online medical strategies and outcomes during an infectious disease epidemic. Infectious diseases like COVID-19 primarily spread through human-to-human transmission in public spaces and during hospital visits, similar in some ways to severe acute

respiratory syndrome coronavirus (SARS-CoV). Potentially infected individuals (i.e., asymptomatic carriers) can also become sources of transmission [8, 13–15]. Patients may not have a fever or obvious symptoms but can still spread the virus to others [16]. Respiratory droplets and contact transmission are the main routes of spread. Individuals with weaker immune systems, such as the elderly, are more susceptible to COVID-19, and these elderly individuals often suffer from various chronic diseases. For highly contagious viruses like COVID-19, which are difficult to control, reducing contact and gatherings among people is an effective way to control the spread. The online consultation and diagnosis model aligns with the principle of reducing population movement and has proven to be an effective method for preventing and controlling infectious diseases. Online psychological consultations for the public provided a safe channel to reduce their panic, despair, and depressive symptoms during the COVID-19 outbreak.

The advantages of the online model include: 1) No need for in-person hospital visits, which reduces hospital traffic and lowers the risk of cross-infection between patients and between patients and healthcare workers; 2) No restrictions of time and space. People can consult doctors anytime and anywhere, without being limited by geographical location and time constraints. Doctors can complete online consultations and provide advice during working hours or even after hours; 3) Online follow-up for chronic diseases. Patients with chronic illnesses can consult professional doctors from home. Doctors issue electronic prescriptions, and medications are delivered to the patient's home, breaking the limitations of traditional healthcare, especially suitable during an epidemic. Over approximately 1 month, the online hospital model facilitated 32,755 online interactions, including 8,783 online consultations, 1,082 telephone consultations, and 22,890 follow-ups for chronic disease patients. The online model enabled rapid screening of high-risk populations, and suspected cases were further diagnosed and treated at designated hospitals. Through online consultations, people were informed about preventive measures such as proper mask-wearing, disinfection, frequent handwashing, reducing outings, and avoiding large gatherings. This model is not only effective for densely populated countries but also invaluable for countries with limited medical resources [17]. However, the online screening protocols evolved gradually, and not all participating clinicians acquired the necessary knowledge in a short period. At the same time, inconsistencies in screening procedures may have occurred, making it challenging to ensure accurate and sensitive screening uniformly.

The internet-based online model provided electronic prescriptions and medication delivery services for chronic disease patients. Most chronic disease patients, such as those with diabetes, cancer, or liver transplants, tend to be relatively stable over short periods. Many patients were able to efficiently communicate with specialized doctors through the online platform. Doctors could assess whether the patient's condition had significantly changed and determine whether the previous treatment plan should continue. If the condition remained stable, medications were delivered directly to the patient's home via electronic prescriptions. This online platform brought significant convenience to chronic disease consultations, electronic prescriptions, and medication delivery, while reducing the risk of cross-infection from contact with others at the hospital. By leveraging this internet-based online model during the epidemic, hospital pressure was alleviated, and it contributed to the broader effort in controlling the epidemic.

During infectious disease outbreaks, the increased tension and anxiety among the public further complicate epidemic prevention and control efforts. Online psychological counseling has been shown to alleviate public tension and anxiety [17]. Public emergencies, especially epidemics like COVID-19, often trigger emotional responses under emergency conditions. Many people experience tension and anxiety, with some even panicking. The public frequently worries about whether they have come into contact with infected individuals or whether they themselves are at risk of infection. They experience tension, fear, anxiety, and even become suspicious of everyone around them, harboring negative and pessimistic emotions toward others. If the public's tension and anxiety are not addressed promptly, it may lead to widespread panic. These behaviors can be assessed through online evaluation tools on the platform. After online consultations, as people gain knowledge about the epidemic and understand their own circumstances, their tension and anxiety are significantly reduced.

A robust information system is crucial for epidemic prevention and control in an internet-based online model [18]. Such a system must be supported by healthcare institutions with strong medical backing and a comprehensive information platform. The development of internet hospitals has met the needs of epidemic prevention. To ensure the smooth implementation of the online model, an "Online Project Task Force for COVID-19 Epidemic" was urgently established. Before the outbreak, the IT department had already developed an internet hospital platform, including applications for use by both doctors and the public. After the outbreak, the IT department developed online channels for epidemic consultations and chronic disease follow-ups, providing an internet platform for epidemic-related consultations, psychological counseling, and chronic disease management. The platform also allows for the issuance of electronic prescriptions. After patients make online payments through social insurance, medications are delivered to their homes by courier services.

In some infectious disease outbreaks, the rapid development of online models based on internet hospitals may lead to less

user-friendly experiences and insufficient levels of intelligent interaction. The overall process can be quite complex and requires further optimization and improvement. With the continuous advancement of artificial intelligence methods, big data, and 5G technology [19], an "intelligent decision-based online model" (further discussion) could better support epidemic prevention and control in the future.

To increase the level of intelligence, we considered using artificial intelligence methods for further improvement work as follows.

1) Risk Warning Module in Telephone Consultation System: A risk warning module could be constructed within the telephone consultation system. Potential risk factors, such as fraudulent calls or malicious complaints, might arise during telephone consultations. A federated learning model could be trained to identify these potential risks and take corresponding preventive measures. Since participants share model updates rather than raw data, this approach can effectively provide risk warnings while protecting user privacy.
2) System Interface Optimization and Customization for Departments: The user interface and operational processes of the Clinical Decision Support System (CDSS) should be continuously optimized based on feedback and needs from clinicians. Personalized customization services should be offered to ensure that the CDSS aligns more closely with the working habits of different departments and doctors.
3) Development of an Intelligent Drug Management System: An intelligent drug management system could be developed to improve the efficiency of medication management and dispensing within the pharmacy department. The system would categorize drugs and establish different inventory management strategies based on the importance and usage frequency of each drug. By analyzing historical data and forecasting demand, a scientific and reasonable procurement plan and replenishment strategy could be formulated. Real-time monitoring and automatic inventory checks would enhance the efficiency of drug management. Machine learning algorithms could be employed to analyze drug usage data, establish a risk warning mechanism, and provide real-time alerts for abnormal medication usage or potential drug interactions.
4) Development of an Intelligent Medical Assistant Based on a Knowledge Base: An intelligent medical assistant could be developed for use in smart triage, patient classification, and outpatient guidance. Departments could jointly train an intelligent medical assistant using federated learning technology, integrating a chatbot connected to the established knowledge base. This assistant would automate responses to common patient queries and consultation requests, improving the efficiency and coverage of hospital services. On the doctor's side, the intelligent medical assistant could interconnect with other medical information systems to gather necessary diagnostic data, provide relevant disease knowledge, and recommend personalized medical plans as diagnostic references, helping to address the issue of insufficient knowledge among some clinicians in a short time. Leveraging big data, the intelligent medical assistant could utilize machine learning to analyze large datasets of patient information and consultation records, predict potential trends in issues or changes in user needs, and update models at local levels using their patient data, with updates then aggregated and distributed back to the assistant centers to timely adjust service strategies and prepare the necessary medical resources.

In recent years, online platforms based on internet hospitals have developed rapidly for the prevention and control of infectious diseases. These online platforms typically offer functions such as online consultations, remote diagnostics, health monitoring, and case management Our research provided a remote, contactless hospital online model that provided the public with online medical consultations, professional psychological counseling, and chronic disease management consultations, significantly enhancing the efficiency and precision of infectious disease prevention and control.

Author contributions

XZ was involved in emergency coordination and organization and manuscript structure writing. HH contributed to the construction of the information system and manuscript writing. GZ played a role in the overall planning, coordination, organization of the online consultation, and the construction of information system. QS participated in literature search, chart generation and overall coordination of hospital medical resources. PZ contributed to the conceptualization and modified the manuscript. LZ played a role in follow-up tracking of high-risk populations. LZ and LuL were involved in coordinating the online consultation team, data collection, data analysis and data interpretation. LeL and QS a played a role in data collection and coordinating and organizing doctors for online consultations. LuL played a role in study design, overall coordination of hospital medical resources, and manuscript writing. NH provided infectious disease expertise and reviewed training materials. WL and KY provided suggestions for the project and refined language expression of the manuscript. All authors contributed to the article and approved the submitted version.

Data availability

The original contributions presented in the study are included in the article/supplementary material, further inquiries can be directed to the corresponding author.

Ethics statement

The studies involving human participants were reviewed and approved by the Sichuan University Medical Ethics Committee and have been performed in accordance with the ethical standards as laid down in the 1964 Declaration of Helsinki and its later amendments or comparable ethical standards. Written informed consent was not required in the study, permitted by the Sichuan University Medical Ethics Committee, because the data used in this study were obtained from previous clinical treatment records. (Acquisition Period: January 2020 - March 2020).

Funding

The author(s) declare that financial support was received for the research and/or publication of this article. Primary Project: Research on Intelligent Medical Emergency Models and Applications for Public Safety Incidents. Funded by the Sichuan Provincial Science and Technology Department, Project Number: 2018sz0353. Sichuan University West China Hospital COVID-19 Research Project: Research on an AI-based COVID-19 Monitoring System. Project Number: HX-2019-nCoV-035.

Conflict of interest

The author(s) declared no potential conflicts of interest with respect to the research, authorship, and/or publication of this article.

References

1. Report of the WHO-China joint missionon coronavirus disease 2019 (COVID-19). (2020). Available online at: https://www.who.int/docs/default-source/coronaviruse/who-china-joint-mission-on-covid-19-final-report.pdf (Accessed February 28, 2020).

2. World Health Organization. Novel coronavirus – China (2020). Available online at: https://www.who.int/emergencies/disease-outbreak-news/item/2020-DON233 (Accessed January 12, 2020).

3. Huang C, Wang Y, Li X, Ren L, Zhao J, Hu Y, et al. Clinical features of patients infected with 2019 novel coronavirus in Wuhan, China. *The Lancet* (2020) **395**(10223):497–506. doi:10.1016/s0140-6736(20)30183-5

4. Xu Z, Shi L, Wang Y, Zhang J, Huang L, Zhang C, et al. Pathological findings of COVID-19 associated with acute respiratory distress syndrome. *The Lancet Respir Med* (2020) **8**:420–2. doi:10.1016/s2213-2600(20)30076-x

5. Xu Z, Li S, Tian S, Li H, Kong LQ. Full spectrum of COVID-19 severity still being depicted. *The Lancet* (2020) **395**:947–8. doi:10.1016/s0140-6736(20)30308-1

6. World Health Organization. Corona-virus disease (COVID-19) outbreak (2025). Available online at: https://www.who.int (Accessed August 16, 2024).

7. Wang D, Hu B, Hu C, Zhu F, Liu X, Zhang J, et al. Clinical characteristics of 138 hospitalized patients with 2019 novel coronavirus-infected pneumonia in wuhan, China. *JAMA* (2020) **323**:1061. doi:10.1001/jama.2020.1585

8. Chan JF, Yuan S, Kok KH, To KKW, Chu H, Yang J, et al. A familial cluster of pneumonia associated with the 2019 novel coronavirus indicating person-to-person transmission: a study of a family cluster. *The Lancet* (2020) **395**(10223):514–23. doi:10.1016/s0140-6736(20)30154-9

9. Defilippo A, Veltri P, Lió P, Guzzi PH. Leveraging graph neural networks for supporting automatic triage of patients. *Scientific Rep* (2024) **14**(1):12548, doi:10.1038/s41598-024-63376-2

10. Mutegeki H, Nahabwe A, Nakatumba-Nabende J, Marvin G. Interpretable machine learning-based triage for decision support in emergency care. In: *2023 7th international conference on trends in electronics and informatics (ICOEI), tirunelveli, India* (2023). p. 983–90.

11. Salman M, Zolait A, Alaafia M, Almalood S, Fateel Z. Continuity of project's follow-up practice during COVID-19: identifying predictors and challenges. In: *2021 international conference on innovation and intelligence for informatics, computing, and technologies (3ICT)*. Zallaq, Bahrain (2021). p. 112–9.

12. Rothe C, Schunk M, Sothmann P, Bretzel G, Froeschl G, Wallrauch C, et al. Transmission of 2019-nCoV infection from an asymptomatic contact in Germany. *N Engl J Med* (2020) **382**:970–1. doi:10.1056/nejmc2001468

13. Phan LT, Nguyen TV, Luong QC, Nguyen TV, Nguyen HT, Le HQ, et al. Importation and human-to-human transmission of a novel coronavirus in vietnam. *N Engl J Med* (2020) **382**(9):872–4. doi:10.1056/nejmc2001272

14. Gilbert M, Pullano G, Pinotti F, Valdano E, Poletto C, Boëlle PY, et al. Preparedness and vulnerability of African countries against importations of COVID-19: a modelling study. *The Lancet* (2020) **395**:871–7. doi:10.1016/s0140-6736(20)30411-6

15. Rosso C. How COVID-19 may impact mental health (2020). Available online at: https://www.psychologytoday.com/us/blog/the-future-brain/202003/how-covid-19-may-impact-mental-health (Accessed August 16, 2024).

16. Guan WJ, Ni ZY, Hu Y, Liang W, Ou C, He J, et al. Clinical characteristics of coronavirus disease 2019 in China. *N Engl J Med* (2020) **382**:1708–20. doi:10.1056/nejmoa2002032

17. Zhu N, Zhang D, Wang W, Li X, Yang B, Song J, et al. A novel coronavirus from patients with pneumonia in China, 2019. *N Engl J Med* (2020) **382**(8):727–33. doi:10.1056/nejmoa2001017

18. Nyarko Y, Goldfrank L, Ogedegbe G, Soghoian S, de-Graft Aikins A, Group N-U-KGEW. Preparing for Ebola Virus Disease in West African countries not yet affected: perspectives from Ghanaian health professionals. *Glob Health* (2015) **11**:7. doi:10.1186/s12992-015-0094-z

19. Li D. 5G and intelligence medicine-how the next generation of wireless technology will reconstruct healthcare? *Precision Clin Med* (2019) **2**(4):205–8. doi:10.1093/pcmedi/pbz020

EBM Experimental Biology and Medicine

TYPE Original Research
PUBLISHED 25 April 2025
DOI 10.3389/ebm.2025.10422

OPEN ACCESS

*CORRESPONDENCE
Kyriacos Mitrophanous,
k.mitrophanous@oxb.com

RECEIVED 02 November 2024
ACCEPTED 15 April 2025
PUBLISHED 25 April 2025

CITATION
Guzman E, Khoo C, O'Connor D, Devarajan G, Iqball S, Souberbielle B, Mitrophanous K and Lad Y (2025) Gender difference in pre-clinical liver-directed gene therapy with lentiviral vectors.
Exp. Biol. Med. 250:10422.
doi: 10.3389/ebm.2025.10422

Gender difference in pre-clinical liver-directed gene therapy with lentiviral vectors

Efrain Guzman, Cheen Khoo, Deirdre O'Connor, Gayathri Devarajan, Sharifah Iqball, Bernard Souberbielle, Kyriacos Mitrophanous* and Yatish Lad

Oxford Biomedica (UK) Limited, Oxford, United Kingdom

Abstract

Viral vector-based therapies are effective therapeutics for the correction of several disorders, both in mouse models and in humans. Several pre-clinical studies have demonstrated differences in transduction efficiencies and therapeutic effect between male and female mice dosed with AAV-based gene therapy product candidates. Here, we report gender-specific transduction and transgene expression differences in mice dosed systemically with lentiviral vectors (LVV). Male mice systemically dosed with LVV carrying the reporter gene luciferase showed at least a 12-fold higher expression of luciferase and a higher vector copy number (VCN) in their livers compared with female mice. Lastly, PAH^{Enu2} male mice dosed with a LVV carrying the human phenylalanine hydroxylase (PAH) transgene were observed to have a higher VCN than their female littermates. These findings suggest that sex-based differences initially observed in AAV-mediated therapies also apply to LVV, but the exact mechanism remains to be determined.

KEYWORDS

lentiviral vectors, adeno-associated virus, AAV, liver, PAH, gender, murine

Impact statement

There are many reports of lower expression of adeno-associated virus (AAV) transgenes in female compared to male mice. The reason for this difference has not been explained with different theories proposed. This report is the first report that describes the same phenomenon with a different viral vector, i.e. lentiviral vectors, and suggests universality for the phenomenon, not exclusive to AAV, thus excluding a receptor-specific phenomenon explanation. It is hoped that this report will stimulate other groups working with lentiviral vectors to confirm, or refute, this observation from their own data, and potentially other groups working with viral vectors other than lentiviral vectors and AAV. If confirmed, this report will help understand the reasons for this sex-difference phenomenon in murine models and stimulate specific experimental work to explain the phenomenon. Whether this phenomenon is also observed in humans, this is not currently known, but it should also be investigated in humans.

Introduction

Lentiviral vectors (LVV) are an established platform for gene delivery. LVV integrate into the host's genome providing long-term expression of the therapeutic transgene. They are the preferred platform for the *ex vivo* transduction of haematopoietic cells or generation of CAR-T cells in clinical applications with good safety and efficacy profiles with several approved products on the market [1]. There are numerous pre-clinical reports of *in vivo* delivery of LVV targeting the liver for the correction of metabolic disorders [2–8], however none have yet to be translated into the clinic in contrast to AAV based vectors.

Achieving optimal transduction and therapeutic transgene expression following *in vivo* delivery is essential for demonstrating the efficacy of gene therapy candidates during pre-clinical studies. In general, laboratory mice are the chosen model to do so for gene therapy products. However, there are multiple reports of reduced transduction efficiency, lower expression of the transgene and product efficacy in female mice compared to male mice in liver-directed gene therapy studies with adeno-associated virus (AAV) [9–12].

Several mechanisms for the observed gender differences in transduction and transgene expression in mice have been proposed [10]. It is unlikely that the observed differences are solely due to differential expression of the AAV binding receptor(s) on liver cells, as gender differences have been demonstrated in mice across different AAV serotypes that bind and enter through unrelated receptors [10]. In addition, whether the transduction efficiencies and transgene expression differences in the livers of male vs. female laboratory mice is strain-specific or serotype-specific is not currently known. It has been suggested that transgene expression difference observed in both genders of mice could be due to specific binding of the AAV to liver proteins in an androgen-dependent pathway [10]. Whether this hypothesis applies solely to AAV based vector or to other vector formats remains to be tested.

With AAV based vectors, several routes of delivery have been evaluated for liver-based gene therapies targeting the liver in both pre-clinical models and in the clinic. Intravenous (IV) administration is by far the simplest route of administration that can be translated from pre-clinical models to patients. In addition to IV administration, portal vein (PV) and hepatic artery injections have also been evaluated, as well as direct administration into the liver tissue.

In this study we evaluated *in vivo* transduction efficiency of hepatocytes and transgene expression of the liver with LVV in both male and female mice. To our knowledge, such a comparison of transduction and transgene expression of vector-encoded transgenes has not been reported with LVV. Here, we report an increase in the transduction efficiencies and transgene expression in the livers of male laboratory mice compared to female mice following delivery of LVV.

Materials and methods

Cell lines

The human embryonic kidney cell line expressing the SV40 large T antigen (HEK293T) was obtained from ATCC (LGC Standards, Teddington, United Kingdom) and cultured in Dulbecco's modified Eagle's medium (DMEM, Merck Life Science, Dorset, United Kingdom) supplemented with 10% heat-inactivated fetal bovine serum (FBS; ThermoFisher Scientific, United Kingdom), 2 mM L-glutamine (Merck Life Science) and 1% non-essential amino acids (NEAAs; Merck Life Science). HEK293T cells adapted to culture in suspension phase were maintained in Freestyle™ 293 Expression Medium (FS; ThermoFisher Scientific) with 0.1% cholesterol lipid concentrate 250X (CLC; ThermoFisher Scientific) (FS + 0.1% CLC).

Vector construction

Third generation lentiviral vector carrying Gaussia luciferase cDNA (LVV-GLuc) was generated as follows: the coding sequence for GLuc followed by a T2A and the enhanced green fluorescent protein (eGFP) sequences were synthesized by ThermoFisher Scientific and cloned into a minimal self-inactivating, third generation HIV-1 transfer vector downstream of a mouse transthyretin promoter preceded by a synthetic enhancer [13], also referred to as ETpro. OXB-401 was generated by cloning synthetic cDNA encoding the human codon optimized phenylalanine hydroxylase gene (PAH, ThermoFisher Scientific) into a minimal self-inactivating, third generation HIV transfer vector downstream of the ETpro mentioned above. OXB-Null did not contain any coding sequences downstream of the ETpro.

Vector production

Third generation, VSVG-pseudotyped LVV were produced and titrated in HEK293T cells as described before [14] and resuspended in a formulation buffer of Tromethamine, NaCl, Sucrose and Mannitol (TSSM) [15] which was also used as vehicle control.

Mice

All animal studies were carried out by Charles River (CR) Discovery Services and approved by the local ethics committee. For the initial gene transfer study, 5–8 week-old male and female BTBR mice (BTBR T^+ Itpr3/J, n = 5/group, The Jackson Laboratory) of an average weight of 25g, were dosed with 1.5×10^{10} TU/kg [intravenously (IV) via the tail vein] or 7.5×10^9 TU/kg [via the intrahepatic portal vein (PV)] of LVV-GLuc (n = 5/group) or with TSSM buffer (n = 1/group) either via IV or PV routes (Table 1).

TABLE 1 Study design for the long-term gene transfer study.

Name	Sex	Route	Treatment	Vector dose (TU/kg)
Group 1	Female	IV	TSSM	N/A
Group 2	Female	IV	LVV-GLuc	1.5×10^{10}
Group 3	Male	IV	TSSM	N/A
Group 4	Male	IV	LVV-GLuc	1.5×10^{10}
Group 5	Female	PV	TSSM	N/A
Group 6	Female	PV	LVV-GLuc	7.5×10^{9}
Group 7	Male	PV	TSSM	N/A
Group 8	Male	PV	LVV-GLuc	7.5×10^{9}

TABLE 2 Study design for the OXB-401 study.

Name	Sex	Route	Treatment	Vector dose (TU/kg)
Group 1	Female	IV	OXB-Null	4×10^{10} TU/kg
Group 2	Male	IV	OXB-401	4×10^{10} TU/kg
Group 3	Female	IV	OXB-Null	4×10^{10} TU/kg
Group 4	Male	IV	OXB-401	4×10^{10} TU/kg

Dosing was performed according to the average weight of the male or female mice respectively. Due to the maximum volume that could be administered by intrahepatic portal vein injection limited to 100 µL compared to the 200 µL by tail vein administration there is a 2-fold lower total dose administered to the mice via this route. The study designs are summarized in Table 2.

Whole body bioluminescent imaging was performed as described before [9, 16] on days 1, 8, 15, 22, 29, and then once every 2 weeks until day 83 post dosing. Two mice each from Groups 2, 4, 6, and 8 were sacrificed at day 29 to determine VCN. D-luciferin was administered (150 mg/kg) intraperitoneally (IP) and 10 min post substrate injection, dorsal and ventral images were taken, and the scaled images quantified.

For the second study, BTBR-*Pah*^{enu2}/J mice [17], also referred to as Pah^{enu2}) were obtained from The Jackson Laboratory and dosed IV with TSSM buffer (200 µL), OXB-Null (4×10^{10} TU/kg) or OXB-401 (4×10^{10} TU/kg) and observed for the duration of the study (85 days). All animals were euthanized at the end of the studies and the livers collected and snap-frozen.

Genomic DNA extraction from liver tissues

Liver tissues from median and right lobes were weighed and 22 mg to 26 mg were homogenised in PBS using the TaKaRa® BioMasher standard micro homogenizers. Genomic DNA was extracted using DNeasy Blood and Tissue Kit (Qiagen) following the manufacturer's instructions.

Quantification of integrated vector copies (VCN)

Duplex qPCR (QuantStudio 7, Thermo ABI) was performed on the liver-extracted DNA to obtain LVV integrated VCN per cell as described before [7] using the transferrin receptor protein 1 (*tfrc*) as a housekeeping gene. The primer probe set for *tfrc* was purchased from (ThermoFisher catalogue number 4458366) and primer probe set for HIV Ψ were synthesized by ThermoFisher.

The formula to calculate integrated VCN is as follows:

$$\text{VCN} = \frac{\text{Copies of Psi}}{\text{Copies of tfrc (divide by 2)}}$$

Statistical analysis

Data analysis and generation of graphs was performed using GraphPad Prism v.9 for Windows (GraphPad, San Diego, CA, United States) with descriptive statistics. Normality tests were used to evaluate the Gaussian distribution of data. Normally distributed data were analyzed using ordinary one-way ANOVA, and data not normally distributed were analyzed using Kruskal-Wallis and Dunn's multiple-comparisons tests.

Results

Long-term expression of LVV-encoded transgenes in mice treated systemically

An initial *in vivo* gene transfer study was designed to determine the transduction efficiency of LVV carrying the luciferase transgene (Table 1). Mice were dosed with pre-clinical grade preparations of LVV-GLuc, delivered via the intravenous (IV) or portal vein (PV) routes. *In vivo* imaging was carried out at regular intervals to determine transgene expression over time. LVV-encoded luciferase activity was observed as soon as day 8 and until the end of the study on day 83 (Figure 1A). Two mice, from Groups 2, 4, 6, and 8, were sacrificed at day 29 to determine VCN with the remaining three mice continuing to day 83. Luciferase expression, measured by whole body luminescence, was observed almost exclusively within the anatomical area which corresponds to the liver and was observed across all vector treated groups, males and females, and via both routes of delivery, IV and PV, from day 8 to the end of the study at day 83 (Figure 1A). In contrast, no luciferase expression was observed in the TSSM-treated groups (Figure 1B).

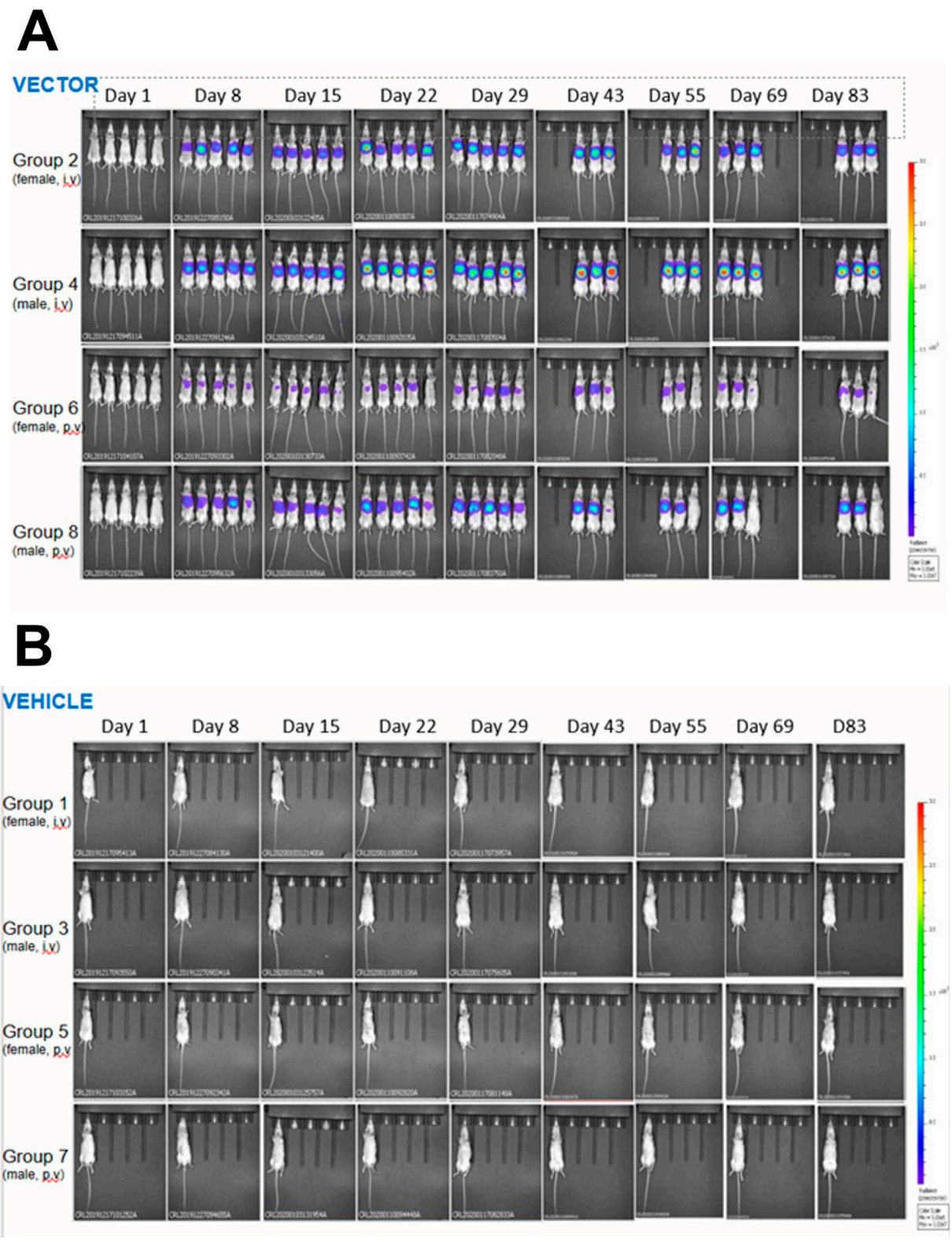

FIGURE 1
In vivo bioluminescent imaging of the expression of LVV-encoded luciferase in mice dosed with LVV- GLuc **(A)** or the vehicle TSSM **(B)** via either the intravenous (IV) or the portal vein (PV) routes. Mice were imaged as described in *Materials and Methods*.

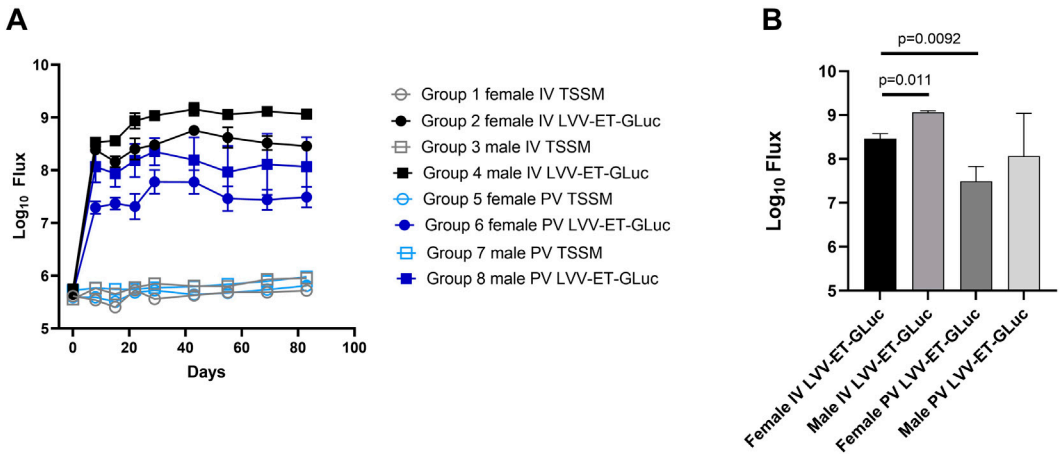

FIGURE 2
Quantification of luciferase expression of LVV-encoded luciferase in mice dosed with LVV-GLuc. **(A)** Quantification of *in vivo* expressed luciferase of all groups over time. **(B)** Quantification and statistical analysis of the *in vivo* expressed luciferase of all groups at day 83.

A quantitative analysis of luciferase expression *in vivo* showed that the maximum transgene expression was achieved between days 22 and 43 post-dosing and was sustained until the end of the study at day 83 (Figure 2A). Luciferase activity in the TSSM-treated group was considered background activity. *In vivo* expression of luciferase was higher in the groups dosed IV compared to the groups dosed PV at all time points (Figure 2A). It should be noted that the IV groups had a 2-fold higher dose of vector than the PV groups. A final statistical analysis at the end of the study showed that male mice dosed with LVV-GLuc had higher expression of luciferase than females dosed with the same vector in both IV (12-fold, $p = 0.011$) and PV (12-fold, $p = 0.3867$) routes (Figure 2B). In comparing routes of delivery within female and male groups, IV delivery of the vector resulted in higher luciferase expression than PV administration in both females (13-fold, $p = 0.0092$) and males (13-fold, $p = 0.1498$).

In conclusion, this analysis of the LVV *in vivo* gene transfer study demonstrated stable transgene expression out to the end of the study at day 83 and that as observed with AAV based vectors there is a higher transgene expression in the male mice compared to the female mice. In addition, the IV route mediated an increase in transgene expression compared to the PV route greater than the two-fold increase in vector dose administered via this route.

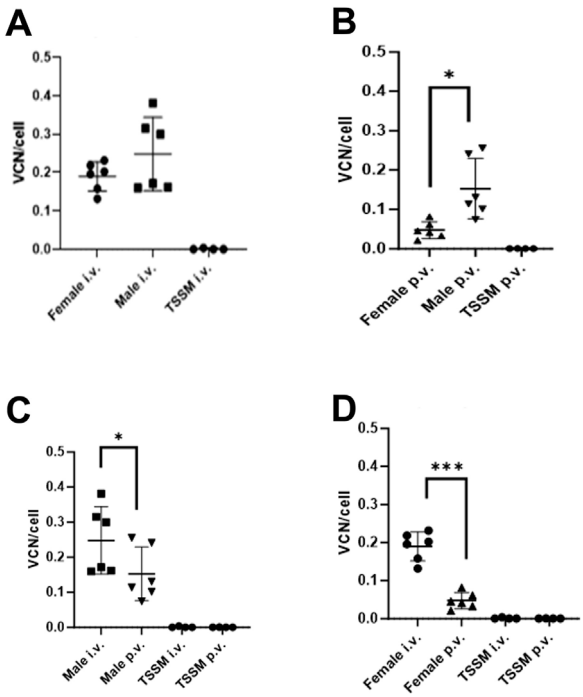

FIGURE 3
Integrated vector copy number (VCN) in livers of male and female mice dosed via two different routes of administration. Livers were collected at day 83 post dosing. **(A)** Male vs. female dosed IV. **(B)** Male vs. female dosed PV; * indicates $p = 0.014$. **(C)** Males dosed IV vs. PV; * indicates $p = 0.0008$. **(D)** Females dosed IV vs. PV; *** indicates $p = 0.0301$.

Transduction efficiency differences between male and female mice

To determine if the differences in transgene expression observed above were due to differential transduction efficiencies *in vivo*, integrated vector copy number (VCN) analysis was carried out on the livers of all animals at the end of the study. Two mice from each group were euthanised at day 29 and VCN/cell was measured in the median and right liver lobes. VCN/cell was 4.8-fold higher in males (0.24 VCN/cell)

compared to females (0.05 VCN/cell) dosed through the PV route (p = 0.0218) but with mice dosed through the IV route there was no significant difference between the male (0.24 VCN/cell) and female mice (0.21 VCN/cell, p = 0.3935, result not shown).

In the remaining mice taken to the end of the study at day 83, VCN was higher overall in males compared to females for both IV and the PV routes (Figures 3A, B). VCN obtained from male mice in the IV group was 0.25 VCN/cell and not significantly different to VCN obtained from female mice (0.20 VCN/cell, p = 0.4237, Figure 3A) and similar to that observed in the mice taken at day 29. With the mice administered vector via the PV route there is a 5.9-fold increase in VCN/cell in male (0.176 VCN/cell) versus female mice (0.03 VCN/cell, p = 0.014, Figure 3B), which is consistent with the significant difference seen at day 29. In comparing routes of delivery within sexes, male mice dosed IV had 2-fold higher VCN/cell compared with male mice dosed via the PV route (p = 0.0301, Figure 3C). Similarly, female mice dosed IV had 4.9-fold higher VCN/cell compared with female mice dosed via the PV route (p = 0.0008, Figure 3D).

In summary there was a 12 to 13-fold difference in gene expression (from Figure 2 data), a higher VCN in male vs. female mice, and a higher VCN in the IV-dosed vs. PV-dosed groups, therefore we can conclude that the difference in transgene expression between these groups can be partly attributed to differences in transduction efficiencies.

Differences in *in vivo* transduction efficiencies between male and female mice using a clinically-relevant therapeutic vector and transgene

To determine if the differences in transgene expression observed above were only seen using the reporter gene Gaussia luciferase, an analysis was conducted on a *in vivo* study using a therapeutic cargo and a mouse model of a human disease. OXB-401 is a third-generation LVV carrying a full-length copy of the human codon-optimized phenylalanine hydroxylase (PAH) open reading frame driven by the liver-specific ET promoter (ETpro). Both male and female Pah^{enu2} mice (n = 5) were dosed intravenously with OXB-401 or OXB-Null as described in *Materials and Methods*. VCN analysis was performed on the livers harvested at the end of the study at day 85 days post-dosing. Male mice showed 2 to 3-fold higher but not significant (p > 0.05) VCN/cell than females in both treatment groups (Figure 4).

When the VCN/cell data in this study were compared with the data from the previous experiment it was observed that male mice had an average of 0.54 VCN/cell and females had an average of 0.25 VCN/cell, however these differences were not statistically significant (p = 0.1792). The spread of the data suggested that the transgene itself (GLuc, PAH or Null) does not have a significant effect on transduction efficiencies (data not shown).

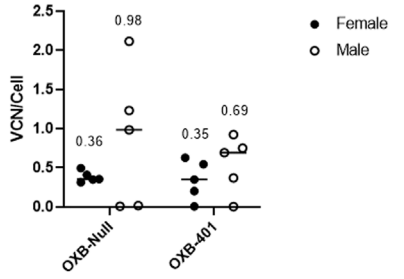

FIGURE 4
Differential transduction efficiencies in male vs. female Pah^{enu2} mice dosed IV with either OXB-401 or OXB-Null. Median VCN is shown for each group at day 85 post dosing. No significant differences were observed between the groups (p > 0.05).

These results are further evidence of the differential LVV transduction efficiencies in laboratory mice.

Discussion

In this report we have shown that the liver expression of a reporter gene administered *in vivo* using a systemic lentiviral vector was significantly higher in male mice compared to female mice. Vector copy number per cell was also higher in male mice compared to female mice. In addition, an increased trend in transduction between male and female, although not significant, was also observed in a therapeutic model of disease with both the therapeutic vector, OXB-401 and a control vector OXB-Null.

To date there have been no reports comparing the expression of *in vivo*-delivered LVV between male and female mice. Our initial LVV *in vivo* gene transfer studies were designed to identify the optimal route of delivery for the transduction of the liver, to assess the safety profile of pre-clinical grade vector batches and to determine duration of the reporter transgene. The current study was designed using both male and female outbred laboratory mice. The luciferase signal was observed within 8 days and peaked between 22 and 43 days post dosing and was stable until the end of the study at day 83 post dosing, indicating long term expression of the transgene following a single administration of the vector. We and others have demonstrated stable transgene expression in other tissues and the liver in pre-clinical models [18]. In the clinic, with a gene therapy for wet-AMD, we have demonstrated stable and long-term transgene expression from a lentiviral vector in the eye for greater than 6 years [19].

In our studies, IV delivery of LVV post 83 days resulted in a 12-13-fold increase in luciferase activity than PV delivery during *in vivo* imaging in both male and female mice. While there was a two-fold increase in vector dose administered IV compared to

the PV route due to constraints in total volumes able to be administered this only partly provides a reason for the increase in luciferase signal. Integrated vector copy number (VCN) analysis, carried out at the end of the study, demonstrated that IV dosing resulted in higher (2 to 5-fold) VCN compared to PV dosing (Figures 3A–D). With AAV based vectors, hepatic artery delivery has been assessed in pre-clinical models [20] and unlike our study they found that intravenous injection of AAV2 resulted in 4-10 fold less hepatic transduction when compared to intra portal injection [21]. For humans, portal vein and hepatic artery injections are more invasive than peripheral intravenous injection and need trained individuals who are experts in interventional radiology or surgical procedures, therefore increasing the complexity of the therapeutic approach compared to an approach based on peripheral injection.

When we compared the transgene expression differences between genders, we observed a higher luciferase expression in mice dosed via the IV route and the PV route post 83 days transduction. The increase was observed as soon as 8 days post dosing in both the IV and PV groups. A similar finding has also been reported with AAV-Luciferase dosed mice [16] This difference in transgene expression has been extensively reported with AAV based vectors in laboratory mice and this is the first report of this observation with LVV.

When VCN/cell analysis was performed at day 29 and day 83 there is a trend of an increase in transduction efficiency in male mice compared to female mice. These increases in VCN/cell may partly account for the increased expression in male versus female mice but other contributing factors may also be involved. To our knowledge this is also the first report of sex-specific differences in LVV transduction efficiencies and transgene expression.

To determine if the differences observed in VCN/cell using the reporter gene luciferase and outbred laboratory mice were specific to this study, a study was conducted using a therapeutic transgene and a mouse model of a human disease. OXB-401 is a third-generation LVV carrying a full-length copy of the human codon-optimized phenylalanine hydroxylase (PAH) gene driven by the liver-specific ET promoter (ETpro). Pah^{enu2} (BTBR-*Pah*^{enu2}/J) mice carry a T835C missense mutation, yielding an F263S single amino acid substitution that causes severely diminished PAH catalytic activity in homozygotes and provide a model of severe phenylketonuria. VCN analysis from the livers of Pah^{enu2} mice harvested 85 days post-dosing demonstrated a higher, but not statistically significant, change in transduction efficiency between male and female mice (Figure 4) with both therapeutic OXB-401 and the OXB-null vectors. Interestingly, two previous publications also reported sex-specific differences in Pah^{enu2} mice systemically dosed with AAV carrying a human PAH cDNA transgene [11, 22]. These results are further evidence of sex-differential LVV transduction efficiencies in at least two strains of laboratory mice. In our studies we used the liver-specific promoter ETpro, and so it would be important to determine if other promoters result in same or different results.

It has been suggested that androgens are likely responsible for the enhanced AAV transduction in male mice as castration was shown to reduce AAV transgene expression, whereas treatment of female mice with testosterone improved AAV transduction to levels observed in males [10, 23]. Additionally, AAV transduction differences between male and female mice have also been reported in organs other than the liver [24]. Our data indicate that sex-specific differences in AAV transduction efficiencies also apply to VSVG-pseudotyped LVV, but further analysis is required to better understand the mechanism of the gender differences observed in this report, including the effect of LVV envelopes other than VSVG. To date, these gender-specific differences have not been reported in species other than laboratory mice, as most AAV and LVV-related pre-clinical studies only use mice as the model species. When the gender difference expression is also confirmed by other groups, it would be important to assess the relative effects of different LVV envelops. In addition, the effect of age and sexual maturity has not been evaluated in pre-clinical studies. To evaluate gender-specific differences in non-human primates or even humans, the design of relevant studies must be carefully evaluated to obtain statistically significant values. Whether these effects are also relevant in other viral and non-viral vectors, the exact mechanism and whether this also applies to other species, including humans, remains to be investigated. In future studies, it would be of interest to evaluate the efficacy of transduction and transgene expression in *in vitro*-transduced cells, for example freshly isolated hepatocytes, from male and female subjects. Indeed, if the gender effect is caused by some hormonal factors, the gender difference would not be seen *in vitro* between female and male cells. Whether there is gender difference on cell lines originally isolated from female or male donors (from either mice of humans) would be a complementary and additional way to tackle this question. On the same line, the inverse *in vitro* experiments were conducted by Davidoff and colleagues who showed that androgens increased AAV-transgene expression *in vitro* by upregulating its receptors [10].

With the increase in transduction efficiency observed with AAV based vectors in male mice compared to female mice, numerous initial AAV-related gene therapy studies only used single sex mice thereby increasing the likelihood of observing a therapeutic benefit, with the simplicity and reduce cost of such studies [23, 25–32]. In addition, the effect of sexual maturity has been overlooked so far. Pre-clinical studies using both genders with AAV based vectors are therefore carried out later in the development pathway. Pre-clinical efficacy studies in mice using systemic delivery of LVV are not very common, and the relatively few reports published only use male mice or don't describe the sex of the animals [2, 3, 6]. Identifying the differences in sex-

dependent transduction efficiencies in gene therapy candidates is important because most studies do not factor these differences. A recent report using a therapeutic AAV8 product candidate for MPSIVA where correction was only observed in male mice highlights the importance of using both male and female mice in efficacy studies [12] in that both groups need to be evaluated to inform pre-clinical efficacy of product candidates. Therefore, accounting for sex-specific differences is a critical variable for the development of safe and efficacious AAV and LVV gene therapy candidates.

In summary, we report for the first-time sex-specific differences in LVV transduction efficiencies and transgene expression in pre-clinical models, similar to those reported for rAAV.

Author contributions

CK and DO'C managed the *in vivo* studies. SI and GD carried out *in vitro* studies. EG and BS wrote the manuscript. All authors contributed to the article and approved the submitted version.

Data availability

The original contributions presented in the study are included in the article/supplementary material, further inquiries can be directed to the corresponding author.

Ethics statement

The animal study was approved by Charles River Laboratories, accredited by the Association for Assessment and Accreditation of Laboratory Animal Care International (AAALAC). The study was conducted in accordance with the local legislation and institutional requirements.

Funding

The author(s) declare that financial support was received for the research and/or publication of this article. The authors declare that this study received funding from Oxford Biomedica (UK) Limited. The funder was not involved in the study design, collection, analysis, interpretation of data, the writing of this article or the decision to submit it for publication.

Acknowledgments

The authors thank Lucy Barnes, Victoria Kennedy, Robert Powels, Federico Zambon and Melissa Sorci and other members of Oxford Biomedica (United Kingdom) Ltd (OXB) for help data acquisition and analysis and in generating and titrating lentiviral vectors used in these studies.

Conflict of interest

All authors were employees of OxfordBiomedica (UK) Ltd.

Generative AI statement

The authors declare that no Generative AI was used in the creation of this manuscript.

References

1. Bulcha JT, Wang Y, Ma H, Tai PWL, Gao G. Viral vector platforms within the gene therapy landscape. *Signal Transduction Targeted Ther* (2021) **6**:53. doi:10.1038/s41392-021-00487-6

2. Carbonaro DA, Jin X, Petersen D, Wang X, Dorey F, Kil KS, et al. *In vivo* transduction by intravenous injection of a lentiviral vector expressing human ADA into neonatal ADA gene Knockout mice: a novel form of enzyme replacement therapy for ada deficiency. *Mol Ther* (2006) **13**:1110–20. doi:10.1016/j.ymthe.2006.02.013

3. Carbonaro-Sarracino DA, Tarantal AF, Lee CCI, Kaufman ML, Wandro S, Jin X, et al. Dosing and Re-administration of lentiviral vector for *in vivo* gene therapy in rhesus monkeys and ADA-deficient mice. *Mol Ther - Methods and Clin Development* (2020) **16**:78–93. doi:10.1016/j.omtm.2019.11.004

4. Dalsgaard T, Cecchi CR, Askou AL, Bak RO, Andersen PO, Hougaard D, et al. Improved lentiviral gene delivery to mouse liver by hydrodynamic vector injection through tail vein. *Mol Ther - Nucleic Acids* (2018) **12**:672–83. doi:10.1016/j.omtn.2018.07.005

5. Brown BD, Cantore A, Annoni A, Sergi LS, Lombardo A, Della Valle P, et al. A microRNA-regulated lentiviral vector mediates stable correction of hemophilia B mice. *Blood* (2007) **110**:4144–52. doi:10.1182/blood-2007-03-078493

6. Milani M, Canepari C, Liu T, Biffi M, Russo F, Plati T, et al. Liver-directed lentiviral gene therapy corrects hemophilia A mice and achieves normal-range factor VIII activity in non-human primates. *Nat Commun* (2022) **13**:2454. doi:10.1038/s41467-022-30102-3

7. Cantore A, Ranzani M, Bartholomae CC, Volpin M, Valle PD, Sanvito F, et al. Liver-directed lentiviral gene therapy in a dog model of hemophilia B. *Sci Transl Med* (2015) **7**:277ra28. doi:10.1126/scitranslmed.aaa1405

8. Nicolas CT, VanLith CJ, Hickey RD, Du Z, Hillin LG, Guthman RM, et al. *In vivo* lentiviral vector gene therapy to cure hereditary tyrosinemia type 1 and prevent development of precancerous and cancerous lesions. *Nat Commun* (2022) **13**:5012. doi:10.1038/s41467-022-32576-7

9. Berraondo P, Crettaz J, Ochoa L, Pañeda A, Prieto J, Trocóniz IF, et al. Intrahepatic injection of recombinant adeno-associated virus serotype 2 overcomes gender-related differences in liver transduction. *Hum Gene Ther* (2006) **17**:601–10. doi:10.1089/hum.2006.17.601

10. Davidoff AM, Ng CYC, Zhou J, Spence Y, Nathwani AC. Sex significantly influences transduction of murine liver by recombinant adeno-associated viral vectors through an androgen-dependent pathway. *Blood* (2003) **102**:480–8. doi:10.1182/blood-2002-09-2889

11. Mochizuki S, Mizukami H, Ogura T, Kure S, Ichinohe A, Kojima K, et al. Long-term correction of hyperphenylalaninemia by AAV-mediated gene transfer leads to behavioral recovery in phenylketonuria mice. *Gene Ther* (2004) **11**:1081–6. doi:10.1038/sj.gt.3302262

12. Piechnik M, Amendum PC, Sawamoto K, Stapleton M, Khan S, Fnu N, et al. Sex difference leads to differential gene expression patterns and therapeutic efficacy in mucopolysaccharidosis IVA murine model receiving AAV8 gene therapy. *Int J Mol Sci* (2022) **23**:12693. doi:10.3390/IJMS232012693

13. Vigna E, Amendola M, Benedicenti F, Simmons AD, Follenzi A, Naldini L. Efficient tet-dependent expression of human factor IX *in vivo* by a new self-regulating lentiviral vector. *Mol Ther* (2005) **11**:763–75. doi:10.1016/j.ymthe.2004.11.017

14. Iqball S, Beck DK, Devarajan G, Khoo CP, O'Connor DM, Ellis S, et al. Lentiviral delivered aflibercept OXB-203 for treatment of neovascular AMD. *Mol Ther - Methods and Clin Development* (2023) **30**:350–66. doi:10.1016/j.omtm.2023.07.001

15. Senova S, Poupon C, Dauguet J, Stewart HJ, Dugué GP, Jan C, et al. Optogenetic Tractography for anatomo-functional characterization of cortico-subcortical neural circuits in non-human primates. *Sci Rep* (2018) **8**:3362. doi:10.1038/s41598-018-21486-8

16. Pañeda A, Vanrell L, Mauleon I, Crettaz JS, Berraondo P, Timmermans EJ, et al. Effect of adeno-associated virus serotype and genomic structure on liver transduction and biodistribution in mice of both genders. *Hum Gene Ther* (2009) **20**:908–17. doi:10.1089/hum.2009.031

17. Shedlovsky A, McDonald JD, Symula D, Dove WF. Mouse models of human phenylketonuria. *Genetics* (1993) **134**:1205–10. doi:10.1093/genetics/134.4.1205

18. Balaggan KS, Binley K, Esapa M, Iqball S, Askham Z, Kan O, et al. Stable and efficient intraocular gene transfer using pseudotyped EIAV lentiviral vectors. *The J Gene Med* (2006) **8**:275–85. doi:10.1002/jgm.845

19. Campochiaro PA, Lauer AK, Sohn EH, Mir TA, Naylor S, Anderton MC, et al. Lentiviral vector gene transfer of endostatin/angiostatin for macular degeneration (GEM) study. *Hum Gene Ther* (2017) **28**:99–111. doi:10.1089/hum.2016.117

20. Bell P, Gao G, Haskins ME, Wang L, Sleeper M, Wang H, et al. Evaluation of adeno-associated viral vectors for liver-directed gene transfer in dogs. *Hum Gene Ther* (2011) **22**:985–97. doi:10.1089/hum.2010.194

21. Arruda V, Scallan C, Jian H, Couto L, Herzog R, Nichols T, et al. Comparison of the efficacy on gene transfer by AAV vectors delivered by distinct routes of administration to the liver of hemophilia B dogs. *Mol Ther* (2004) **9**:S40–S41.

22. Kaiser RA, Weber ND, Trigueros-Motos L, Allen KL, Martinez M, Cao W, et al. Use of an adeno-associated virus serotype Anc80 to provide durable cure of phenylketonuria in a mouse model. *J Inherit Metab Dis* (2021) **44**:1369–81. doi:10.1002/jimd.12392

23. Han SO, Gheorghiu D, Chang A, Mapatano SH, Li S, Brooks E, et al. Efficacious androgen hormone administration in combination with adeno-associated virus vector-mediated gene therapy in female mice with pompe disease. *Hum Gene Ther* (2022) **33**:479–91. doi:10.1089/hum.2021.218

24. Han S, Li S, McCall A, Arnson B, Everitt JI, Zhang H, et al. Comparisons of infant and adult mice reveal age effects for liver depot gene therapy in pompe disease. *Mol Ther - Methods and Clin Development* (2020) **17**:133–42. doi:10.1016/j.omtm.2019.11.020

25. Maturana CJ, Chan A, Verpeut JL, Engel EA. Local and systemic administration of AAV vectors with alphaherpesvirus latency-associated promoter 2 drives potent transgene expression in mouse liver, kidney, and skeletal muscle. *J Virol Methods* (2023) **314**:114688. doi:10.1016/j.jviromet.2023.114688

26. Bell P, Wang L, Chen S-J, Yu H, Zhu Y, Nayal M, et al. Effects of self-complementarity, codon optimization, transgene, and dose on liver transduction with AAV8. *Hum Gene Ther Methods* (2016) **27**:228–37. doi:10.1089/hgtb.2016.039

27. Wang L, Wang H, Morizono H, Bell P, Jones D, Lin J, et al. Sustained correction of OTC deficiency in spfash mice using optimized self-complementary AAV2/8 vectors. *Gene Ther* (2012) **19**:404–10. doi:10.1038/gt.2011.111

28. Cunningham SC, Spinoulas A, Carpenter KH, Wilcken B, Kuchel PW, Alexander IE. AAV2/8-mediated correction of OTC deficiency is robust in adult but not neonatal spfash mice. *Mol Ther* (2009) **17**:1340–6. doi:10.1038/mt.2009.88

29. Bell P, Wang L, Lebherz C, Flieder DB, Bove MS, Wu D, et al. No evidence for tumorigenesis of AAV vectors in a large-scale study in mice. *Mol Ther* (2005) **12**:299–306. doi:10.1016/j.ymthe.2005.03.020

30. Kok CY, Tsurusaki S, Cabanes-Creus M, Igoor S, Rao R, Skelton R, et al. Development of new adeno-associated virus capsid variants for targeted gene delivery to human cardiomyocytes. *Mol Ther - Methods and Clin Development* (2023) **30**:459–73. doi:10.1016/j.omtm.2023.08.010

31. Anderson JM, Arnold WD, Huang W, Ray A, Owendoff G, Cao L. Long-term effects of a fat-directed FGF21 gene therapy in aged female mice. *Gene Ther* (2023) **31**:95–104. doi:10.1038/s41434-023-00422-0

32. Sun B, Zhang H, Franco LM, Young SP, Schneider A, Bird A, et al. Efficacy of an adeno-associated virus 8-pseudotyped vector in glycogen storage disease type II. *Mol Ther* (2005) **11**:57–65. doi:10.1016/j.ymthe.2004.10.004

EBM Experimental Biology and Medicine

TYPE Correction
PUBLISHED 24 April 2025
DOI 10.3389/ebm.2025.10614

OPEN ACCESS

*CORRESPONDENCE
EBM Production Office,
production@ebm-journal.org

RECEIVED 02 April 2025
ACCEPTED 02 April 2025
PUBLISHED 24 April 2025

CITATION
EBM Production Office (2025) Erratum: Retraction: Pyridoxal 5′ phosphate protects islets against streptozotocin-induced beta-cell dysfunction – *in vitro* and *in vivo*.
Exp. Biol. Med. 250:10614.
doi: 10.3389/ebm.2025.10614

Erratum: Retraction: Pyridoxal 5′ phosphate protects islets against streptozotocin-induced beta-cell dysfunction – *in vitro* and *in vivo*

EBM Production Office*

Frontiers Media SA, Lausanne, Switzerland

An Erratum on
Retraction: Pyridoxal 5′ phosphate protects islets against streptozotocin-induced beta-cell dysfunction – *in vitro* and *in vivo*

by EBM Editorial Office (2025). Exp. Biol. Med. 249:10441. doi: 10.3389/ebm.2024.10441

In the published article, there was an error in the terminology used.

A correction has been made to the second and third sentences, which previously stated the following:

"Particularly, in the β-Actin band in **Figure 6A**, two sets of western blots appear to be duplicated if reversed horizontally. Further, in the Glut2 band in the same **Figure 6A**, two sets of western blots appear to be duplicated as well."

The corrected sentence appears below:

"Particularly, in the β-Actin bands in **Figure 6A**, two sets of PCR bands appear to be duplicated if reversed horizontally. Further, in the Glut2/Reg-1 bands in the same **Figure 6A**, two sets of bands appear to be duplicated as well."

The publisher apologizes for this error. The original version of this article has been updated.

EBM Experimental Biology and Medicine

TYPE Retraction
PUBLISHED 10 April 2025
DOI 10.3389/ebm.2025.10605

OPEN ACCESS

*CORRESPONDENCE
EBM Editorial Office,
ebm@ebm-journal.org

RECEIVED 28 March 2025
ACCEPTED 02 April 2025
PUBLISHED 10 April 2025

CITATION
EBM Editorial Office (2025) Retraction: Hydrogen-rich saline protects myocardium against ischemia/reperfusion injury in rats.
Exp. Biol. Med. 250:10605.
doi: 10.3389/ebm.2025.10605

Retraction: Hydrogen-rich saline protects myocardium against ischemia/reperfusion injury in rats

EBM Editorial Office*

A Retraction of the Original Research Article
Hydrogen-rich saline protects myocardium against ischemia/reperfusion injury in rats

by Sun Q, Kang Z, Cai J, Liu W, Liu Y, Zhang JH, Denoble PJ, Tao H and Sun X (2009). Experimental Biology and Medicine. 234(10):1212–9. doi: 10.3181/0812-RM-349

Following publication, concerns were raised on the PubPeer platform regarding the integrity of the images in the published figures. Specifically, highlighted sections of the Sham and H2 images in Figure 6 appear to be duplicated.

The authors remained unresponsive and failed to provide a satisfactory explanation during the investigation, which was conducted in accordance with Experimental Biology and Medicine's policies. As a result, the data and conclusions of the article have been deemed unreliable, and the article has been retracted.

This retraction was approved by the Editor-in-Chief of Experimental Biology and Medicine. The authors received communication regarding the retraction. EBM would like to thank the users on PubPeer for bringing the published article to our attention.

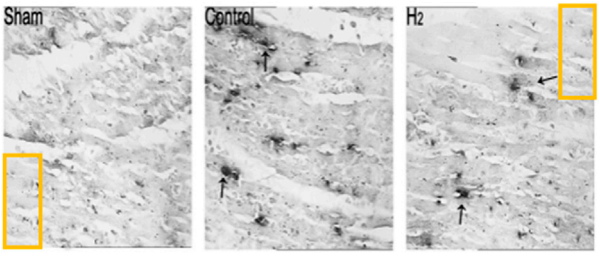

FIGURE 6
Detection of apoptotic cell death by TUNEL staining in the Sham, Control, and H2 groups at the end of 24 h of reperfusion. Relative to the Control group, H2 significantly reduced the number of TUNEL-positive cells (blue staining). Values are mean ± SEM; $P < 0.01$ compared to Control group, $n = 6$ for each group.

Scope

Experimental Biology and Medicine (EBM) is a global, peer-reviewed journal dedicated to the publication of multidisciplinary and interdisciplinary research in the biomedical sciences. The journal covers the spectrum of translational research from T0, basic research, to T4, population health. Articles in EBM represent cutting edge research at the overlapping junctions of the biological, physical and engineering sciences that impact upon the health and welfare of the world's population. EBM is particularly appropriate for publication of papers that are multidisciplinary in nature, are of potential interest to a wide audience, and represent experimental medicine in the broadest sense of the term. However, manuscripts reporting novel findings on any topic in the realm of experimental biology and medicine are most welcome.

EBM publishes Research, Reviews, Mini Reviews, and Brief Communications in the following categories.

- Anatomy/Pathology
- Artificial Intelligence/ Machine Learning Applications to Biomedical Research
- Biochemistry and Molecular Biology
- Bioimaging
- Biomedical Engineering
- Bionanoscience
- Cell and Developmental Biology
- Clinical Trials
- Endocrinology and Nutrition
- Environmental Health/Biomarkers/ Precision Medicine
- Genomics, Proteomics, and Bioinformatics
- Immunology/Microbiology/Virology
- Mechanisms of Aging
- Neuroscience
- Pharmacology and Toxicology
- Physiology and Pathophysiology
- Population Health
- Stem Cell Biology
- Structural Biology
- Synthetic Biology
- Systems Biology and Microphysiological Systems
- Translational Research

EBM Experimental Biology and Medicine

EBM is the official journal of the Society for Experimental Biology and Medicine

Experimental Biology and Medicine (EBM) is a global, peer-reviewed journal dedicated to the publication of multidisciplinary and interdisciplinary research in the biomedical sciences.

Discover more of our Special Issues

See more →

Contact

development@ebm-journal.org

See more

ebm-journal.org

publishingpartnerships.frontiersin.org/our-partners